K^--p Interaction at 2.24 BeV/c*

G. W. LONDON†, R. R. RAU, N. P. SAMIOS, AND S. S. YAMAMOTO
Brookhaven National Laboratory, Upton, New York

AND

M. GOLDBERG‡, S. LICHTMAN,‡ AND M. PRIME
Syracuse University Syracuse New York

AND

J. LEITNER
Syracuse University, Syracuse, New York and Brookhavan National Laboratory, Upton, New York

(Received 14 October 1965)

K^--p interactions at 2.24 BeV/c were studied in several exposures of the Brookhavan National Laboratory 20-in. hydrogen bubble chamber at the alternating-gradient synchrotron. We give an account of all aspects of the experiment, including: experimental procedures, scanning and measuring techniques, data-reduction methods, and experimental results and their consistency with the current theories of strong and weak interactions. The experimental results are grouped as follows: meson and baryon resonance spectroscopy; other two-body and three-body reactions; the Ξ hyperon; and total cross sections. For completeness, we include information published elsewhere but add important details not previously given. In addition, we report a considerable range of new results.

I. INTRODUCTION

DATA concerning K^--p interactions at 2.24 BeV/c were obtained in several exposures of the 20-in. hydrogen bubble chamber at the Brookhaven AGS, beginning in February 1961. Data reduction and analysis of 40 separable reaction channels were carried out both at Brookhaven National Laboratory (BNL) and Syracuse University over a four-year period during which many results of unusual interest were reported on a preliminary basis. In this paper we update these preliminary results using more complete samples. We give an account of all aspects of the experiment, including features such as sample selection and analysis procedures which were not treated in detail in previous publications. In addition, we report a considerable range of completely new results.

Section II is a description of the general experimental procedure. Included are details of the beam detection apparatus, scanning-measuring techniques, data-reduction methods and general event-identification criteria. Experimental results are presented in Secs. III to VI under the self-descriptive headings: III. Meson and Baryon Resonance Spectroscopy; IV. Other Two-Body and Three-Body Reactions; V. The Ξ Hyperon and VI. Total Cross Sections. The content of these sections is discussed briefly below.

The material of Sec. III concerns the existence and properties of all resonances for which we have new or significant results. The K^--p interaction is well known to be a prolific source of unstable resonance particles. Indeed, virtually all the known resonant states whose production is allowed by energy conservation have been observed in one or more of the multiparticle final states of this experiment. Three resonances were, in fact, discovered in the course of this study; they are the $\eta^*(960)$, the $\phi(1020)$ and $\Xi^*(1530)$. In several cases the data are sufficient to provide the determination of all essential properties: mass, width, spin, parity, isospin, G parity (where relevant) and decay modes. In other cases only partial information is available. We compare our findings with other available experimental results and, wherever possible, examine their consistency with the predictions of currently promising theories of strong interaction symmetries.

In Sec. IV we consider special two-body reactions such as $\bar{K}^0N$, $\Lambda\pi^0$, etc, quasi-two-body reactions in which one body is a resonant state, such as $\bar{K}^0N^*$, etc., and some three-body reactions. The dynamical features of most reactions are compared and summarized. In Sec. V the intrinsic properties of the Ξ hyperon are discussed. Total cross sections for all reaction channels which could be identified are given in Sec. VI.

The organization described above is designed primarily to elucidate the role of resonances and reactions rather than *final states*. For this reason, and also because of the broad scope of the experiment, we include a tabulation of the contents for Secs. II–VI with cross reference to the major final state or states involved in each study.

II. Experimental Procedures
A. Experimental Layout
B. Data Analysis
C. Kinematic Analysis and Event Identification

* This work was supported by the Office of Naval Research, National Science Foundation, and the U. S. Atomic Energy Commission.

† Part of this paper forms the subject of a thesis submitted in partial fulfillment of the requirements for the degree of Doctor of Philosophy, University of Rochester (1964).

‡ Part of this paper forms the subject of a thesis submitted in partial fulfillment of the requirements for the degree of Doctor of Philosophy, Syracuse University (1965).

III. Meson and Baryon Spectroscopy
  A. The $\eta^*(960)$
    1. Existence
    2. Decay Modes: $\eta\pi\pi$, $\rho\gamma$
    3. Properties: M, Γ, C, G, I, J, P
    4. Production: K^* Exchange
    5. Discussion: Symmetries
    Major Final States: $\Lambda^0\pi^+\pi^-\pi^0$, $\Lambda^0\pi^+\pi^-\pi^+\pi^-\pi^0$, Λ^0MM, $\Lambda^0\pi^+\pi^-MM$
  B. The ϕ
    1. Existence
    2. Decay Modes: K_1K_2, K^+K^-, $\pi\rho$
    3. Properties: M, Γ, C, P, I, G, J
    4. Kaon Permutation Symmetry
    5. Production: K, K^* Exchange
    6. Discussion: Symmetries
    Major Final States: $\Lambda^0K^0\bar{K}^0$, $\Lambda^0K^+K^-$, $\Sigma^0K^+K^-$, $\Sigma^+K^0K^-$, $\Sigma^-\bar{K}^0K^+$, $\Lambda^0\pi^+\pi^-\pi^0$
  C. The $\kappa(730)$ and $\Xi^*(1530)$
    1. Existence and Decay Modes
    2. Properties of the $\Xi^*(1530)$: M^-, M^0, Γ^-, I
    3. Discussion: Symmetries, Electromagnetic Mass Differences
    Major Final States: $\Xi^-K^+\pi^0$, $\Xi^-K^0\pi^+$, $\Xi^0K^+\pi^-$, $\Xi^0K^0\pi^0$
  D. The $Y_1^*(1385)$ and $Y_0^*(1405)$
    1. Decay Modes: $\Lambda^0\pi^+$, $\Sigma^+\pi^0$, $\Sigma^+\pi^-$
    2. Properties of $Y_1^*(1385)$: J, M^+, M^-, Γ^+
    3. Production of $Y_1^*(1385)$ and $Y_0^*(1405)$: K^* Exchange
    Major Final States: $\Lambda^0\pi^+\pi^-$, $\Sigma^+\pi^-\pi^0$
  E. The $Y_1^*(1660)$
    1. Existence
    2. Decay Modes: $Y_0^*(1405)\pi^+$
    3. Properties: J, P
    Major Final States: $\Sigma^{\pm}\pi^{\mp}\pi^+\pi^-$, $\Lambda^0\pi^+\pi^-\pi^0$

IV. Other Two and Three-Body Reactions

A. Two-Body Reactions	Major Final States
1. $\bar{K}^0N$, $\bar{K}^0(N^*)^0$	$\bar{K}^0MM$
2. $(K^*)^-p$	$\bar{K}^0\pi^-p$
3. $\Lambda^0\pi^0$, $\Lambda\eta$	Λ^0MM
$\Lambda^0\rho^0$	$\Lambda^0\pi^+\pi^-$
$\Lambda^0\omega$	$\Lambda^0\pi^+\pi^-\pi^0$
$\Sigma^+\pi^-$, $\Sigma^+\rho^-$, $Y_0^*(1520)\pi$	$\Sigma^{\pm}\pi^{\mp}\pi^0$
Ξ^-K^+	Ξ^-K^+
$\Xi^-(K^*)$	$\Xi^-K^+\pi^0$, $\Xi^-K^0\pi^+$

B. Three-body reactions	Major Final States
1. $K^*N\pi$, $N^*\bar{K}\pi$, $Y^*(1520)\pi\pi$	$\bar{K}^0N\pi^+\pi^-$, $\bar{K}^0p\pi^-\pi^0$ $K^-p\pi^+\pi^-$ $K^-p\pi^+\pi^-\pi^0$
2. $\Sigma\eta\pi$, $\Sigma\omega\pi$, $Y^*(1405)\pi\pi$, $Y^*(1520)\pi\pi$	$\Sigma^{\pm}\pi^{\mp}\pi^+\pi^-\pi^0$, $\Sigma^{\pm}\pi^{\mp}MM$

V. The Ξ Hyperon
  A. Properties: M^-, M^0, τ^-
  B. Decay Modes: $\Lambda^0e\bar{\nu}$
  C. Weak-Interaction Parameters: α_{Ξ^-}, β_{Ξ^-}, γ_{Ξ^-}, α_{Ξ^0}
  Major Final States: $\Xi^-K^+\pi^0$, $\Xi^-K^0\pi^+$, $\Xi^0K^+\pi^-$

VI. Total Cross Sections

II. EXPERIMENTAL PROCEDURES

A. Experimental Layout

1. Targeting and Beam

The layout of the beam used in this experiment is shown in Fig. 1. The target, located in the F-10 straight section of the AGS, was a tungsten parallelopiped 0.01-in. high, 0.25-in. wide, and 2-in. long (in the circulating beam direction). The beam was kicked onto the target with the Rapid Beam Deflector[1] system producing a beam-burst length of the order of 50μsec, appropriate for bubble-chamber operation where the sensitive time is $\sim$3msec. The ejected beam was taken off at 8° to the circulation direction in order to avoid the AGS fringe field and thus permit independent variation of the internal-beam energy and secondary-beam momentum and charge. Under typical conditions the beam was operated at an internal energy of 25 BeV, with an intensity of $\sim 3\times 10^{11}$ protons/pulse.

The separated secondary beam has been described in considerable detail elsewhere,[2,3] Here, we shall review the important beam characteristics, referring to the block diagram shown in Fig. 1. The beam was 270 ft long and consisted of four distinct stages connected by a continuous vacuum pipe extending from the AGS to the final mass-resolving slit. The four stages performed distinct functions; the first stage gave primary momentum resolution and image demagnification, the second and third performed the π-K separation, and the fourth produced the desired image at the chamber. Each of these is described briefly below.

The angular acceptance of the secondary beam was defined by slit No. 1 to be 3.6×10^{-2} msr. The first stage consisting of a quadrupole doublet, a bending magnet and slit No. 2, demagnified the vertical image height (by a factor of 2), thus increasing the ratio of relative π-K separation to image height which was the primary measure of system efficiency. The bending magnet gave a rough momentum selection ($\Delta p/p \approx \pm 6\%$) at slit No. 2. The next two stages were identical, each containing a pair of quadrupoles, a 15 ft electrostatic velocity spectrometer,[4] a mass-resolving slit (slits 3

[1] H. N. Brown *et al.*, Brookhaven Internal Report, AGS Dept., HNB/BBC/EFB-1 (unpublished).
[2] C. Baltay *et al.*, Nucl. Instr. Method **20**, 37 (1963).
[3] J. Leitner, G. Moneti, and N. P. Samios, *Proceedings of the International Conference on High Energy Instrumentation, 1962*, edited by F. J. M. Farley (North-Holland Publishing Company, Amsterdam, 1963), p. 42.
[4] W. Fickinger *et al.*, Brookhaven National Laboratory Internal Report, AGS Dept. (unpublished).

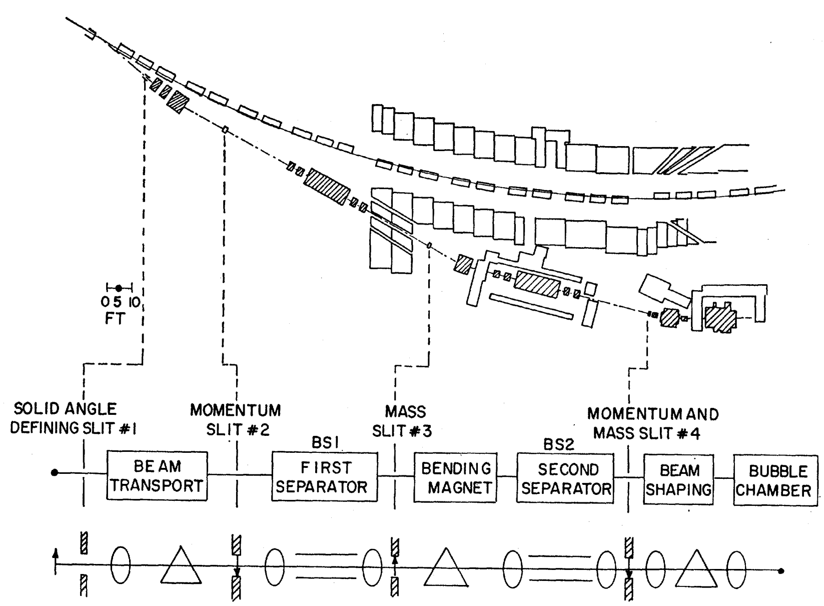

FIG. 1. Schematic layout of the beam used for separating K^- particles from the undesired μ^-, π^-, and $\bar{p}$ particles.

and 4), and had an over-all magnification of unity. The separators were operated at a nominal potential of 380 kV across a 2-in. gap. The first quadrupole pair in the second stage produced a parallel beam which was mass separated by the first separator and refocused by the second quadrupole pair at slit No. 3, where most of the pions were removed. The bending magnet between stages 2 and 3 removed slit-scattered background and gave a momentum selection of $(\Delta p/p)_{\max} = \pm 2\%$. The third stage culminating at the final mass slit No. 4, provided a π-K separation of $\sim$0.15 in., an image width of 0.1 in. and a K^-/background ratio of $\sim$4. The final beam-shaping section served to spread the image to fill the entrance window of the chamber and compensate for the chamber fringe field.

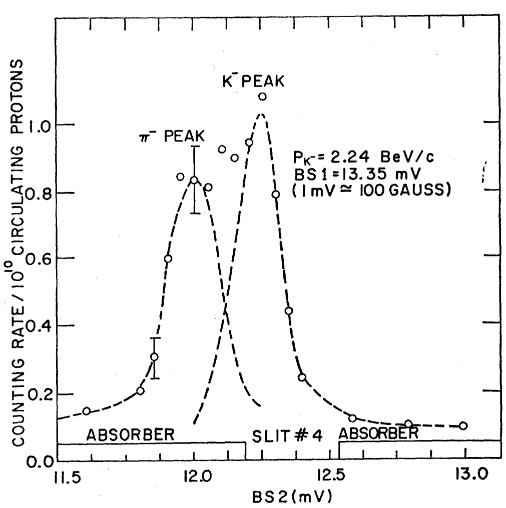

FIG. 2. Counting rate as a function of the second electrostatic-separator magnetic-field current for typical operating conditions. The dotted curves indicate roughly the contribution from π^- and K^- particles.

The actual beam performance was studied using both counters and the bubble chamber. Beam images were obtained using a counter telescope directly in front of the final mass resolving slit. The system was tuned by setting the magnetic field of the first separator (BS1) to transmit either π's or K's and then varying the magnetic field in the second separator (BS2). In this way BS2 was used as an analyzer for the beam transmitted by BS1. By taking counting rates versus BS2 magnetic field for a fixed BS1 magnetic field, we were able to study both image widths and image separation. Figure 2 shows the curve corresponding to typical running conditions, i.e., six particles/picture per 10^{11} circulating protons. The width of each image is about 0.18 mV ($\sim$0.1 in.) and their separation is 0.27 mV ($\sim$0.15 in.). The position of the mass-resolving slit is also shown in Fig. 2. Using this slit position, we estimate that only $\sim$5% of the transmitted particles are pions. However, the main background, which appears as a constant contribution to both peaks of Fig. 2, constitutes 15% of the transmitted beam, and consists of slightly off-momentum muons coming from in-beam pion decays. These percentages of K, π and μ's in the beam agree well with those obtained in bubble chamber studies of K^- decays and identified pion events. The latter indicate a $K^-:\mu^-:\pi^-$ content of 80:15:5 with an error of $\pm 3\%$.

2. *Bubble Chamber*

The 20-in. BNL liquid-hydrogen bubble chamber has been fully described elsewhere.[5] Here we briefly describe the features relevant to the subsequent analysis. The chamber (see Fig. 3) is 20 in. along the beam direction,

[5] R. I. Louttit *et al.*, in *Proceedings of an International Conference on Instrumentation for High Energy Physics, 1960*, edited by C. E. Mauk, A. H. Rosenfeld, and R. K. Wakerling (University of California Press, 1961), Berkeley, California, p. 117.

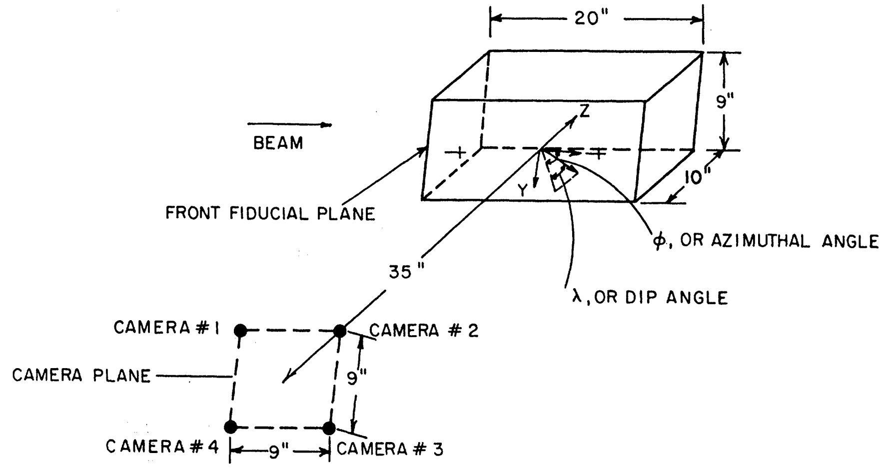

FIG. 3. Schematic diagram of the relevant geometry of the 20-in. hydrogen bubble chamber.

9 in. high and 10 in. wide, with an illuminated volume of $\sim$25 l. The magnetic field is 17 kG in the horizontal plane perpendicular to the beam direction, with variations of up to $\pm 3\%$ of roughly linear nature from the nominal value at the center. Using a through-illumination system, four 35-mm photographs are taken by 4 separate cameras located at the vertices of a 9-in. square about 40 in. from the chamber center (see Fig. 3). Fiducial marks on both the front and rear windows provide the necessary reference for stereo reconstruction. The average stereo angle is 15°, and the reconstruction may be done using any of four different camera combinations. Under typical operating conditions, i.e. temperature 25.6°K and pressure 52 psi(gauge), the bubble density is $\sim$12 bubbles/cm for a minimum ionizing track. Since the beam burst is short (50μsec) and the chamber sensitive time is long ($\sim$3msec) the bubble size can be sensitively controlled by varying the light-flash delay. With $\sim$150 μsec delay, bubble size was diffraction-limited, corresponding to $\sim$0.3 mm in true space. The track intensity and bubble density were maintained at desired levels by manual monitoring.

Three separate exposures were taken containing 80 000, 100 000, and 160 000 pictures, respectively, with an average of about 7, 8 and 14 tracks/picture, respectively, over the course of a year. We shall refer to these exposures as data runs I, II, and III. The K^- content of the beam was very close to 80% in all three runs.

B. Data Analysis (Scanning and Measuring)

Portions of the film were scanned independently at both BNL and Syracuse using standard reprojection devices with magnifications of the order of 10–20. Each frame was scanned in at least two views and a third was always available in the event of topological confusion or optical obscuration.

The complete scanning operation was carried out in four separate stages. To begin with, a "fast scan" of a preliminary nature was undertaken to select rare final states involving two or more strange particles. For the most part, such events are characterized by two visible decays of either the charged or neutral (V^0) variety, and so are easily recognizable. This search was done primarily by physicists at the rate of $\sim$100 frames/h, and served to isolate the final states $\Lambda^0 K^0 \bar{K}^0$, ΞK, $\Xi K\pi$, and $\Sigma K\bar{K}$, making them available for study while slower, more exhaustive, scans were in progress. In order to obtain as much data as possible, all three data runs were "fast scanned" and no fiducial criteria were employed. For this reason, special care must be taken in the evaluation of the differential and total cross sections for rare final states.

The "fast scan" was followed by two independent "normal" scans in which all final states with one or more visible decays of either the charged or V^0 variety were recorded (the independence of these scans provided scanning efficiencies). The above criteria is designed to select the vast majority of all strange-particle events except those involving a K^- in the final state. These are highly biased because most K^-'s escape from the chamber before decaying. The normal scan was carried out only for data runs I and II and with slightly different fiducial regions. The fiducial regions consist of cutoffs along all edges of the illuminated region which effectively reduce the chamber volume by 15%. At the far edge two cutoffs were imposed, one for production vertices and one for decay vertices.

Specially trained technicians proceeding at a rate of $\sim$40 frames/h, recorded all information necessary for the measurement of the event. This included the event topology (in terms of a code[6] suitable for programming), a rough sketch with numerical ordering of the tracks, alternative interpretations such as other possible origins, special information such as whether a positive track stopped or left the chamber, and finally the best views for measurement. The "normal" pair of views chosen was that in which the majority of the tracks make an

[6] This code was developed by J. Kopp for use in association with BNL programs, see Brookhaven National Laboratory Internal Report F-55 (unpublished).

angle $>20°$ with the intercamera line (see Fig. 3). For each track making an angle $<20°$ with the normal intercamera line, one of 3 alternate camera pairs was chosen. In addition, information useful to subsequent event identification was noted. This included ionization estimates for all tracks, unusual topology, whether the V^0 was potentially associated with the production vertex and the existence of γ pairs associated with either the production or decay vertex. All V^0 candidates were measured unless (a) the vertex occurred within 4 mm of the origin or (b) one track was clearly identified as an electron on the basis of curvature and ionization. However, candidates were noted as possible γ pairs if the projected opening angle was less than 3° in two views. Events with charged Σ decays were recorded only if scanners also recorded information necessary for cross section determinations. This included: (a) whether the event is measurable (it may be unmeasurable either because of optical obscuration or, for rare topologies, because of the insufficient length of 2 or more tracks); (b) the number of τ decays and single prong K^- decays (of angle $\geqslant 5°$) in each frame; (c) the beam count in every 50th frame; and (d) the number of blank pictures.

The final stage of scanning was designed to obtain the remaining sample of $\Sigma^{\pm}\pi^{\mp}\pi^+\pi^-(\pi^0)$ events and to select a useful sample of 4 and 5 body final states containing a K^- meson. This was accomplished (using the rules described above) by selecting "4 prong with one-charged-decay" topologies in run III and all "4 prong and no-decay" topologies in a partial sample of data from run I and III.

Measurement of events was carried out using standard measuring machines, all capable of 2-μ reproducibility on the film. Coordinate information was automatically read out through 1μ least-count binary encoders. An average of 6–10 points and a minimum of 3 points were measured over the useful visible length of each track, avoiding crossing tracks and δ rays and ending before any kink visible in any view. Special care was given to measurement of fiducials, end points and vertices. The average measurement time was 15 min/event with $\sim 30\%$ spread depending upon the complexity of the event and the number of views required. After measurement (and remeasurement), events were processed at the BNL 7094 and analyzed at both BNL and Syracuse (SYR).

C. Kinematic Analysis and Event Identification

Measurements were analyzed using the basic BNL programs for geometrical reconstruction (TRED) and kinematic analysis (KICK and PRINT B) which have been described in great detail elsewhere.[7] TRED provides unfitted information for all possible hypotheses for each track in the event. KICK attempts to fit TRED data to all kinematically determined event-type hypotheses consistent with the known conservation laws, beginning with the decay vertex. Successful[8] decay-fit information is used as input to the production vertex fit, and again if successful, the charged decay vertex is refitted. For all hypotheses the missing neutral mass at production is calculated (provided there is sufficient information to do so).

The output of the entire sequence of event-analysis programs provides the following information: (1) *unfitted* angles, momenta and expected ionization densities for all tracks; (2) for each event-type hypothesis, the decay and production χ^2 probabilities $P(\chi^2)$ provided $P(\chi^2)\geqslant 0.1\%$, along with the *fitted* angles, momenta and expected ionization densities of all tracks; (3) the neutral missing mass for *all* hypotheses; and (4) relevant position and length information. On the basis of such output, taking any fit with $P(\chi^2)\geqslant 1\%$ as acceptable, events were temporarily classified as either unique fits ($\sim 25\%$), nonunique fits ($\sim 65\%$) or missing mass (MM) fits containing more than one missing neutral ($\sim 10\%$). Studies of the expected versus observed ionization densities, the χ^2 distributions and the relative proportions of rare events, indicated that most of the alleged ambiguities could be resolved with good reliability. However, MM events were sometimes erroneously fitted as events with one missing neutral, when the error in MM was large.

On the basis of such studies and many event-by-event comparisons, we developed the following set of criteria for the *rejection* of event-type hypotheses passed by KICK: (1) $P(\chi^2)\leq 1\%$; (2) observed ionization inconsistent with predicted ionization; (3) $P(\chi^2)$ lower by a factor of 10 than that for the most probable fit; (4) neutral missing mass greater than two standard deviations from m_{π^0}, for one-constraint fits only; (5) for Σ^- versus K^- ambiguities, the K^- hypothesis is rejected if the (fitted) decay time is <3 Σ^- lifetimes.

Application of the above criteria yielded a single successful hypothesis (i.e. a unique fit or MM identity) for $\sim 90\%$ of all events. The majority of the remaining multiple fits are due to Σ^0-Λ^0 ambiguity. The first two of the above criteria are by far the most important. After application of (1) in most cases the ionization estimates of trained scanners were sufficient to decide identity, but in others, especially the rare topology events, physicists carefully re-examined the event. It was found that under "normal" circumstances π-K ambiguities were distinguishable up to 800 MeV/c and π-p ambiguities up to 1.5 BeV/c with ionization estimates accurate to $\approx\pm 0.4\times$minimum.[9] It is important

[7] Brookhaven National Laboratory Bubble Chamber Group Internal Reports: T. W. Morris, F-18(1959), W. J. Willis, F-28(1960), J. K. Kopp, F-55(1961), F-49(1961), F-62(1962), F-68(1962), F-67(1960), I. O. Skillicorn, F-94(1962), (all unpublished).

[8] The term "successful" in the context of KICK means that a fit could be achieved where the fitted missing mass of a given vertex was less than six standard deviations from the unfitted value.

[9] Of course, there are many exceptional circumstances which preclude accurate estimates, such as high dip ($>70°$), short tracks ($\lesssim 2$ cm), perpendicularity to the beam direction, poor chamber conditions, etc. Most of the multiple fits, aside from Σ^0-Λ^0 ambiguities, are due to such effects.

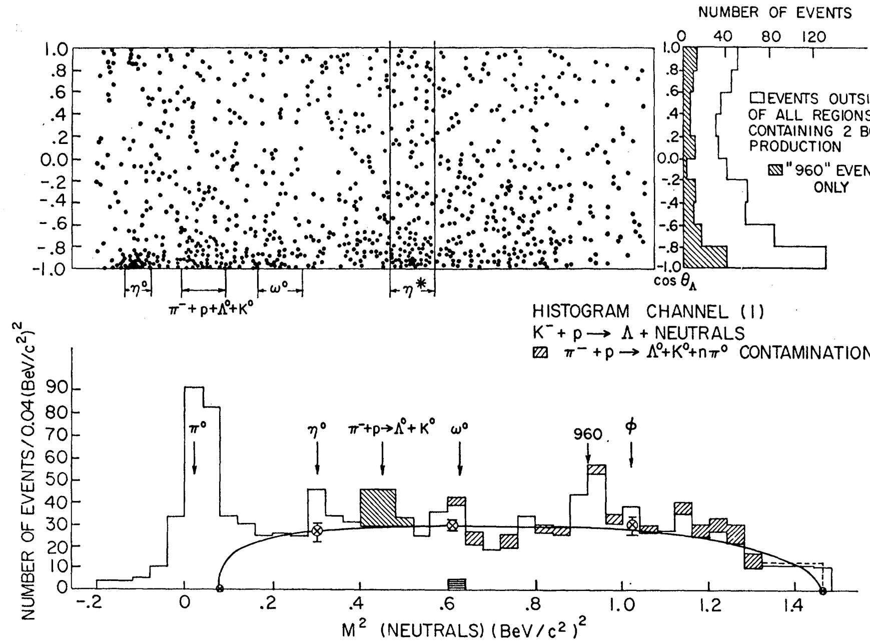

FIG. 4. Scatter plot of Λ-production angle as a function of M^2 (neutrals) for 1277 $K^-p \to \Lambda^0$ +neutrals events, with production angle and mass-squared projections.

to note that the above criteria identify *final states* rather than reaction channels. The additional criteria used to identify the many reaction channels contained within a given final state are more appropriately discussed in Secs. III–VI. The same is true of biases and detailed background problems which are usually different for each final state.

III. MESON AND BARYON SPECTROSCOPY

A. The η^* Meson

In this section we discuss the evidence pertinent to the existence and properties of a strangeness-zero meson of mass 960 MeV/c^2 and narrow width. This particle originally called[10,11] the "X^0", might more appropriately be called the η^*, since it appears to be an excited η^0. The η^* is found to have zero isospin, positive G parity and most probably spin parity 0^-, although 2^- cannot be conclusively ruled out. Similar studies of the η^* and its properties have been reported by a Berkeley Group,[12] and a University of California at Los Angeles (UCLA) group.[13] We shall make use of these published data for various analyses and comparisons.

1. Existence

Evidence for the existence of the η^* comes primarily from effective mass studies in the following final states:

$$K^- + p \to \Lambda^0 + \text{neutrals}, \quad (1)$$

$$K^- + p \to \Lambda^0 + \pi^+ + \pi^- + \pi^+ + \pi^- + \pi^0, \quad (2)$$

$$K^- + p \to \Lambda^0 + \pi^+ + \pi^- + (\text{neutrals with mass} > m_{\pi^0}). \quad (3)$$

The number of events in each[14] channel is 1277, 43, and 415, respectively, all coming from a complete sample occurring within a suitable fiducial region. The effective-mass spectra of all final-state particles, except the Λ^0, for the above reactions, are shown as the lower projection of Figs. 4, 5, and 6, respectively. In each case, a clear peak occurs at $[M \text{ (all except } \Lambda^0)]^2 = (960\ \text{MeV}/c^2)^2$, of width no larger than the mass resolution. Additional evidence indicating that events in the 960 peaks are different from those in neighboring

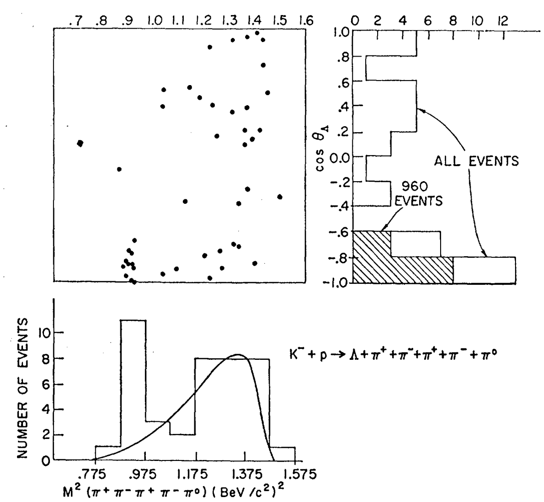

FIG. 5. Scatter plot of Λ-production angle as a function of M^2 ($\pi^+\pi^-\pi^+\pi^-\pi^0$) for 43 $K^-p \to \Lambda^0\pi^+\pi^-\pi^+\pi^-\pi^0$ events, with production angle and mass-squared projections.

[10] M. Goldberg *et al.*, Phys. Rev. Letters **12**, 546 (1964).
[11] M. Goldberg *et al.*, Phys. Rev. Letters **13**, 249 (1964).
[12] G. R. Kalbfleisch *et al.*, Phys. Rev. Letters **12**, 527 (1964); **13**, 349 (1964).
[13] P. M. Dauber *et al.*, Phys. Rev. Letters **13**, 449 (1964).

[14] These numbers do not include 2% of the total number of events where the V^0 was not uniquely identified as a Λ^0. Such events were studied separately and apportioned on the basis of (decay) χ^2 probability and the ratio of Λ^0 to K^0 in the unique sample and are included in the graphs.

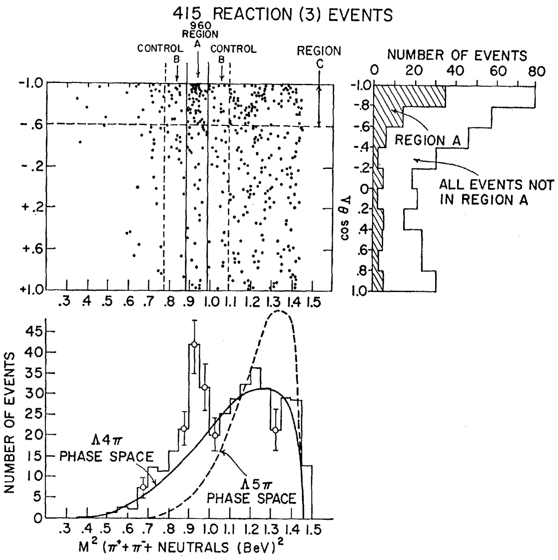

FIG. 6. Scatter plot of Λ^0-production angle as a function of M^2 ($\pi^+\pi^-$+neutrals) for 415 $K^-p \rightarrow \Lambda^0\pi^+\pi^-$+neutrals events, with production angle and mass-squared projections.

mass regions is apparent from a study of $[M$ (all except $\Lambda^0)]^2$ versus momentum transfer (or similarly versus $\cos\theta_\Lambda$, the center-of-mass production angle of the Λ^0). As shown in Figs. 4, 5, and 6, the percent age of extremely backward Λ's, i.e., peripheral events, is much higher in the 960 distribution than it is for the remainder of the M^2 distributions. (Hereafter when we have occasion to use a "peripheral criterion" to select η^* events, what is meant is the condition $-1\leq\cos\theta_\Lambda\leq-0.6$.)

All of these results taken together constitute unequivocal evidence for the production of a 960 MeV/c^2 meson via the reaction

$$K^-+p\rightarrow\Lambda^0+\eta^*, \tag{4}$$

where the η^* subsequently decays into the following modes:

$$\eta^*\rightarrow \text{neutrals}, \tag{5}$$

$$\eta^*\rightarrow\pi^+\pi^-\pi^+\pi^-\pi^0, \tag{6}$$

$$\eta^*\rightarrow\pi^+\pi^-+\text{neutrals}. \tag{7}$$

We discuss details concerning the reliability of this evidence for each of the channels (1), (2), and (3) in sequence below.

In channel (1) 98% of all events contain a uniquely identified Λ^0. Aside from (1), the topology "Λ^0+neutrals" may include the reaction channels

$$K^-+p\rightarrow\Sigma^0+\text{neutrals}, \tag{8a}$$

$$\pi^-+p\rightarrow(\Lambda^0 \text{ or } \Sigma^0)+K^0, \tag{8b}$$

$$\pi^-+p\rightarrow(\Lambda^0 \text{ or } \Sigma^0)+K^0+\pi^0. \tag{8c}$$

The reaction (8a) cannot of course be distinguished from (1) and is included in Fig. 4 within the general background contribution. The contribution of reaction (8b) and (8c) can be ascertained from a study of kinematically fitted π^-+p events in which *both* the Λ^0 and K^0 decay visibly in the chamber. Because of the vast difference in missing mass between pion and kaon-induced double V^0 events, this study permits the identification of the former with essentially no ambiguity. From this study we find that in Fig. 4 there are included $\sim$37 reaction (8b) events and $\sim$60 reaction (8c) events. Moreover, since the background missing-mass spectra are known from the double V^0 event study, we are able to subtract the pion-induced background events in a reliable way. This subtraction is indicated by the shaded areas of Fig. 4. (Since the pion-induced contamination is negligible within the 960 region, we have made no correction to the $\cos\theta_\Lambda$ versus M^2 scatter plot.)

After subtraction of the pion contamination, the general features of the M^2 (neutrals) distribution become apparent. As indicated in the figure, there are peaks of varied size corresponding to the known two-body production of Λ^0, together with either a π^0, η, ω, or ϕ. From an ideogram of the data of Fig. 4, we find that these peaks occur at 130±30 MeV/c^2, 550±20 MeV/c^2, 780±15 MeV/c^2 and 1020±15 MeV/c^2, respectively, in excellent agreement with the accepted masses of these mesons. In addition, one sees the new peak at $\sim$960 MeV/c^2 of width $\approx$40 MeV/c^2, roughly equal to the experimental width.

We have investigated a number of alternative production mechanisms such as $Y^*+\eta^0$, $Y^*+\omega^0$, $\Sigma^0+\omega^0$, etc., and find that none of them is capable of giving rise to a peak of width as narrow as that observed. In particular we emphasize that Σ^0 contamination (if it were significant) cannot account for the 960 peak; in any special Σ^0 production mechanism the missing γ ray would give rise to a wide peak—for example in $\Sigma^0+\omega^0$ the peak would have a width about four times the observed one. (For the same reason $\Sigma^0+\eta^*$ production would be much broader than the experimental peak.)

A quantitative estimate of the size of the new peak may be obtained only after a reliable estimate of the "phase space" background due to $K^-+p\rightarrow(\Lambda^0$ or $\Sigma^0)$ $+n\pi^0$. We make such an estimate by first studying the *charged* decay rates of the various resonances in the peaks of Fig. 4. More specifically, as discussed in Sec. IIIE, from the M^2 ($\pi^+\pi^-\pi^0$) spectrum of the reaction $K^-+p\rightarrow\Lambda^0+\pi^-+\pi^++\pi^0$, we determine the number of ω, and η's decaying via the charged ($\pi^+\pi^-\pi^0$) mode. Similarly, the charged K^++K^- mode of ϕ decay is directly observed from $K^-+p\rightarrow\Lambda^0+K^++K^-$ (see Sec. IIIB for details). From this information and the known charged to neutral branching ratios[15] of the η, ω, and ϕ we predict that 30±10, 20±5, and 10±3 events should appear in the η, ω, and ϕ peaks of Fig. 4, re-

[15] G. Puppi, Ann. Rev. Nucl. Sci. **13**, 287 (1963); P. L. Connolly *et al.*, Phys. Rev. Letters **10**, 371 (1963); S. Lichtman, Syracuse University, thesis (unpublished).

spectively. These normalization points are indicated by "$\oplus$" under the appropriate peaks in Fig. 4. The other two $\oplus$ marks correspond to the onset of $\Lambda^0\pi^0\pi^0$ phase space and the end point of the "Λ^0+neutrals" spectrum Using the normalization points and assuming that the. initial slope of the background is determined by $\Lambda^0\pi^0\pi^0$ phase space, we obtain the smooth background curve of Fig. 4, representing $K^-+p\to(\Lambda^0 \text{ or } \Sigma^0)+n\pi^0$. On this basis the "960" peak is found to contain 39 ± 10 events, representing reaction (5). It should be pointed out, however, that the angular-distribution information is ignored in this estimate; we shall use this information later to obtain a better estimate of the true number of η^*'s in the peak.

Next, we turn to the five-pion channel (2), which contains only one π^0, so that all events are kinematically fitted with one constraint. Of the total of 43 events, 38 are unambiguous and 5 are ambiguous with $\Sigma^0\pi^+\pi^-\pi^+\pi^-$. None of the latter, however, contribute to the 960 peak of Fig. 5. The background can be accounted for very well by phase space for the $K^-+p\to\Lambda^0+5\pi$ reaction, as indicated by the solid curve of Fig. 5. We have studied the two and three-particle mass spectra of channel (2) and found evidence for $Y_1^*(1385)$ and ω^0 production, but we believe that this circumstance cannot account for any appreciable distortion in $M^2(5\pi)$, let alone the 960 peak itself. To further investigate the effect of such intermediate resonance production on multipion mass distributions, we studied an 83 event sample of the reaction $K^-+p\to\Lambda^0+4\pi$ which we know to contain a strong $Y_1^*(1385)$. As shown in Fig. 7, the $M^2(4\pi)$ distribution from this reaction fits phase space very well, indicating that resonance effects do not markedly distort the $M^2(4\pi)$ spectrum, and implying a similar situation for reaction (2). From Fig. 5 we estimate that the peak located at 960 ± 10 MeV/c^2 and of width ±25 MeV/c^2 contains 10 ± 3 η^* events representing reaction (6). From Fig. 5 one sees that all these events are highly peripherally produced.

Finally, we consider channel (3). Here events are defined by the criteria: (a) the V^0 is a uniquely identified Λ^0; (b) each of the charged prongs is consistent with a pion identity on the basis of momentum and ionization; (c) no kinematic fit consistent with any of the hypotheses $K^-+p\to(\Lambda^0 \text{ or } \Sigma^0)+\pi^++\pi^-$, $\Lambda^0+\pi^++\pi^-+\pi^0$, or $\pi^-+p\to\Lambda^0+K^++\pi^-(+\pi^0)$ is possible with a χ^2 probability of 1% or greater; and (d) the calculated missing mass of the neutrals is greater than m_{π^0}. In practice about 90% of the events in this sample have a neutral missing mass $\gtrsim 2m_{\pi^0}$. The only source of contamination in this sample is due to pion-induced final states of the type $(\Lambda^0)+K^0+\pi^++\pi^-$. From a study of the visible "double-V^0+2-prong" topology, we conclude that only 6 ± 4 events of this type are contained in the 415-event sample of channel (3) considered here. The criteria outlined above discriminate against reaction (3) events with low M^2 (neutrals). From a study of the 1–10% χ^2 tail of unique $\Lambda^0\pi^+\pi^-\pi^0$ events we

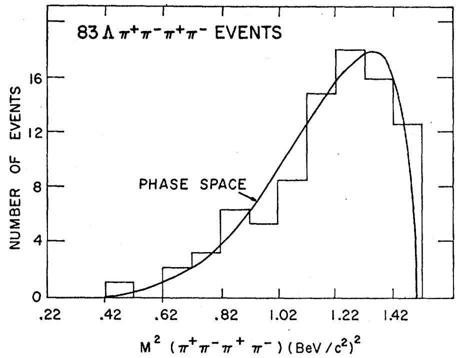

FIG. 7. M^2 $(\pi^+\pi^-\pi^+\pi^-)$ histogram for 83 $K^-p\to\Lambda\pi^+\pi^-\pi^+\pi^-$ events.

estimate that 30 ± 10 events which are really reaction (3) events have been spuriously fit as $\Lambda^0\pi^+\pi^-\pi^0$ and thus omitted from Fig. 5. However, a study of their M^2 (neutrals) distribution indicates that they consist almost entirely of $\Lambda^0\pi^+\pi^-\pi^0\pi^0$ final states, and as we shall see in the next section, η^* decay does not lead to such final states, so that our relative η^* estimate is unbiased by this omission. The $\Lambda^0 4\pi$ phase space (shown as the solid curve of Fig. 6) fits the background very well. The "$\Lambda^0 5\pi$" reaction $(K^-+p\to\Lambda^0\pi^+\pi^-3\pi^0)$ is shown for comparison. We conclude that at least in the region of the 960 peak the $\Lambda^0 4\pi$ phase space is a good estimate to the background level. Using the former, we find that channel (3) contains 39 ± 10 $(\eta^*\to\pi^++\pi^-+\text{neutrals})$ events. The angular-distribution information of Fig. 6 bears out this estimate very well.

2. Decay Modes

We turn now to an investigation of the detailed nature of η^* decay, i.e. an examination of the structure within the final states (5), (6), and (7). The simplest of the above modes to consider is (6), which can be ascribed to either of the decay chains:

$$\eta^*\to5\pi(\text{direct}) \qquad (9a)$$

or

$$\eta^*\to\eta^0\pi^+\pi^-,\quad \eta^0\to\pi^+\pi^-\pi^0. \qquad (9b)$$

No other possibilities are consistent with the relative rates of (5), (6), (7) given in the previous section. Since, as we shall see later, the η^* decay is mediated by a strong interaction, the 5π and $\eta^0\pi^+\pi^-$ hypotheses are mutually exclusive since they have different G parity. Direct evidence against $\eta^*\to5\pi$ comes from considerations based on the distribution of the four possible $(\pi^+\pi^-\pi^0)$ mass combinations for each 5-pion final state. The striking feature of the distribution is that every one of the available 45 η^* events[16] contains at least one $M(\pi^+\pi^-\pi^0)$ combination consistent with the η^0 mass (taken to be 550 ± 25 MeV/c^2 for all these well-measured

[16] This sample consists of 10 events from this experiment and 35 events from Ref. 12 (produced at momenta 2.45–2.7 BeV/c).

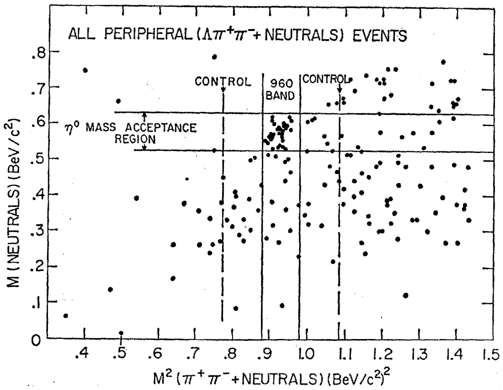

FIG. 8. Scatter plot of M^2 (neutrals) as a function of $M^2(\pi^+\pi^- +\text{neutrals})$ for peripheral $K^-p \to \Lambda^0\pi^+\pi^- +$neutrals events.

events). It is easy to see that this circumstance is inconsistent with the assumption $\eta^* \to 5\pi$. We estimate the probability P_{η^0}, that three pions from $960 \to 5\pi$ have $M(3\pi) = 550\pm25$ MeV/c^2, from the appropriate 3π phase space. Including resolution broadening, we find $P_{\eta^0} = 0.2\pm0.05$. Then, ignoring correlations among the 4 possible mass choices, the expected number of events with at least one "successful" mass combination is only $45[1-(1-0.2\pm0.05)^4] \approx 27\pm5$ events which is $(45-27)/5 \approx 3.5$ standard deviations from the observed value. It is important to note that although correlations certainly do exist here, their effect is small, because for this sample the η^0 mass acceptance region is very narrow compared with the range over which $M(3\pi)$ phase space is appreciable. In similar fashion we have computed the expected distribution of "successful" mass combinations based upon either the 5π or the $\eta^0\pi^+\pi^-$ hypothesis. The results are summarized in Table I. The evidence for (9b) is quite conclusive, establishing the hypothesis $\eta^* \to \eta^0\pi^+\pi^-$.

In the final state (7) we have two possible contributing $\eta^0\pi\pi$ modes:

$$(\alpha) \quad \eta^* \to \eta^0\pi^+\pi^-, \quad \eta^0 \searrow \text{neutrals } (70\%),$$

$$(\beta) \quad \eta^* \to \eta^0\pi^0\pi^0, \quad \eta^0 \searrow \pi^+\pi^-\pi^0 \ (24\%).$$

Assuming the η^* decay to be strong, decay (α) is allowed for either $I=0$ or $I=1$, while (β) is allowed only for $I=0$. For $I=0$, the ratio $(\eta^* \to \eta^0\pi^+\pi^-)/(\eta^* \to \eta^0\pi^0\pi^0)$ must be 2/1. This, together with the η^0 decay branching ratios[15] $\approx 70\%$ for $\eta^0 \to$ neutrals and $\approx 24\%$ for $\eta^0 \to \pi^+\pi^-\pi^0$, gives $(\alpha)/(\beta) = 2\times0.7/0.24 \approx 6/1$. Thus for either value of I one expects to see a dominant η^0 contribution in the mass subspectrum M^2 (neutrals) from the final state (7). A scatter plot of M^2 (neutrals) versus $M^2(\pi^+\pi^- +\text{neutrals})$, show in Fig. 8 for peripheral events only, clearly demonstrates the preference for η^0 masses among the 960 events. The

TABLE I. $\Lambda^0\pi^+\pi^+\pi^-\pi^-\pi^0$ mass combinations.

Number of $(\pi^+\pi^-\pi^0)$ combinations with $M^2(3\pi) = 0.282-0.322$ $(\text{BeV}/c^2)^2 \approx (\eta^0 \text{ mass})^2$	Expected from $\eta^0\pi^+\pi^-$ hypothesis	Expected from 5π hypothesis	Number observed	Number of standard deviations of disagreement with 5π hypothesis
0	0 ± 1	18.5 ± 2	0 ± 1	6
1	19 ± 2	18 ± 2	18 ± 4	0
2	19.5 ± 2	7 ± 2	21 ± 5	3
3	6 ± 2	1 ± 1	4 ± 2	1
4	0	0	2 ± 1.5	0

effect of background subtraction is shown in Fig. 9(a) where the M^2 (neutrals) spectrum is compared with that from an appropriate control region surrounding the 960 region (defined in Fig. 6). Figure 9 shows two important points. First, the control spectra are consistent with 2π phase space from the $\Lambda^0 4\pi$ reaction, as expected from arguments given in the previous section. Second, if one subtracts an estimated (30%) background contamination from the 960 region using the control-spectrum shape as indicated by the shaded area of Fig. 9, the resulting neutrals spectrum is very well fit by either the hypothesis (α) alone (shown as the solid curve) or the hypothesis[17] $(\alpha)/(\beta) = 6/1$ (shown as the dashed curve).

It is of interest to note that there is a weak indication of a final-state-interaction effect as evidenced by the failure of the $M^2(\pi^+\pi^-)$ spectrum [the 960 MeV/c^2 events shown in Fig. 9] to fit $\pi^+\pi^-$ phase space from $\eta^* \to \eta^0\pi^+\pi^-$. There seems to be a preference for mass values[18] of ≈ 380 MeV/c^2, i.e. a possible π-π "σ en-

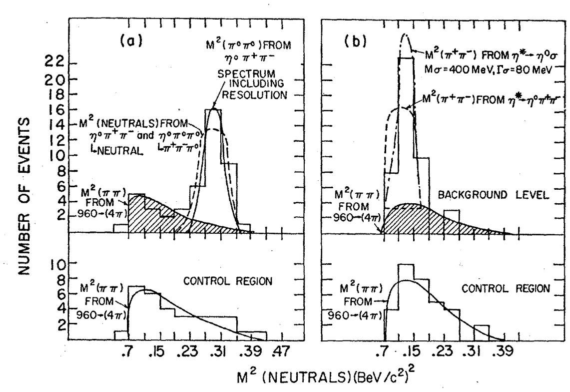

FIG. 9. $M^2(\pi^+\pi^-)$ and M^2 (neutrals) histograms for peripheral $K^-p \to \Lambda^0\pi^+\pi^- +$neutrals events in both the "960" region and in the control region defined in Fig. 6.

[17] If one considers a model for (β) of the type: $\eta^* \to \eta^0 + \sigma^0$; $\eta^0 \to \sigma^0 + \pi^0$, then the neutral mass spectrum $M^2(\sigma^0\pi^0)$ is essentially flat over the range 500–600 MeV/c^2. Including resolution, the η^0 mass from (α) extends over the same region. Since the latter is dominant for either $I=0$ or $I=1$, there is no possibility of distinguishing a contribution from (β) within the neutrals mass subspectrum. We shall show later that $I=0$ is correct on the basis of other evidence.

[18] N. P. Samios *et al.*, Phys. Rev. Letters **9**, 139 (1962).

hancement" of the type suggested[19] to explain η^0 and τ decay final-state interactions. However, in view of the uncertainties introduced by subtraction and the sample size, no strong conclusions concerning this point can be drawn from the data of Fig. 9. A compilation of all published data consisting of 32 BNL-SYR channel-(3) events and 111 channel-(2) and channel-(3) events from Berkeley and UCLA (containing $\sim 20\%$ background) is shown in Fig. 10. There seems to be no compelling evidence for an appreciable final-state interaction in the total data.

The purely neutral decay mode (5) cannot be further studied at this point. We shall see later, however, that the isospin of the η^* is 0, indicating that the dominant contribution to (5) comes from the chain $\eta^* \to \eta^0\pi^0\pi^0$; $\eta^0 \to$ neutrals.

In addition to the modes (5), (6), and (7) we have searched for 2π, $2\pi+\gamma$, 3π and 4π decay modes in the final states of the reaction channels

$$K^- + p \to \Lambda^0\pi^+\pi^- \tag{10a}$$

$$\to \Sigma^0\pi^+\pi^- \tag{10b}$$

$$\to \Lambda^0\pi^+\pi^-\pi^0 \tag{10c}$$

and

$$\to \Lambda^0\pi^+\pi^-\pi^+\pi^-, \tag{10d}$$

respectively. There is no indication of any 2π, 3π or 4π mode; however, significant evidence for the existence of

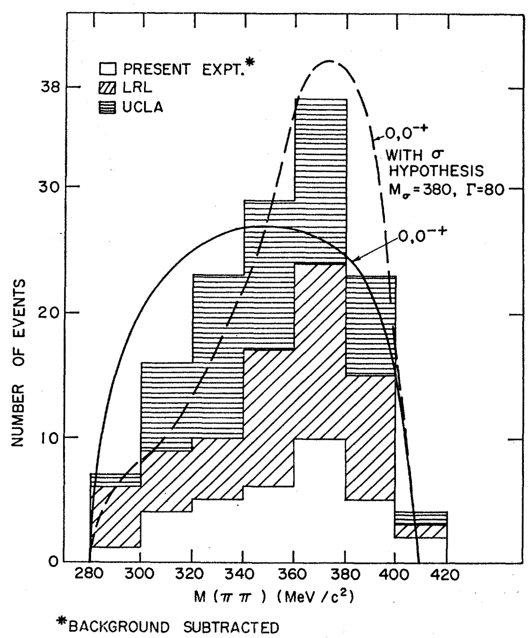

FIG. 10. Combined $M(\pi^+\pi^-)$ histogram for 143 $K^-p \to \Lambda^0\eta^*$ events for $\eta^* \to \eta^0\pi^+\pi^-$.

[19] See, for example, the summary of such final state interaction effects by L. Brown and P. Singer, Phys. Rev. Letters **8**, 460 (1962); D. Berley *et al.*, *ibid.* **10**, 114 (1963). Also see F. Crawford *et al.*, *ibid.* **11**, 564 (1963); L. Brown and P. Singer, Phys. Rev. **133**, B812 (1964); and R. Dell Fabbro *et al.*, Phys. Rev. Letters **12**, 674 (1964).

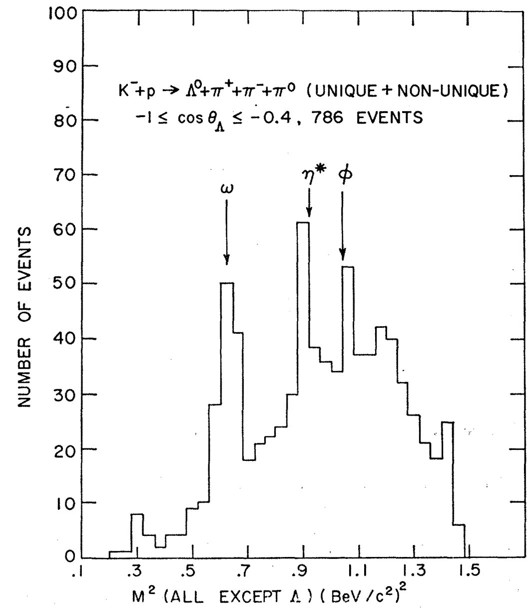

FIG. 11. $M^2(\pi^+\pi^-\pi^0)$ histogram for 786 peripheral, unique and non-unique, $K^-p \to \Lambda^0\pi^+\pi^-\pi^0$ events.

$\pi^+\pi^-\gamma$ mode was found. Details of this search are described below.

Initially all "two-prong plus V" events were kinematically tested only for the hypothesis 10(a), 10(b), and 10(c); the $\Lambda^0\pi^+\pi^-\gamma$ hypothesis was ignored. It was found that 85% of the events were consistent with one or more of 10(a)–(c), the remaining 15% having a large neutral missing mass ($\gtrsim 2m_{\pi^0}$), constituting the (unfitted) reaction (3) sample. The results of this kinematic analysis led us to subdivide the *fitted* events into 2 groups: (i) events consistent with either 10(a), 10(b) or both, (appropriate for the $\eta^* \to 2\pi$ search). (ii) events which uniquely fit 10(c) or were ambiguous among 10(c) and 10(a) and/or 10(b), (appropriate for the $\eta^* \to 3\pi$ search). It must be emphasized, however, that $\Lambda^0\pi^+\pi^-\gamma$ final states might be hidden in either category. A study of the M^2 (all except Λ^0) versus $\cos\theta_\Lambda$ scatter plot of type (i) events (Fig. 24, Sec. IIIB) revealed no significant peaking at 960 MeV/c^2 for peripheral events, from which we estimate the upper limit of the $(\eta^* \to 2\pi)/(\eta^* \to \eta^0\pi^+\pi^-)$ branching ratio to be $\lesssim 10\%$.

On the other hand, a study of the mass spectrum of the type (ii) events (see Fig. 11), revealed a significant peaking at 960 MeV/c^2 for peripheral events. Subsequent study showed that almost all the presumed η^* events were, in fact, contained within a subsample of type (ii) in which the 2π effective mass lay within the ρ band (768 ± 50 MeV/c^2), as one can see in Fig. 12. On the basis of the above-mentioned selection criteria for type (ii) events, the 960 enhancement could represent either a $\rho\pi$ or a $\rho\gamma$ mode[20] of the η^*. An attempt to choose

[20] We ignore the remote possibility of a significant contribution due to $\eta^* \to \rho\pi^0\gamma$, on the grounds of simple phase-space estimates.

TABLE II. Search for η^* decays.

Total BNL-SYR events used in search	K^-p final state used in search	η^*-Decay final state	Number events	Branching/ ratios BNL-SYR	Berkeley[a] +UCLA[b] and this experiment
900	$\Lambda^0\pi^+\pi^-$ $\Sigma^0\pi^+\pi^-$	2π	...	<0.10	<0.07
1900	$\Lambda^0\pi^+\pi^-\pi^0$	3π	...	<0.15	<0.07
110	$\Lambda^0\pi^+\pi^-\pi^+\pi^-$	4π	...	<0.15	<0.01
...	...	6π	...	...	<0.01
415	$\Lambda^0\pi^+\pi^-$+neutrals; $m_{\text{neutrals}}>m_{\pi^0}$	$\pi^+\pi^-$+neutrals; $\eta^0\pi^+\pi^-$ and/or $\eta^0\pi^0\pi^0$	39 ± 10	0.4 ± 0.1	$0.4\ \pm0.05$
1277	Λ^0+neutrals	all neutrals	32 ± 12	0.3 ± 0.1	0.28 ± 0.05
43	$\Lambda^0\pi^+\pi^-\pi^+\pi^-\pi^0$	$\pi^+\pi^+\pi^-\pi^-\pi^0$ $(\eta^0\pi^+\pi^-)$	10 ± 3	0.1 ± 0.04	0.12 ± 0.02
399	all $\Lambda^0\pi^+\pi^-\pi^0$	$\pi^+\pi^-\gamma$	20_{-10}^{+6}	0.2 ± 0.1	0.20 ± 0.06
2000	all V^0+2 prong	$e^+e^-\pi^0$, $e^+e^-\eta_0$	...	<0.3	...

[a] Reference 12. [b] Reference 13.

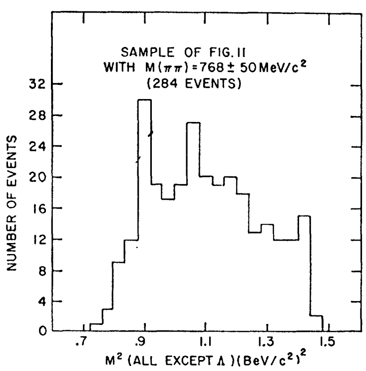

FIG. 12. $M^2(\pi^+\pi^-\pi^0)$ histogram for peripheral, unique and nonunique $K^-p\rightarrow\Lambda^0\pi^+\pi^-\pi^0$ events where $M(\pi\pi)=768\pm50$ MeV/c^2.

between $\rho\pi$ and $\rho\gamma$ on the basis of further kinematic analysis, i.e. a comparison of the fits to the $\Lambda^0\pi^+\pi^-\pi^0$ versus the $\Lambda^0\pi^+\pi^-\gamma$ hypothesis proved fruitless. However, the two alternatives can be distinguished by studying the frequency of η^* in $\rho^\pm$, and ρ^0 subsamples separately. If the $\eta^*\rightarrow\rho\pi$ hypothesis were valid, one would expect the η^* to appear in each of these distributions; on the other hand, if $\eta^*\rightarrow\rho^0\gamma$ were correct, one would expect an η^* enhancement to appear only in the ρ^0 distribution. The latter expectation is supported by the experimental distributions shown in Fig. 13 (peripheral events only). Moreover, when the η^* events are characterized as $\Lambda^0\pi^+\pi^-MM$, their MM spectrum peaks very close to zero in agreement with the $\rho^0\gamma$ hypothesis. After correcting for background effects,[21] we find that the number of $\eta^*\rightarrow\rho+\gamma$ events is 20 ± 5, corresponding to a branching ratio relative to $\eta^*\rightarrow\eta\pi\pi$ of 1/5. This ratio is consistent with an earlier estimate[11] based upon a somewhat different subsample of "$\Lambda3\pi$" final states, and in excellent agreement with that of other groups.[12,13] The existence of a $\rho\gamma$ decay mode of the η^* plays an essential role in the determination of its quantum numbers.

Finally, we report a search for the modes

$$\eta^*\rightarrow e^+e^-\pi^0\,, \tag{11a}$$

and/or

$$\eta^*\rightarrow\eta^0e^+e^-\,, \tag{11b}$$

as the result of suggestions by Bernstein *et al.*[22] and Feinberg[23] that such modes may be appreciable if there exists a medium-strong C-violating interaction. From the measured momentum of all "V^0+2 prong" events, the mass of the recoiling system was calculated. An event was accepted as a candidate if the latter was 960 ± 35 MeV/c^2. All such candidates which had already been fit to 10(a)–(10(d) were then refit to 11(a) or 11(b). There were *no* events which fit either 11(a) or 11(b) uniquely. For ambiguous events it is in principle possible to remove the π-electron ambiguity only if the charged prong has momentum ≤200 MeV/c. All seven events with this characteristic turned out to be pions. Estimating the efficiency[24] of the search as 30%, this corresponds to an upper limit for the branching ratio $[\eta^*\rightarrow e^+e^-+(\pi^0 \text{ or } \eta^0)]/[\eta^*\rightarrow \text{all modes}]$ of the order of 3%.

The results of our search for all decay modes of the η^* are summarized in Table II and combined with rates reported by other groups.

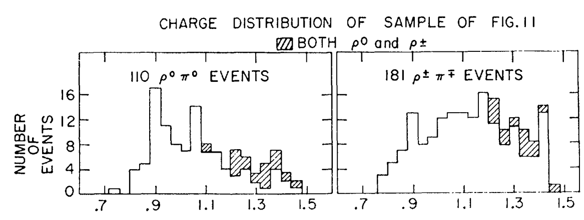

FIG. 13. $M^2(\rho^0\pi^0)$ and $M^2(\rho^\pm\pi^\mp)$ histogram for peripheral, unique and nonunique, $K^-p\rightarrow\Lambda^0\pi^+\pi^-\pi^0$ events where $M(\rho)=768\pm50$ MeV/c^2.

[21] We have made this study both with and without the $Y_1^*(1385)$ events which constitute 50% of the $\Lambda3\pi$ final state and find the same effect within statistical limitations.

[22] J. Bernstein, G. Feinberg, and T. D. Lee, Phys. Rev. **139**, B1650 (1965).

[23] G. Feinberg, Phys. Rev. **140**, B1402 (1965).

[24] This efficiency represents fraction of the e^+ and/or e^- laboratory momentum spectrum below 100 MeV/c, i.e., the momentum below which electrons are clearly recognizable. The theoretical spectrum is obtained by rough numerical integration and scaling of the matrix elements for the equivalent $\eta^0\rightarrow\pi^0+e^++e^-$ decay given in Refs. 22 and 23.

3. *Properties of the* η^*

To obtain the best values of mass and width, we take advantage of the known production and decay characteristics of the η^* to select a sample whose mass spectrum will have relatively little background. This sample is required to satisfy the following criteria: (i) $\cos\theta_\Lambda$ must lie between -1.0 and -0.6 (see Figs. 4, 5, 6); (ii) For channel (3) events $M(\text{neutrals})=550\pm50$ MeV/c^2; (iii) For channel (2) events $M(\pi^+\pi^-\pi^0)=550\pm25$ MeV/c^2; (iv) For channel (1) events, only those with M(neutral) greater than the ω^0 mass are accepted. Aside from its inherent purity, this sample affords the advantage of better mass resolution because it contains only peripheral Λ's which emerge slowly in the laboratory system. The mass histogram of this selected sample is shown in Fig. 14. The solid curve represents our estimation of the background. Also included is a Gaussian ideogram of events in the region of the "960" peak and the experimental resolution function for these events.[25] These are shown as the solid and dashed curves in the insert of Fig. 14, respectively. The best values of the mean mass and experimental width are

$$M=959\pm3\ \text{MeV}/c^2,\quad \Gamma_{\text{obs}}=25\pm5\ \text{MeV}/c^2.$$

As is seen from Fig. 14, the experimental width of the η^* is consistent with that of the resolution function. From this we estimate the true width $\Gamma_{\text{rue}}<15$ MeV/c^2 and is consistent with zero. These values are in excellent agreement with the observations of other groups[11,12] and lead to "world average" values

$$M=958\pm1\ \text{MeV}/c^2,\quad \Gamma<4\ \text{MeV}/c^2.$$

We now consider possible quantum number assignments of the η^*, starting with the G parity. Let us first assume that G is $+1$. With this assumption, the $\eta^0\pi^+\pi^-$ decay is G-allowed. The relatively small observed width

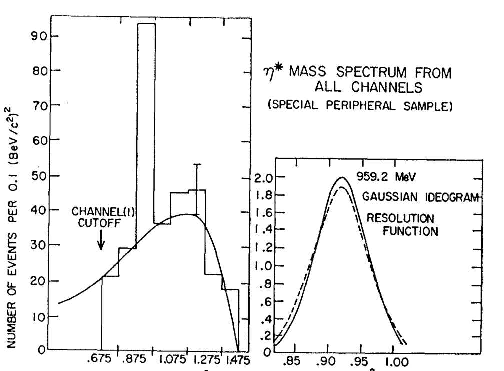

FIG. 14. η^* mass spectrum from all channels for a special peripheral sample (see text), with Gaussian ideogram and superimposed resolution function shown at the right.

[25] The Gaussian ideogram of the experimental resolution function has been obtained by multiplying the error of each individual event by $\sqrt{2}$ and summing over the events in the "960" peak region.

TABLE III. Predicted η^*-decay rates assuming $G=+1$ ($J^P=0^-$).

η^* decay channel	Predicted	Observed
5π	0.13 ($\eta^0\pi^+\pi^-$)	0.12 ± 0.02
$\pi^+\pi^-$+neutral(s), $M>m_{\pi^0}$	0.46 ($\eta^0\pi\pi$)	0.4 ± 0.06
all neutral	0.21 ($\eta^0\pi^0\pi^0$)	0.28 ± 0.06
4π	~0	<0.01
Subtotal	0.8	0.8
$\pi^+\pi^-\gamma$	~0.25	0.2
		100%

of the $\eta^*(\Gamma<15\ \text{MeV}/c^2)$ is entirely consistent with this hypothesis. Neglecting barriers and taking an interaction radius of $M_{\eta^0}^{-1}$, we find $(\eta^*\to\eta^0\pi\pi)\approx10$ keV. This is, of course, only a consistency argument. The rate is very sensitive to the choice of radius—it increases to 10 MeV, if one takes M_π^{-1}. The important consequence of the $G=+1$ hypothesis is that the 3π mode is forbidden.[26] Moreover, *all* observed decay rates are in agreement with estimates based on phase space and the known η^0 decay rates. Detailed comparison is given in Table III. On the other hand, if we assume $G=-1$, the 3π model is G-allowed for all permissible J^P values, and its expected dominance is in significant disagreement with the observed upper limit to its relative rate (see Table II). Similarly, with $G=-1$, $\eta^0\pi\pi$ decay would be G forbidden; thus its existence must be attributed to the electromagnetic interaction giving a rate $\approx\alpha^2$, while $\pi^+\pi^-\gamma$ decay would occur (for all permissible J^P) values with a rate $\approx\alpha$. Ignoring barriers, we estimate[27] $(\eta^*\to\rho^0\gamma)/(\eta^*\to\eta^0\pi\pi)\approx5\times10^3$, and find that this predominance persists even if we assume two-body phase space corresponding to a "σ enhancement" for the denominator and 3-body phase space for the numerator. In spite of the obvious criticism that no simple phase-space estimate (nor, at this stage even a detailed model) can be trusted to within an order of magnitude, we conclude that the $\eta^*\to\eta^0\pi\pi$ decay is strong, i.e., that $G=+1$, since the discrepancy between the observed and estimated $\pi^+\pi^-\gamma$ rate is almost 4 *orders of magnitude.*

Next, we turn to the isospin (I) of the η^*, which we know to be either 0 or 1 on the basis of isospin conservation in the reaction (4). Some direct evidence against $I=1$ comes from a null result in a search for a charged counterpart of the η^* in the production channel $(\Sigma^\pm\eta^{*\mp})$. However, the amplitude could be too small to detect within our limited sample (150 events). Fortunately, conclusive evidence on I is furnished indirectly by the existence of a $\rho\gamma$ decay mode. The exist-

[26] This ignores the possibility of a new selection rule which is specially designed to forbid 3π decay. Such a rule has recently been proposed by J. B. Bronzan and F. E. Low, Phys. Rev. Letters **12**, 522 (1964). We note, however, that the "A-parity" suppression is not relevant here because both the 3π and $\eta^0\pi\pi$ modes consist of 3 pseudoscalars with $A=-1$, so *both* are suppressed (allowed) simultaneously if the η^* is assigned $A=+(-1)$.

[27] This estimate is based on the formulas given in R. H. Milburn, Rev. Mod. Phys. **27**, 1 (1955). We note that the ratio is independent of the choice of interaction radius since both numerator and denominator are 3-body final states.

ence of this mode requires the charge-conjugation quantum number to be +1 and thus the well-known relation $G=Ce^{I\pi}$ for neutral bosons, requires $I=0$. With $I=0$, the all neutral decay mode of the η^* is presumably predominantly due to the chain $\eta^* \to \eta^0\pi^0\pi^0$; $\eta^0 \to$ neutrals. The observed relative neutral rate given in Table II suggests, in fact, that $\eta^* \to \eta^0\pi^0\pi^0$ is the only source of the neutral mode. Knowledge of I considerably simplifies the investigation of possible spin-parity assignments of the η^*.

To investigate possible J^P assignments, we turn now to an analysis of the Dalitz plot data representing all available $\eta^0\pi^+\pi^-$ decays. This data consists of 102 events[28] from channels (2) and (3) which satisfy restrictive selection criteria, as follows: (i) The appropriate M^2 spectra must lie within the η^* acceptance band *and* the peripheral acceptance region; (ii) for channel (2) events, the mass combination closest to the η^0-mass acceptance band (550 ± 25 MeV/c^2) is chosen for the plot. Under these circumstances the wrong mass choice is made in $\sim$13 of the 45 events. In addition, we estimate that the sample contains four ($\Lambda 5\pi$) background events; (iii) for channel (3) events, M(neutrals) lies within ±25 MeV/c^2 of the η^0 mass for the 26 Berkeley events and ±50 MeV/c^2 for the 31 BNL-SYR events. A private communication from Berkeley indicates that their sample contains "no" background, The BNL-SYR sample contains $\lesssim5$ phase-space background events and 5 $\eta^0\pi^0\pi^0$ background events if $I=0$ is correct.

From these considerations we estimate that of the 102 events the background contributions consists of somewhere between 17 and 27 events. These events are shown in Fig. 15, plotted in terms of the Dalitz coordinates:

$$x=\left(\frac{T_+-T_-}{Q}\right)\left(\frac{M+2m}{M}\right)^{1/2},\quad y=\left(\frac{M+2m}{m}\right)\left(\frac{T_3}{Q}\right)-1,$$

where m, m, M, T_+, T_-, T_3 are the masses and kinetic energies of the π^+, π^- and η^0, respectively. The coordinates are a generalization of those used in τ-decay analysis,[29] appropriately normalized to avoid interpretive complications due to the finite-mass spread of the η^*. Since the point density is symmetric[30] to the interchange of π^+ and π^-, the plot has been folded about the y axis. The I, J^P dependence of the Dalitz plot density (i.e. the square of the η^*-decay matrix element), is analyzed below.

We describe the $\eta^0\pi^+\pi^-$ final state in terms of the usual systems, i.e. a dipion ($\pi^+\pi^-$) with relative momentum $\mathbf{q}$ and relative angular momentum $\mathbf{L}$, together with the η^0, characterized by its momentum $\mathbf{p}$ and angular momentum $\mathbf{l}$ in the over-all center-of-mass system (c.m.s.). Given that $I=0$, for each spin-parity assignment of the decaying η^*, straightforward application of isospin, angular momentum and parity conservation along with Bose symmetry restrictions for the dipion system yields certain permissible combinations of l and L. The *simplest* of all these possibilities (for $I=0$ and J values less than 3) are listed in the second column of Table IV. All assignments lead to unique matrix elements with the exception of $(0,2^-)$ which has two equally low-lying states $(L,l)=(0,2)$ or $(2,0)$ and thus involves an arbitrary parameter, b/a, representing the $(L=0)/(L=2)$ ratio. As in τ decay, it is convenient to describe the behavior of the Dalitz plot density by means of the θ dependence ($\cos\theta=\mathbf{p}\cdot\mathbf{q}$) and momentum dependence, given in Table IV. The simplest nonrelativistic matrix elements $M(\mathbf{q},\mathbf{p},\theta)$ consistent with the (L,l) dependences described above, and their appropriate spin-parity assignments are listed in the third column of Table IV.

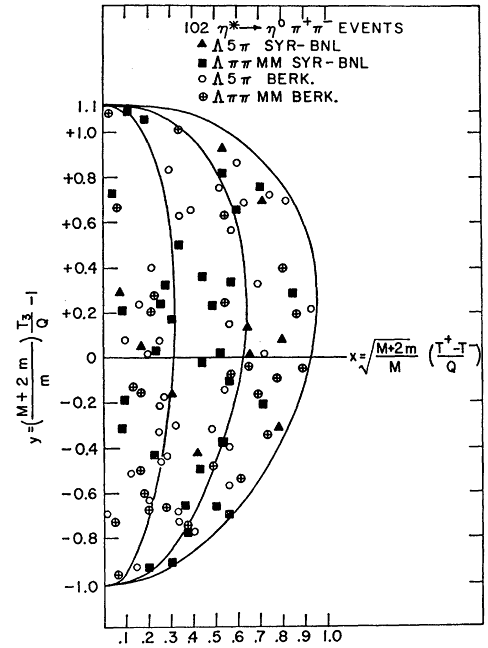

FIG. 15. Dalitz plot for 102 $\eta^* \to \eta^0\pi^+\pi^-$ decays for special sample. (See text.)

The variations in y and θ are compared with various theoretical distributions in Figs. 16(a) and 16(b). Before we draw conclusions from this analysis, we wish to point out that there are several potential sources of error whose effects are difficult to assess. In the first place, the background contamination is nontrivial; moreover, the density distribution of this contamination is unknown (we assume that it is given by phase space). Second, measurement errors have been ignored; this is of particular importance for (7) events where the η^0 mass spread is large. Finally, we have ignored final

[28] These consist of 31 channel-(3) and 10 channel-(2) events from this experiment, together with 26 channel-(3) and 35 channel-(2) events from Ref. 12.

[29] R. Dalitz, Phil. Mag. 44, 1068 (1953).

[30] This symmetry follows from assumed invariance under C. The validity of the latter assumption has been recently questioned by J. Bernstein *et al.*[22] Experimentally, there is no indication for a C-violating asymmetry.

TABLE IV. $I=0$ η^* decay matrix elements.

J^P	Simplest L, l	$M(\mathbf{q},\mathbf{p})$	$M^2(q,p)$ momentum dependence	$M^2(\theta)$ angular dependence
0^+	...	Forbidden	...	...
0^-	0, 0	1	1	1
1^+	0, 1	$\mathbf{p}$	p^2	1
1^-	2, 2	$(\mathbf{q}\cdot\mathbf{p})(\mathbf{q}\times\mathbf{p})$	q^4p^4	$\sin^2\theta\cos^2\theta$
2^+	2, 1	$(\mathbf{q}\times\mathbf{p})_\alpha q_\beta+q_\alpha(\mathbf{q}\times\mathbf{p})_\beta$	q^4p^2	$\sin^2\theta$
2^-	$\begin{cases}0, 2\\2, 0\end{cases}$	$\begin{matrix}a p_\alpha p_\beta\\ b q_\alpha q_\beta\end{matrix}$	$\|a\|^2p^4+\|b\|^2q^4+3\,\mathrm{Re}\,ab^*p^2q^2(\cos^2\theta-\frac{1}{3})$	

state interactions which are known to be non-negligible in the case of such similar decays as η^0 and τ.

In spite of the uncertainties contributed by these effects, the density distribution for all the assignments (I,J^P) except $(0,0^-)$ and $(0,2^-)$ disagree so markedly with the data that they may be rejected with a high degree of confidence. On the basis of statistical errors only, analysis yields χ^2 probabilities considerably less than 0.1% for all the assignments[31] except the two listed above. Because of the arbitrary parameter occurring in the $(0,2^-)$ distribution, only its extreme limits can be comfortably ruled out. Both $(0,0^-)$ and $(0,2^-)$ (with $b/a\sim 3$) are in good agreement with the data. These conclusions are essentially unaffected if a σ final-state interaction is included according to the method of Brown and Singer.[19] Figure 17 shows a typical reasonable ($J=0$) fit obtained for σ mass ≈ 380 MeV/c^2 and width ~ 100 MeV/c^2.

Finally, we note that (in principle) information on the η^* spin-parity can be obtained from its decay angular distribution. The extreme peripherality of η^* production certainly suggests the importance of one particle exchange with a concomitant possibility of strong spin alignment. The folded distribution of the angle between the normal to the η^* decay plane and the incoming K^- direction in the η^* rest frame is shown in Fig. 18 for a selected sample of our data and the UCLA

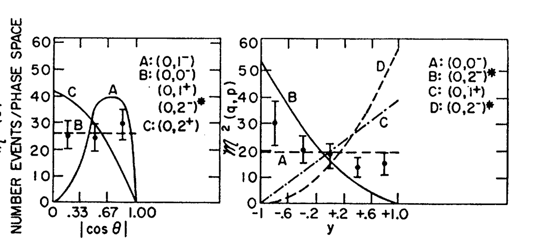

*(FOR 0,2⁻ ONLY LIMITING CASES ARE SHOWN $\left(\frac{L=2}{l=2}\right)$>>1 OR<<1)

FIG. 16. (a) and (b) angular and momentum dependences of the simplest squared η^* matrix elements compared with the theoretical nonrelativistic predictions. See Table IV. Background has been subtracted from experimental points.

sample.[13] The combined distribution is consistent with isotropy, as expected[32] for $J^P=0^-$. Of course the data do not uniquely require 0^-; they can be made consistent with the 2^- distribution,[33]

$$W_2(\theta)=7+5(1-2|b/a|^2)(1+\rho_{00})P_2(\theta)+(5|b/a|^2+1)(5\rho_{00}-2)P_4(\theta),$$

for an appropriate choice of the density matrix element ρ_{00} and polarization parameter $|b/a|$.

Although no unique conclusive results emerge from the above spin-parity analyses, one is certainly led to favor the 0^- hypothesis. First, there is the obvious point that 2^- is almost impossible to rule out because of the arbitrary parameters involved in its distributions. Second, in order to fit the 2^- hypothesis to the Dalitz plot data, one must assume that the dipion angular momentum is dominantly $L=2$ which is not in keeping with the $(L=0)$ σ hypothesis. Finally, the observed $\rho\gamma/\eta\pi\pi$ decay ratio is in agreement with rough expectations if no barriers are assumed in the $\eta\pi\pi$ system, i.e. if $J=0$. In contrast, when appropriate spin 2 barriers are included, the expected ratio would be

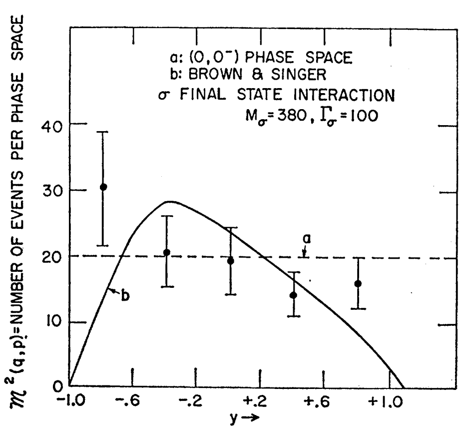

FIG. 17. $J=0$ fit to y distribution for (a) no final state $\pi\pi$ interaction and (b) Brown and Singer final state $\pi\pi$ interaction.

[31] Additional evidence against $(0,2^{++})$ comes from the fact that 2π decay is allowed for this assignment. The observed upper limit to the 2π decay rate is 2 orders of magnitude less than the values estimated from phase space. Also, additional evidence against all $I=1$ possibilities is provided by the observed Dalitz plot densities. This evidence is discussed in Ref. 11.

[32] There is some indication of enhancement near $\cos\theta\approx 0$. As pointed out by Jackson (Ref. 33), absorption effects certainly alter the effective density matrix elements and could conceivably lead to apparent anisotropy.

[33] K. Gottfried and J. D. Jackson, Nuovo Cimento, 33, 309 (1964); K. Gottfried and J. D. Jackson, Phys. Letters 8, 144 (1964).

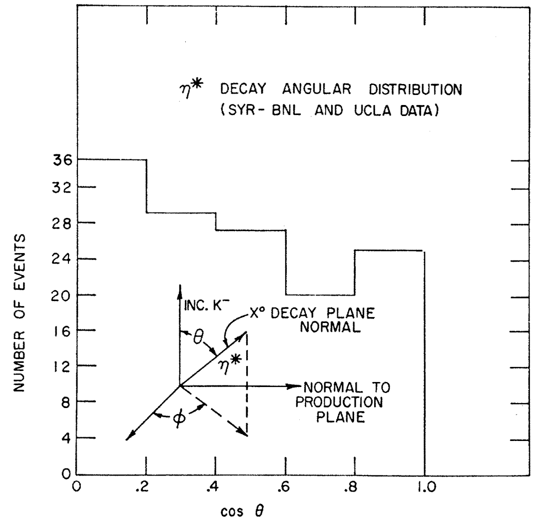

FIG. 18. Combined η^*-decay polar angular distribution.

markedly increased. If these arguments are considered together with the positive evidence for 0^- obtained from a Dalitz plot study of the $\rho\gamma$ mode carried out by the Berkeley Group,[12] the 0^- hypothesis must be strongly favored.

4. *Production Characteristics*

In order to obtain a sample of η^*'s which is unbiased with respect to production angle, we make use of mass and decay-mode information in the two channels with relatively little background. The angular distribution of events in channels (2)+(3) which lie within the 960 band of Figs. 5, 6 and also satisfy M (presumed η^0 decay products)$=550\pm50$ MeV/c^2, is shown in Fig. 19. As noted previously, the evident peripherality of the distribution suggests the importance of one-meson exchange. For J^P values of 0^- or 2^- the only possibility is K^* exchange.

As usual for high-energy interactions, the simple K^*-exchange model does not predict sufficient peaking, but presumably this is due to the omission of absorption effects.[33] No theoretical calculation of these effects has been carried out, but it is known[33] that they can be simulated by a phenomenological form factor of the form $[(\alpha^2-m_\pi^2)/(\alpha^2-\Delta^2)]^2$ where Δ^2 is the momentum transfer. Reasonable agreement can be obtained with a fit of this form as shown in Fig. 19 for $\alpha^2=0.13$ (BeV/c^2).^{2}

5. *Discussion*

It is interesting to speculate as to the role which the η^* would play in various theories of strongly interacting particles. Within the framework of SU_3,[34] if the $(0,0^-)$ assignment is verified,[35] the η^* can be accommodated as a mixture of unitary singlet and octet states along with the η^0, forming a pseudoscalar nonet. In analogy to the situation in the vector meson octet, where one must invoke ω-ϕ mixing,[36] one might expect η^*-η^0 mixing. However, since the observed η^0 mass is within 3% of the octet mass formula,[37] the mixing must be small. One finds, in fact, a mixing angle of $\approx 12°$. Although small, such mixing may lead to appreciable effects in the η^* electromagnetic decay rates (as has been emphasized by Dalitz and Sutherland).[38] Within the framework[39] of $SU(6)$ the η^* may be accommodated within a one-dimensional representation, whereas the pseudoscalar octet is in the 35-fold representation. Dalitz has shown[38] that the observed mixing is compatible with the limits set by the $SU(6)$ theory.

Other generalizations of $SU(3)$ have led to the expectation of more than one η^*-type meson.[40,41] No evi-

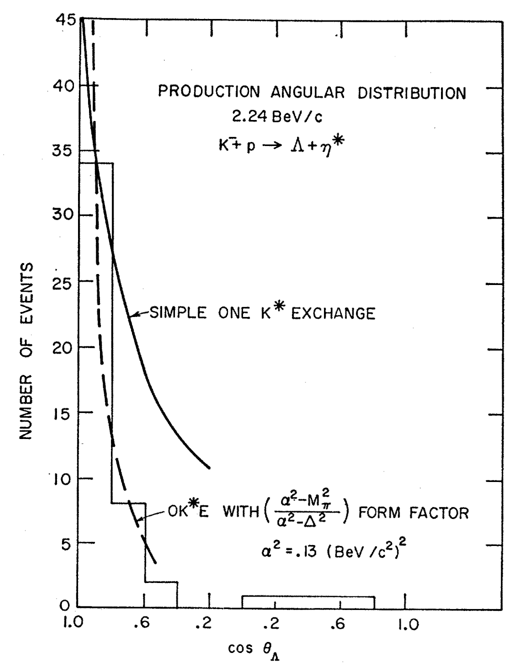

FIG. 19. η^*-production angular distribution with simple one-K^*-exchange fit and modified one-K^*-exchange fit.

[34] M. Gell-Mann, in *The Eight-Fold Way*, edited by M. Gell-Mann and Y. Ne'eman (W. A. Benjamin, Inc., 1964), p. 11; Y. Ne'eman, Nucl. Phys. **26**, 222 (1961).

[35] If the remote possibility $(0,2^-)$ should prove to be correct, the η^* presumably would herald the existence of a new unitary multiplet.

[36] J. J. Sakurai, Phys. Rev. Letters **9**, 472 (1962); S. Okubo, *Proceedings of the Athens Conference on Recently Discovered Resonant Particles*, edited by B. A. Munir and L. J. Gallaher (Ohio University, Columbus, Ohio, 1963), p. 193.

[37] M. Gell-Mann (Ref. 34) and S. Okubo, Progr. Theor. Phys. (Kyoto) **27**, 949 (1962). Using the K, $\bar{K}$ and pion masses as input, one predicts the singlet mass to be 567 MeV/c^2.

[38] R. H. Dalitz and D. G. Sutherland, Nuovo Cimento **37**, 1777 (1965).

[39] F. Gürsey and L. A. Radicati, Phys. Rev. Letters **13**, 173 (1964); F. Gürsey, A. Pais, and L. A. Radicati, *ibid.* **13**, 399 (1964).

[40] H. Bacry, J. Nuyts, and L. Van Hove, Phys. Rev. Letters **12**, 285 (1964).

[41] K. T. Mahanthappa and E. C. G. Sudarshan, Phys. Rev. Letters **14**, 163 (1964).

dence for additional mesons of this type in the mass range 850–1400 MeV/c^2 has been found.

B. The ϕ Meson

In this section we discuss evidence pertinent to the existence of a 1020-MeV $K\bar{K}$ resonance and the determination of its properties. The resonance, known as the ϕ meson, has been found to have isospin 0, spin 1, negative G parity, and negative parity.

1. Existence

The evidence for the existence[42–44] of the ϕ comes primarily from effective-mass studies in the following reaction channels:

$$K^{-}+p\rightarrow\Lambda^{0}+K^{0}+\bar{K}^{0} \tag{12}$$

$$\rightarrow\Lambda^{0}+K^{+}+K^{-} \tag{13}$$

$$\rightarrow\Sigma^{0}+K^{+}+K^{-}. \tag{14}$$

The number of events satisfying preliminary selection criteria[45] in each sample is 85, 59, and 14, respectively. Since the samples come from different fiducial volumes and different combinations of data runs, the numbers are not directly comparable.

The Dalitz plot of $\Lambda^0K^+K^-$ events is shown in Fig. 20 with the effective mass distributions in $M^2(K^+K^-)$, $M^2(\Lambda^0K^+)$ and $M^2(\Lambda^0K^-)$ exhibited separately.[46] While no significant departures from phase space are seen in the Λ^0K^+ and Λ^0K^- mass plots, there is a pronounced peak at 1020 MeV/c^2 in the K^+K^- effective mass plot.

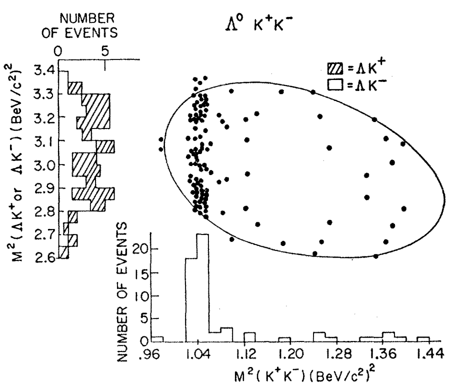

FIG. 20. Dalitz plot and effective-mass projections for the reaction $K^-p\rightarrow\Lambda^0K^+K^-$. Each event appears twice in the plot, but only once in the projections.

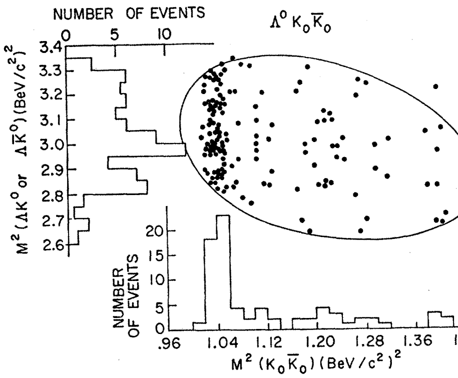

FIG. 21. Dalitz plot and effective-mass projections for the reaction $K^-p\rightarrow\Lambda^0K^0\bar{K}^0$. Each event appears twice in the plot but only once in the projections.

This enhancement is also observed in the $\Lambda^0K^0\bar{K}^0$ sample,[47] shown in Fig. 21, as well as the $\Sigma^0K^+K^-$ sample, shown[46] in Fig. 22. The number of events above background in the 1020 MeV/c^2 peaks of Figs. 20, 21, and 22 are 37, 35, and 7, respectively. Considering the small background levels, these numbers conclusively establish the existence of the reactions:

$$K^{-}+p\rightarrow\Lambda^{0}+\phi \tag{15}$$

$$\rightarrow\Sigma^{0}+\phi, \tag{16}$$

where the ϕ subsequently decays via the modes,

$$\phi\rightarrow K^{0}+\bar{K}^{0}, \tag{17a}$$

$$\phi\rightarrow K^{+}+K^{-}. \tag{17b}$$

Problems connected with sample selection, event identification and background contamination in the (Λ^0 or Σ^0)$K\bar{K}$ final states are discussed below.

First, we consider the criteria used to select the $\Lambda^0K^0\bar{K}^0$ sample. All such events are contained, of course, within four different topological classes according to the number of V^0's which decay visibly in the chamber. Those with no visible V^0's, being undetectable, are ignored. With one exceptional class, events with one visible V^0 cannot be positively identified, and are thus omitted from the $\Lambda^0K^0\bar{K}^0$ sample. The exceptional class, namely $\Lambda^0+\phi$ final state in which the Λ^0 decays visibly, can be detected in the channel Λ^0+neutrals (as described previously in the η^* discussion). Such events are not suitable for establishing existence or properties because the systematic uncertainties involved in distinguishing them from the large background of $\Lambda^0+n\pi^0$ final states vitiates the small statistical gain which could result if they were included. Such single Λ^0 events are used only to obtain rough information on decay rates. Thus, the sample of Fig. 21, and that used in subsequent analyses pertinent to the

[42] L. Bertanza *et al.*, Phys. Rev. Letters **9**, 180 (1962).
[43] P. Schlein *et al.*, Phys. Rev. Letters **10**, 368 (1963).
[44] P. Connolly *et al.*, Phys. Rev. Letters **10**, 371 (1963).
[45] These preliminary criteria produce essentially pure samples of $\Lambda^0K^+K^-$ and $\Sigma^0K^+K^-$ but are not sufficient to remove a small $\Sigma^0K^0\bar{K}^0$ contamination from (12). Final selection criteria will be discussed shortly.
[46] To symmetrize the distribution between (+) and (−) charges, we represent each event by 2 points on the plot. However, the ordinate scale for the $\Lambda^0K^\pm$ is adjusted to properly indicate the observed number of events.

[47] Since the K^0 and $\bar{K}^0$ are indistinguishable, each event is plotted twice, but the scale is again adjusted to reflect the true number of events.

determination of quantum numbers consists only of events in which either two or three V^0's decay visibly. We employ no fiducial cutoff for such events. Since only two events of the $3V^0$ variety were observed, we need only consider background problems for the $2V^0$ configurations.

In this group we classify reactions which can simulate $\Lambda K^0\bar{K}^0$ into four groups; reactions in each group present similar problems:

$$K^-+p\rightarrow\Xi^0+K^0;\quad \pi^-+p\rightarrow\Lambda^0+K^0(+\pi^0);\quad \pi^-+p\rightarrow K^0+\bar{K}^0+N,\qquad \text{(i)}$$

$$\pi^-+p\rightarrow\Lambda^0+K^0+n\pi^0;\quad \pi^-+p\rightarrow K^0+\bar{K}^0+N+n\pi^0,\ (n\geqslant 1),\qquad \text{(ii)}$$

$$K^-+p\rightarrow\Xi^0+K^0+\pi^0,\qquad \text{(iii)}$$

$$K^-+p\rightarrow\Sigma^0+K^0+\bar{K}^0.\qquad \text{(iv)}$$

Owing to the difference in neutral missing mass between $\Lambda^0K^0\bar{K}^0$ and the hypotheses of group (i), the latter are easily distinguished by our χ^2 and ionization criteria. On the other hand, group (ii) events are not so easily distinguished from $\Lambda^0K^0\bar{K}^0$. However, the absence of any appreciable number of the identifiable final states $\Lambda^0K^0\pi^+\pi^-(\pi^0)$ or $K^0\bar{K}^0p\pi^-(\pi^0)$ indicates that group (ii) contamination is negligible (less than 2 events). The number of $\Xi^0\pi^0K^0$ final states can be estimated from a study of the $\Xi^-\pi^+K^0$ channel. We find that of the 7 events expected, in which the K^0 and Λ^0 are visible, *5* were identified on the basis of missing mass and the fact that the visible Λ^0 did not come from the production origin.

Thus the only significant source of background in the $\Lambda K^0\bar{K}^0$ sample is due to the $\Sigma^0K^0\bar{K}^0$ reaction. As we shall see later, the majority of $2V^0$ events consist of one Λ^0 and one K_1^0. Although $\Sigma^0K^0\bar{K}^0$ final states of this type cannot be kinematically fit, their presence can be detected in the neutral missing-mass spectrum of events with a visible Λ^0 and K^0. Here the real $\Lambda^0K^0\bar{K}^0$ events have a missing mass of 498 ± 13 MeV/c^2 while the $\Sigma^0K^0\bar{K}^0$ events have masses from 530 to 620 MeV/c^2. On the basis of the data shown in Fig. 23, we conclude that a missing-mass cut at 535 MeV/c^2 separates the Λ^0

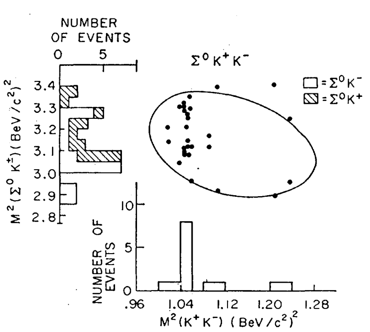

FIG. 22. Dalitz plot and effective-mass projections for the reaction $K^-p\rightarrow\Sigma^0K^+K^-$. Each event appears twice in the plot but only once in the projections.

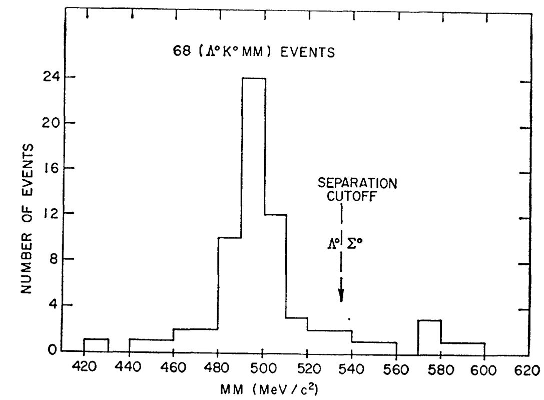

FIG. 23. Missing-mass (MM) spectrum for the hypothesis Λ^0K^0MM of 68 events which fit $\Lambda^0K_1K_2$. (*One event is omitted because of large error).

from Σ^0 events with a very small cross contamination, yielding[48] a sample of 60 $\Lambda^0K^0\bar{K}^0$ events.

Next we discuss the charged kaon channels (13) and (14). Because of severe competition from other modes, candidates for (13) and (14) are used only if the Λ^0 decays visibly. For the "two-prong+V^0" topology the principle sources of potential background are the reactions: $K^-+p\rightarrow(\Lambda^0 \text{ or } \Sigma^0)\pi^+\pi^-(\pi^0)$, $K^-+p\rightarrow\Xi^0K^+\pi^-$ and $\pi^-+p\rightarrow(\Lambda^0 \text{ or } \Sigma^0)K^+\pi^-(\pi^0)$. In practice (with 3 exceptions), kinematic fitting and ionization information resulted in unambiguous separation of these reactions from the $K^-+p\rightarrow(\Lambda^0 \text{ or } \Sigma^0)K^+K^-$ reaction. Thus the only source of ambiguity is between the $\Lambda^0K^+K^-$ and $\Sigma^0K^+K^-$ final states. The 8 ambiguous fits were unraveled by means of a missing mass study analogous to that used in the $\Lambda^0K^0\bar{K}^0$ channel, which indicated that most of these[49] are really $\Lambda^0K^+K^-$. On this basis, we assign seven of the events to the $\Lambda^0K^+K^-$ channel and one to the $\Sigma^0K^+K^-$ channel. This completes our discussion of those $Y^0K\bar{K}$ channels of immediate interest. For purposes of subsequent analysis, it is sometimes necessary to restrict the sample to that obtained in data runs I and II which are completely analyzed. Appropriate members are summarized in Table V. Here all corrections due to ambiguity have been made so that the numbers are directly comparable,

TABLE V. Observed numbers of events after corrections for ambiguities.

Data runs	$\Lambda^0K^0\bar{K}^0$	$\Lambda^0K^+K^-$	$\Sigma^0K^+K^-$	$\Sigma^+K^-K^0$	$\Sigma^-K^+\bar{K}^0$	$\Sigma^0K^0\bar{K}^0$
I & II	34	55	9	2	5	6
III	42	4	5	1	5	6
Total	76	59	14	3	10	12

[48] In addition to these $\Sigma^0K^0\bar{K}^0$ events, others in which two K_1^0's or all $3V^0$'s decay visibly can be detected by direct kinematic fit with essentially no background problem. Three such events were found and are included in Fig. 22.

[49] Note that the attempted fit to $\Lambda^0K^+K^-$ employs 4 constraints while the $\Sigma^0K^+K^-$ fits use only 2 constraints. It is reasonable that the looser criteria should permit accidental ambiguity.

except for neutral decay corrections and (very small) differences in fiducial acceptance criteria.

Evidence for the existence of a meson resonance provided by the $Y^0K\bar{K}$ channels has been corroborated by Schlein *et al.* of UCLA.[43] Other groups[50] have reported a wide enhancement in the $K_1{}^0K_1{}^0$ system at a mass of 1 BeV/c^2. This $K_1{}^0K_1{}^0$ enhancement is clearly unrelated to the ϕ on the basis of the observed widths and differences in decay modes (the ϕ, as we shall see later, decays via the $K_1{}^0K_2{}^0$ mode).[51]

2. Decay Modes

In addition to the $K\bar{K}$ decay modes (3) and (4) discussed above, we have searched for indication of 2π, 3π, 4π, 5π, and electromagnetic decay modes such as $\pi^0\gamma$, $\eta\gamma$, $\rho\gamma$ and $\omega\gamma$. Fairly reliable evidence for a 3π or to be more exact, a $\rho\pi$ decay mode was found; all other searches led to null results with varying degrees of reliability.

The procedures used in the ϕ-decay-mode search are similar to those described in the discussion of η^* decay modes. Since the $\phi\to K\bar{K}$ events are produced preferentially peripherally[52] (see Fig. 26), we use a momentum-transfer criterion ($\cos\theta_\Lambda\leq -0.4$) as well as effective-mass information to select the ϕ sample. Further details are given below.

The "2-prong+V^0" events known to be kinematically consistent with either $\Lambda^0\pi^+\pi^-$ and/or $\Sigma^0\pi^+\pi^-$, i.e. with low neutral missing mass, are appropriate for the 2π mode search. Since $\Lambda^0\pi^+\pi^-\gamma$ final states may well be hidden among this group, it also provides information on a possible $\pi^+\pi^-\gamma$ mode. The plot of effective masses M^2 (all except Λ^0), and in particular that of the peripheral subsample shown in Fig. 24, gives no significant indication of peaking at 1020 MeV/c^2. On this basis we estimate the upper limit of the relative 2π to $K\bar{K}$ branching ratio to be ~ 0.2. Similar studies of the channels $\Lambda^0\pi^+\pi^-\pi^+\pi^-$, $\Lambda^0\pi^+\pi^-\pi^+\pi^-\pi^0$ and $\Lambda^0\pi^+\pi^-$+neutrals of mass $\gtrsim 2m_{\pi^0}$ reveal no indication of 4π, 5π, $\pi^+\pi^-\gamma$, $\omega\gamma$ etc. modes (see Figs. 5, 6, 7 of Sec. IIIA). Neutral counterparts of the above modes in addition to the possible modes $\pi^0\gamma$, $\eta^0\gamma$, $\eta^0\pi^0$ etc., would appear in the Λ^0+neutrals channel. Unfortunately, because the statistics are so limited, and because the experimental resolution happens to be considerably poorer here than it is in the η^* case, this technique yields no significant information. For the sake of calculating branching ratios, we shall simply assume[53] that all the candidates of Fig. 12, IIIA are examples of $\phi\to\rho\pi$.

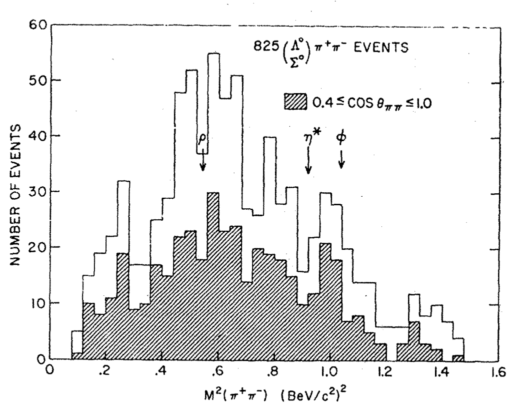

FIG. 24. Effective mass for all 825 events consistent with (Λ^0 or Σ^0)$\pi^+\pi^-$. The shaded insert shows the peripheral subsample.

The above study was carried out including all events regardless of $\Lambda^0\pi^+$ effective mass. It was also carried out with the $Y_1{}^*(1385)^+$ events removed and (within statistical limitations), all previous conclusions remain unaltered. Thus, we use the entire sample of Fig. 12 (Sec. IIIA) from which to obtain the $\rho\pi$ branching ratio. Allowing for: (i) fiducial region, neutral decay and different momentum transfer; (ii) systematics of background subtraction; and (iii) the finite width of the ρ meson, we find

$$(\phi\to\rho\pi)/(\phi\to K\bar{K})=0.3\pm 0.15.$$

This is consistent with values quoted previously[42,54] based upon partial samples of the data, and compares favorably with the ratio of 0.22 ± 0.09 recently reported by Lindsey and Smith.[55]

3. Properties of the ϕ

To determine the mass and width of the ϕ, we use only the $(\Lambda^0,\Sigma^0)K^+K^-$ sample. The Σ^0 contamination is removed on the basis of missing mass studies as described earlier, yielding a pure sample of 59 $\Lambda^0K^+K^-$ events, of which 41 lie in the ϕ region. (The charged K sample provides most of the information on mass and width since its inherent mass resolution is ~ 3 MeV/c^2 compared with ~ 8 MeV/c^2 for the neutral sample.) The mass spectrum of the pure sample was fitted[56] to a Breit-Wigner curve, with the experimental resolution

[50] G. Alexander *et al.*, Phys. Rev. Letters **9**, 460 (1962); A. R. Erwin *et al.*, *ibid.* **9**, 34 (1962).

[51] Thus, the ϕ and the K_1K_1 enhancement have opposite C.

[52] Since 65% of ϕ production is contained within the production angular interval $0.4<\cos\theta_\phi<1.0$, we use the latter interval as our peripheral criterion here.

[53] As we shall see later with the quantum numbers of the ϕ established as $J^{PG}=1^{--}$ and $C=-1$, the $\rho\pi$ mode is presumably strong (G allowed) while the $\rho\gamma$ mode presumably is forbidden ($C=+1$). It has been recently suggested, however, that a $\rho\gamma$ mode may exist as the result of a semistrong C-violating interaction [T. D. Lee (private conversation)]. Thus, one may consider the possibility of both modes existing simultaneously. Since the presumed $\rho\pi$ mode is observed to be anomalously small, the latter possibility is enhanced.

[54] P. L. Connolly *et al.*, *Proceedings of the Sienna Conference on Elementary Particles, 1963*, edited by G. Bernardini and G. P. Puppi (Societa Italiana di Fisica, Bologna, 1963), p. 130.

[55] J. S. Lindsey and G. A. Smith, Bull. Am. Phys. Soc. **10**, 502 (1965).

[56] The general fitting technique is described in detail in the thesis of G. W. London, Rochester University, 1964 (unpublished). In the particular case of the ϕ, we used a modified version of this technique, which utilizes only the resonance portion of the spectrum.

folded in. Adequate fits are obtained for mass values in the range 1020 ± 2 MeV/c^2 and natural widths of $\Gamma=6\pm4$ MeV/c^2. The errors include our estimates of possible systematic uncertainties.[57] The above values are in good agreement with other determinations.[43,58] Since the width appears to be nonzero,[58] we shall assume that the ϕ decay is mediated primarily by a strong interaction.

We turn now to a discussion of the ϕ, beginning with its charge-conjugation number (C). Determination of C rests upon the observation by Goldhaber *et al.*[59] that a $K^0\bar{K}^0$ system can decay strongly into the $K_1^0K_1^0$ and $K_2^0K_2^0$ mode if $C=+1$, but only into the $K_1^0K_2^0$ mode if $C=-1$. In the ϕ mass region the division of $K^0\bar{K}^0$ final states into the $(K_1^0K_1^0)$, $(K_2^0K_2^0)$ and $(K_1^0K_2^0)$ modes can be ascertained on a statistical basis using the $[(K_1^0\rightarrow \text{neutral})/(K_1^0\rightarrow\text{charged})]$ branching ratio.[60] If we label the detectable topological configurations of the $\Lambda^0K^0\bar{K}^0$ sample by the visible V^0's as follows: $\Lambda^0K_1K_1$, Λ^0K_1, K_1K_1, then we can predict[61] their *relative* rates on the basis of either the $C=+1$ or $C=-1$ hypothesis. These predictions are compared with the observed rates in Table VI. The results conclusively establish $C=-1$ for the ϕ meson.

TABLE VI. Predicted and observed relative rates for different topological types of channel (1) on basis of charge conjugation.

Topological type of Channel (1)	Predicted relative rates $C=-1$ $(\Lambda^0K_1K_2)$	$C=+1$ (ΛK_1K_1) $(\Lambda^0K_2K_2)$	Observed relative rates for events in peak
$(\Lambda^0$ or $\Sigma^0)K_1K_1$	0	0.4	0 ± 0.04
$(\Lambda^0$ or $\Sigma^0)K_1$	1	0.4	1 ± 0.2
K_1K_1	0	0.2	0 ± 0.04

With the usual assumption of Bose symmetry for the $K\bar{K}$ system,[62] the operations of charge conjugation and spatial inversion are identical, so the ϕ parity must be negative. This in turn means that the ϕ spin must be odd, the most likely values being $J=1$ or 3.

We have determined the ϕ spin using two methods. The first of these[63] involves a comparison of the K_1K_2 and K^+K^- decay rates, the ratio of which is sensitive to the assumed spin. If p_{12} and $p_\pm$ are the center-of-mass momenta of the K_1K_2 and K^+K^- decays, then the branching ratio may be written[64] in the form:

$$\beta_1=\frac{\varphi\rightarrow K_1K_2}{\varphi\rightarrow K^+K^-}=C_1\left(\frac{p_{12}}{p_\pm}\right)^3\left[\frac{p_\pm^2+m^2}{p_{12}^2+m^2}\right],\ \text{for } J=1, \quad (18)$$

$$\beta_3\approx C_3\left(\frac{p_{12}}{p_\pm}\right)^7\left[\frac{225m^2+45p_\pm^2}{225m^2+45p_{12}^2}\right],\quad \text{for } J=3. \quad (19)$$

Here C_J is a small Coulomb correction (4% for $J=1$ and 3% for $J=3$), and m^{-1} is the interaction radius. It may be emphasized that for any reasonable interaction radius, $m\gtrsim 2m_\pi$, the value of β_J is essentially given by the spin-dependent term. Moreover, the value of β_J is sensitive to J because $(p_{12}/p_\pm)$ differs from unity (owing to the K^0, K^+ mass difference and the small available energy). For $m=2m_\pi$, $p_\pm=125$ MeV/c and $p_{12}=107$ MeV/c, we calculate[65] for the related ratio α_J:

$$\alpha_J=\frac{\varphi\rightarrow K_1K_2}{(\varphi\rightarrow K_1K_2)+(\varphi\rightarrow K^+K^-)}\begin{matrix}=0.39 \text{ for } J=1\\ =0.26 \text{ for } J=3.\end{matrix} \quad (20)$$

Comparing this with the observed value of $\alpha_{\mathrm{EXPT}}=0.44\pm0.07$, one sees that $J=1$ is favored by ~2.5 standard deviations. This result is in agreement with that of the UCLA group[43] who use the same technique.

The second method of determining the ϕ spin makes use of the theorem due to Wigner[66] relating the sum of the reduced channel widths γ_α to the interaction radius m^{-1}:

$$\textstyle\sum_\alpha \gamma_\alpha=3m^2/2\mu\,, \quad (21)$$

where μ is the reduced mass of the $K\bar{K}$ system. The reduced widths γ_α are related to the observed width Γ_α according to[67] $\Gamma_\alpha=2(p_\alpha/m)v_{J,\alpha}\gamma_\alpha$, where p_α is the c.m. momentum and $v_{J,\alpha}$ is a spin-dependent angular-momentum barrier factor discussed in the previous determination. It follows from (21) that

$$\Gamma\leq(3m/\mu)(\textstyle\sum_\alpha B_\alpha/p_\alpha v_{J,\alpha})^{-1}\,, \quad (22)$$

where $B_\alpha=\Gamma_\alpha/\Gamma$ is the branching ratio of the channel α. Evaluating this for the channels $\alpha=(K^+K^-)$ and $(K^0\bar{K}^0)$ assuming $m=2m_\pi$ and using the barrier factors

[57] To check our mass resolution against systematic errors, we studied the $M(\pi^-p)$ distribution from identified Λ^0's, which, of course, are known to have a "zero" width and Q value close to φ decay. The control distribution (fitted with a Gaussian) gave $M_{\Lambda^0}=1115.5\pm0.5$ MeV/c^2 and Γ_{true} consistent with 0.

[58] N. Gelfand *et al.*, Phys. Rev. Letters **11**, 438 (1963).

[59] M. Goldhaber, T. D. Lee, and C. N. Yang, Phys. Rev. **112**, 1796 (1958).

[60] We use the ratio $(K_1\rightarrow 2\pi^0)/(K_1\rightarrow \text{all decays})=\frac{1}{3}$. See F. S. Crawford, *Proceedings of the 1962 International Conference on High Energy Physics*, edited by J. Prentki (CERN, Geneva, 1962), p. 836.

[61] As pointed out earlier, the one visible V^0 topology of the $\Lambda^0+\phi$ final state has been estimated at 10 ± 4 events (over a background of 40). This number is in agreement with the 8 expected on the basis of the $C=-1$ hypothesis and in significant disagreement with the 24 expected from the $C=+1$ hypothesis. If the 10 ± 4 events in the 1020 Mev/c^2 peak contained a small contribution from another mode, the disagreement would become even more marked.

[62] That this is a nontrivial assumption has been emphasized by O. Greenberg and A. Messiah, Phys. Rev. **136**, B238 (1964).

[63] J. J. Sakurai, Phys. Rev. Letters **9**, 472 (1962).

[64] We assume, of course, that K_1K_2 and K^+K^- decay are characterized by identical coupling constants and interaction radii.

[65] These values are entirely insensitive to the choice of m provided $m\gtrsim2m_\pi$. For example, if $m=m_K$, we find $\alpha_1=0.38$ and $\alpha_3=0.26$.

[66] E. P. Wigner, Am. J. Phys. **17**, 99 (1949). We use $n=1$ throughout the paper.

[67] J. M. Blatt and V. F. Weisskopf, *Theoretical Nuclear Physics* (John Wiley & Sons, New York, 1952), p. 383 ff.

TABLE VII. Summary of φ decay rates.

Mode	Rate relative to total $K\bar{K}$
K^+K^-	0.59 ± 0.07
$K^0\bar{K}^0(K_1K_2)$	0.41 ± 0.07
$\rho\pi$	$0.3\ \pm0.15$
$\pi\pi$	<0.2 (90% confidence)
4π	<0.2 (90% confidence)
5π	<0.1 (90% confidence)
neutrals (aside from $K^0\bar{K}^0$)	<0.2 (90% confidence)

$v_{J,\alpha}$ of (18), (19) together with the branching ratios of Table VII, we find[68]

$$\Gamma\leq 58\ \text{MeV}/c^2 \quad \text{for } J=1$$

and

$$\Gamma\lesssim 10^{-3}\ \text{MeV}/c^2 \text{ for } J=3.$$

Since the best experimental value of Γ is 3 ± 1 MeV/c^2, the $J=3$ inequality is violated by about 3 standard deviations, while the $J=1$ inequality is well satisfied. These results taken together with the previous decay-rate analysis[69] and the UCLA study provide convincing evidence that the spin of the ϕ is $J=1$, and the ϕ is a vector particle.[70]

We turn now to the discussion of the remaining quantum number, the isospin I. From the existence of the 2-body reaction (15), we know only that the isospin of the ϕ must be either 0 or 1. However, we have obtained direct evidence against $I=1$ from a study of the $\Sigma K\bar{K}$ channels listed below

$$K^-+p\rightarrow\Sigma^0+K^++K^- \qquad (23)$$

$$\rightarrow\Sigma^++K^0+K^- \qquad (24)$$

$$\rightarrow\Sigma^-+K^++\bar{K}^0 \qquad (25)$$

$$\rightarrow\Sigma^0+K^0+\bar{K}^0. \qquad (26)$$

The identification of events from the reaction (23) has already been described. The samples from (24) and (25) consist entirely of events in which *two* decays are visible. This class of events is essentially uniquely identified[71] and appropriate numbers are given in Table V. The invariant mass distribution of the $K\bar{K}$ combinations from these three channels are shown in Figs. 22 and 25. The ϕ is clearly present in the $I=0(K^+K^-)$ distribution and apparently absent in the $I=1(K^0K^-)$ or $(K^+\bar{K}^0)$ distributions.

[68] The choice of m is not critical to the conclusion in the text. If $m=m_\pi$, we get $\Gamma\leq80$ ($J=1$) or $\Gamma\leq0.3$ ($J=3$) MeV/c^2. For $m=2m_k$, these become 26 and 10^{-5} MeV/c^2, respectively.

[69] Both methods depend upon the assumption that the spin dependence is properly given by the usual barrier factors. If this assumption is found wanting for some as yet unsuspected reason, both determinations would be open to criticism.

[70] In principle, some information on the ϕ spin is available from the ϕ decay angular distributions. In fact, however, the observed angular distributions show no striking behavior, and may be made consistent with various spin hypotheses for appropriate choices of the density-matrix parameters. See discussion on production characteristics.

[71] Three ambiguous events of the type $\Sigma^-K^+\bar{K}^0$ were apportioned on the basis of their population in the unique samples.

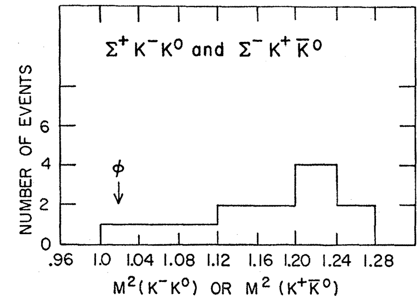

FIG. 25. Effective-mass plot for all unique $\Sigma^+K^-K^0$ and $\Sigma^-K^+\bar{K}^0$ final states.

A quantitative test of the $I=1$ hypothesis may be carried out by examining the charge-independence[72] triangular inequality:

$$2\sqrt{\sigma\begin{bmatrix}\Sigma^0\phi & \\ & \searrow \\ & \text{all } K\bar{K}\end{bmatrix}}\leqslant\sqrt{\sigma\begin{bmatrix}\Sigma^+\phi^- & \\ & \searrow \\ & K^-K^0\end{bmatrix}}+\sqrt{\sigma\begin{bmatrix}\Sigma^-\phi^+ & \\ & \searrow \\ & K^+\bar{K}^0\end{bmatrix}} \qquad (27)$$

From the data of Figs. 22 and 25, correcting for neutral decay and using the ratio (20), one finds that (27) is violated to the extent that

$$9\pm2\leq0\pm3,$$

establishing that the isospin of the ϕ is zero.

Knowing that $I=0$ and $J=1$, the relation $G=(-1)^{I+J}$ applicable to the decay into two spinless bosons, immediately gives $G=-1$. This is consistent with the absence of two-pion decay.[73] On the other hand, one expects a relatively large three-pion, i.e. $\rho\pi$, decay. When we estimate the decay ratio $\delta=(\phi\rightarrow\rho\pi/\phi\rightarrow K\bar{K})$ on the basis of phase space, barrier penetration factors, $m=2m_\pi$ and spin and isospin weights, we find that the ratio expected in the absence of selection rules is $\delta\approx4$. This value is an order of magnitude larger than $\delta_{\text{exp}}\cong0.25\pm0.2$, which is the combined value of our data and the Berkeley data. This discrepancy could be due only to uncertainties in our crude theoretical estimate. If the discrepancy is taken literally, however, it indicates that a special mechanism and/or selection rule is operating to inhibit the $\rho\pi$ decay mode. (This point will be taken up again in the discussion.) Similar remarks apply to the $\pi^0\gamma$ decay mode—here the crudely estimated rate is also about an order of magnitude larger than the observed upper limit.

This concludes our discussion of the properties of the ϕ. Since these properties have some relevance to the

[72] Here we neglect the relatively minor violation of charge independence due to the $K^\pm K^0$ mass difference.

[73] We may estimate the decay rates $(\phi\rightarrow\pi\pi)/(\phi\rightarrow K\bar{K})$ expected in the absence of selection rules forbidding it, on the basis of phase space and barrier penetration factors. For $m\leq2m_\pi$, we find $(\phi\rightarrow2\pi)/(\phi\rightarrow K\bar{K})\gtrsim10$. Since this is 2 orders of magnitude more than the observed upper limit, it indicates the existence of a selection rule, most naturally ascribed to G parity conservation.

subject of kaon permutation symmetry, we digress from our current topic, the ϕ meson, to briefly discuss this question.

4. *Kaon Permutation Symmetry*

As mentioned in the course of our analysis leading to the determination of ϕ properties, one usually assumes that the kaon is a boson in the conventional (Pauli) sense, i.e. that integral spin particles must have a completely symmetric wave function.[74] However, this assumption has been challenged in two independent ways. First, the possibility has been raised[75] that strange particles might have an inverted spin-statistics correlation, e.g. kaons might be fermions. Second, it has been suggested[76] that particles might not obey either Fermi or Bose statistics, but might obey a "mixed statistics." In fact, within the language of field theory, a detailed version of the "mixed" type has been recently developed.[77,78] Since very little direct experimental information on the statistics of strange particles exist,[79] it is worthwhile to note the relevance of our experimental results to the question of kaon statistics, even though they are not conclusive.

We emphasize that this experiment can shed no light on the possibility of mixed statistics for the $K\bar{K}$ system. At most, it can decide between the pure Bose and pure Fermi alternatives (in principle). The argument is given below.

First, as indicated in Sec. IIIB 3, the $K\bar{K}$ system under study here has a charge-conjugation quantum number $C=-1$, independent of any assumptions concerning kaon permutation symmetry. However, the relation between C and $P=(-1)^J$ does depend upon the nature of kaon statistics. It can be shown[79] that $C=(-1)^J$ if kaons are bosons while $C=-(-1)^J$, if kaons are fermions, i.e. odd spin implies Bose statistics. Now, the spin analyses used in Sec. IIIB.3 may be carried out for even spin as well as odd. We find the $J=1$ is favored over $J=2$, but $J=0$ cannot be ruled out. If future experiments are able to eliminate $J=0$ from consideration then, given the choice between pure Fermi and pure Bose statistics, the hypothesis that kaons are bosons would be established. In this connection it is interesting to note that present evidence, evaluated by Gatto[80] using $\bar{p}+p\rightarrow K+\bar{K}$ data, favors the boson hypothesis.

[74] W. Pauli, Phys. Rev. **58**, 716 (1940); G. Luders and B. Zumino, Phys. Rev. **110**, 1450 (1958).
[75] S. Drell, *Proceedings of the Ninth International Annual Conference on High Energy Physics at Kiev 1959* (Moscow, 1960), Vol. II, p. 137 ff.
[76] H. S. Green, Phys. Rev. **90**, 270 (1953).
[77] O. Greenberg and A. Messiah (private communication).
[78] H. Feshbach, Phys. Letters **3**, 317 (1963). This work contains an extended list of references on the subject).
[79] This has been particularly emphasized by O. Greenberg and A. Messiah who pointed out that conclusive evidence exists only for the nucleon, electron, muon, and photon. Although it is known that pions are not fermions, the recent discovery of the reaction $K_2^0\rightarrow\pi^+\pi^-$ (J. H. Christenson *et al.*, Phys. Rev. Letters **13**, 123 (1964)] leaves open the possibility of mixed statistics for the pion.
[80] R. Gatto, Phys. Letters **5**, 56 (1963).

5. *Production Characteristics of the* ϕ

It has been noted throughout our discussion of the ϕ that its production is predominantly peripheral, suggesting the importance of one meson exchange. The differential cross section for the $K^-+p\rightarrow\Lambda^0+\phi$ reaction[81] is shown in Fig. 26. The observed distribution is compared with a realistic version of the one-meson-exchange model suggested by Jackson.[82] The model assumes that the exchanged meson is a kaon (both K and K^* exchange are possible here) and includes $SU(3)$ couplings and initial and final state absorption. The substantial forward enhancement is reasonably well accounted for by the model; it must be emphasized, however, that there are many parameters involved in the comparison, and it is intended only as a semiquantitative guide.

Quite independent of the details of the production mechanism, ϕ decay may be analyzed in terms of the density-matrix formalism of Jackson and Pilkuhn.[83] In the ϕ rest frame, the decay angles[84] of the K^+ (or K^0) from ϕ decay have expected distributions of the form

$$W(\cos\theta)\approx 1+\left(\frac{3\rho_{00}-1}{1-\rho_{00}}\right)\cos^2\theta\,, \tag{28}$$

$$W(\varphi)\approx 1-\left(\frac{4\rho_{1,-1}}{1+2\rho_{1,-1}}\right)\cos^2\varphi\,. \tag{29}$$

The experimental distributions in $\cos\theta$ and ϕ are shown in Fig. 27.[85] The results of fitting the data of Fig. 27 with the distributions (28), (29) are summarized in Table VIII. Also given are the theoretical estimates of the one-kaon-exchange model; agreement with this model is adequate except for the parameter $\mathrm{Re}\rho_{1,0}$. This disagreement is probably not significant in view of the naiveté of the theoretical estimates.

It is worthwhile to note that K^* exchange is allowed for this reaction and is of great importance in other re-

TABLE VIII. Results of best fits for ϕ decay in terms of density matrix elements. See text.

Experiment Sample with $\hat{q}_{K^-}\cdot\hat{q}_\phi>0.4$		Theory K exchange $+$absorption
$1+(0.73\pm0.76)\cos^2\theta$	$\rho_{0,0}=0.46\pm0.10$	$\rho_{0,0}\approx0.4$
$1+(1.08\pm0.98)\cos^2\phi$	$\rho_{1,-1}=-0.18_{-0.08}^{+0.16}$	$\rho_{1,-1}\approx-0.08$
$\frac{-5}{4\sqrt{2}}\langle\sin2\theta\cos\phi\rangle$	$\mathrm{Re}\rho_{1,0}=0.04\pm0.07$	$\mathrm{Re}\rho_{1,0}\approx-0.2$

[81] The shape of the distribution is taken from the relatively uncontaminated channel (12) and (13) events. However, the ordinate scale is adjusted to include the $\rho\pi$ contribution as well.
[82] J. D. Jackson (private communication).
[83] J. D. Jackson and H. Pilkuhn, Nuovo Cimento 33, 906 (1964).
[84] See the diagram of Fig. 18 which defines the equivalent decay angles for η^* decay. The normal $\hat{n}$ of Fig. 18 is replaced in this case by the c.m. momentum of the kaon. The data are folded so that $K^0\bar{K}^0$ events may be added to K^+K^- events.
[85] Here the sample is restricted to events with ϕ production angles of cosine greater than 0.4 since the one-kaon-exchange model is expected to be best here.

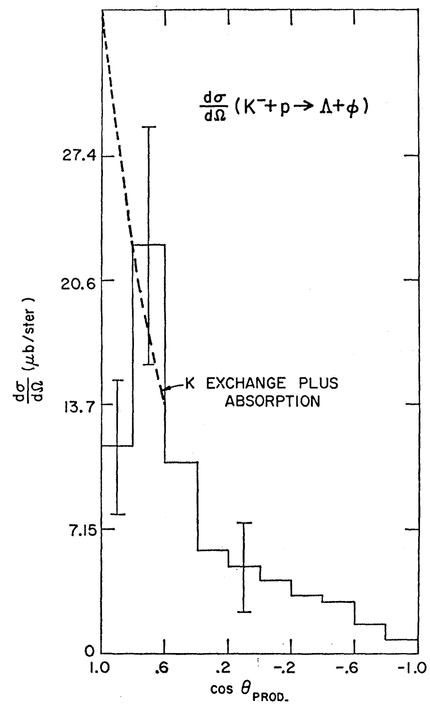

FIG. 26. Production angular distribution for the reaction $K^{-}p\rightarrow\Lambda\phi$.

actions (those which *require* vector meson exchange). Although a theoretical analysis taking into account both K and K^* exchange and absorption effects is certainly possible here, such an analysis is not warranted, in view of the small sample size and the fact that several additional parameters must be introduced.

6. Discussion

The discovery of the ϕ and especially the fact that it has the same quantum numbers as the ω ($J^{PG}=1^{--}$) has played a significant role in the development of $SU(3)$. Both the ω and ϕ may be accommodated in $SU(3)$, one as a unitary singlet and the other as the $I=0$ member of the vector meson octet. However, the experimentally determined masses of neither the ϕ nor the ω satisfy the Gell-Mann–Okubo mass formula which gives 930 MeV/c^2 for the octet member. Gell-Mann,[34] Sakurai,[36] Okubo[36] and others suggested that this circumstance might be due to the mixing of two 1^{--} particles say ϕ_0 and ω_0 which are degenerate in the limit of exact unitary symmetry. The physical particles ϕ and ω would then be linear combinations: $\phi=a\phi_0-b\omega_0$, $\omega=b\phi_0+a\omega_0$, where the mixing parameters, a, b are chosen to satisfy the observed masses and the requirements of the mass formula for the unobserved masses. One finds[86] a mixing angle of $\sim40°$. The ω-ϕ mixing hypothesis also offers a possible explanation of the small $\phi\rightarrow\rho\pi$ decay rate, since (physical) ϕ decay would be governed by a matrix element of the form:

$$|aM(\phi_0\rightarrow\rho+\pi)-bM(\omega_0\rightarrow\rho+\pi)|^2,$$

which may exhibit destructive interference. Of course, other explanations are possible, including the introduction of new quantum numbers and heretofore unsuspected selection rules.[26]

Within the framework of $SU(6)$,[39] the role of the ϕ and ω remain unaltered in the sense that they are accommodated as a singlet and the $I=0$ member of an octet. However, here both the singlet and octet are part of the same (35-fold) representation, so that the degeneracy of the unphysical ϕ_0 and ω_0 is a "natural" consequence of the theory, in contrast to $SU(3)$ where it is fortuitous. Moreover, the mixing angle is *predicted* to be 33° in agreement with the observed angle.

C. The Ξ^* Hyperon and the κ Meson

In this section we discuss our investigation of the three-body Ξ channels which led to the discovery[87–89] of the Ξ^*, a 1530-MeV/c^2 $\Xi\pi$ resonance. This study also yields some supporting evidence for the existence of a ≈730 MeV/c^2 $K\pi$ resonance known as the κ meson.[90] The data provide partial information on the $\Xi^*(1530)$ properties, including masses for the two charge states, isospin and spin. It provides no information on κ properties. No indication of any other new $\Xi\pi$ (or $K\pi$) resonance was found.

1. Existence and Decay-Mode Evidence

The channels of interest here are:

$$K^{-}+p\rightarrow\Xi^{-}+\pi^{+}+K^{0} \quad (30)$$

$$\rightarrow\Xi^{-}+\pi^{0}+K^{+} \quad (31)$$

$$\rightarrow\Xi^{0}+\pi^{-}+K^{+} \quad (32)$$

$$\rightarrow\Xi^{0}+\pi^{0}+K^{0}. \quad (33)$$

The sample consists of *all* events (368) in which the Λ^0 (from Ξ decay) decays visibly, together with a subsample (45 events) of types (30) and (31) in which the Ξ^- decays and the Λ^0 escapes detection. A study of identification and background problems, discussed below, indicates that the sample is quite pure.

When a Λ^0 decays visibly, the Ξ^- final-state topology is ambiguous only with relatively rare configurations containing one charged decay such as $\Lambda^0K^+K^-$ or $\Lambda^0\pi^+\pi^-$. In these cases, χ^2 and ionization information are sufficient to identify unambiguously all candidates. For the subsample of reactions (30) and (31) in which the Λ^0 is not observed, ambiguity with the hypothesis

[86] For a complete discussion see Y. S. Kim, S. Oneda, and J. C. Pati, Phys. Rev. **135**, B1076 (1964).

[87] Bertanza *et al.*, *Proceedings of the International Conference on High Energy Physics, 1962*, edited by J. Prentki (CERN, Geneva, 1962), p. 279.

[88] G. Pjerrou *et al.*, ibid, p. 289 and P. Schlein *et al.*, Phys. Rev. Letters **9**, 368 (1962).

[89] L. Bertanza *et al.*, Phys. Rev. Letters **9**, 472 (1962).

[90] Alexander *et al.*, Phys. Rev. Letters **8**, 447 (1962); D. Miller *et al.*, Phys. Rev. Letters **5**, 557 (1963).

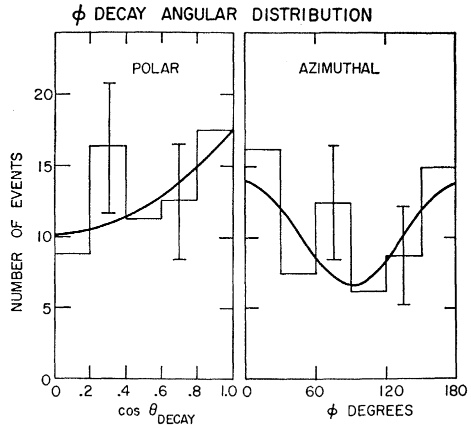

FIG. 27. Decay angular distribution of $\phi \to K\bar{K}$ in the ϕ rest frame for all events in the production-angle region of $+0.4 \leq \cos\theta_\phi \leq 1$.

$\Sigma^-\pi^+MM$ results in a small ($\lesssim$10-event) Σ^- contamination. For channel (32), candidates are accepted only if the Λ^0 is observed and the fit is unique or if the K^+ is clearly identified. This criterion results in the omission of an unknown fraction $\Xi^0K^+K^-$ events, so that the sample is biased as regards branching ratio information. Channel (33) events cannot, of course, be kinematically fit, even if both V^0's decay visibly. A fraction of the latter can be uniquely identified, however, either because the Λ^0 was clearly not associated with production vertex and/or on the basis of missing neutral mass. Out of ten candidates, five were uniquely identified. Because of possible systematic difficulties, this channel gives only rough quantitative information.

The Dalitz plot of the 413-event sample from (30), (31) and (32) is shown in Fig. 28, along with the $\Xi\pi$ and $K\pi$ effective-mass projections. Several indications of structure, both in the $\Xi\pi$ and $K\pi$ system are evident from the plot. First, there is a $\Xi\pi$ enhancement at 1530 MeV/c^2. Second, there is a $K\pi$ enhancement at $\approx$870 MeV/c^2, presumably corresponding to the established $K^*(885)$ resonance. In addition, there is a broad peak in the region $0.5(\text{BeV}/c^2)^2 \leq M^2(K\pi) \leq 0.6(\text{BeV}/c^2)^2$, i.e. in the neighborhood of the (not so well established) κ meson. We shall now consider the significance of this Dalitz plot structure.

The high density ($\approx$140 events over the background) and relatively narrow width of the 1530-MeV/c^2 band strongly suggest the existence of a strangeness-minus-two $\Xi\pi$ resonance, which we call the $\Xi^*(1530)$. The indication is reinforced by the fact that the point density within the Ξ^* band is high throughout the band. In fact, removal of events in the presumed K^* and 730 MeV/c^2 bands leave the resultant $\Xi\pi$ mass spectrum virtually unaltered in shape; the 1530 MeV/c^2 peak remains narrow and $\gtrsim$10 standard deviations above background level. We conclude that the $\Xi^*(1530)$ exists, and accounts for about $\frac{1}{3}$ of the final states (30)–(33), as a result of the reactions

$$K^-+p \to (\Xi^*)^- + K^+ \tag{34}$$

$$\to (\Xi^*)^0 + K^0, \tag{35}$$

where the Ξ^* subsequently decays via

$$(\Xi^*)^- \to \Xi^- + \pi^0 \tag{36a}$$

$$(\Xi^*)^- \to \Xi^0 + \pi^- \tag{36b}$$

and

$$(\Xi^*)^0 \to \Xi^- + \pi^+ \tag{37a}$$

$$(\Xi^*)^0 \to \Xi^0 + \pi^0. \tag{37b}$$

The lack of any further structure in the $\Xi\pi$ mass spectrum is consistent with the absence of other Ξ^*-type resonances with masses in the range $\approx$1575–1800 MeV/c^2. We postpone quantitative estimates of upper limits to such production until the $K\pi$ mass structure has been discussed.

In an attempt to unravel the structure within the $M^2(K\pi)$ spectrum, we may, as a first approximation, compare its shape with that expected[91] from $\frac{1}{3}$ of re-

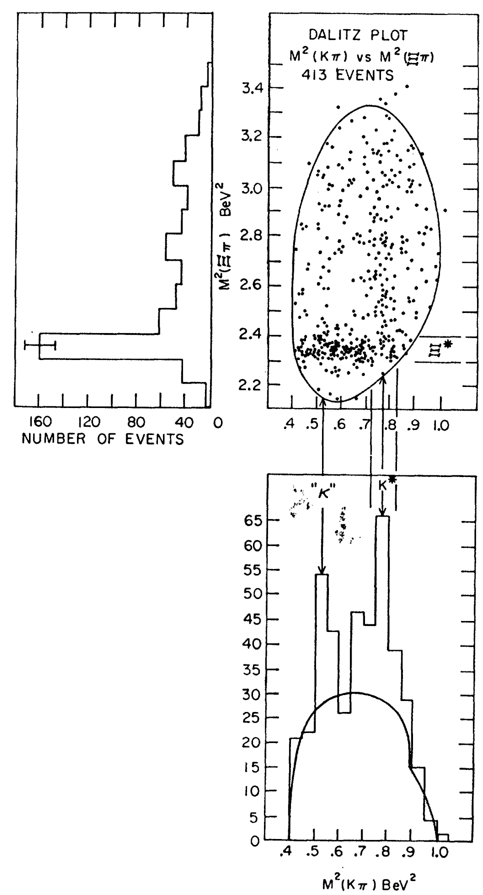

FIG. 28. Dalitz plot for 413 $K^-p \to \Xi\pi K$ events, along with the $M^2(\Xi\pi)$ and $M^2(K\pi)$ projections.

[91] For this purpose it is assumed that the Ξ^* band is uniformly populated—the peculiar shape of the phase-space curve is entirely a kinematic effect.

action (34) plus $\frac{2}{3}$ of reaction (30). As shown in Fig. 28, if one normalizes to the wings of spectrum outside all resonance regions, the presumed K^* peak stands out clearly. We assume then that the K^* peak is real.[92] When viewed in this way, the 730 MeV/c^2 peak also clearly stands out and is a 5-standard-deviation effect.[93] However, the ideogram of $M^2(K\pi)$ (see Fig. 29) makes it evident that the mass and width of the "730" MeV/c^2 peak do not agree with those expected[90] for the κ, namely $M=725\pm5$ MeV/c^2, $\Gamma<12$ MeV/c^2. Since the average experimental mass resolution is only ±8 MeV/c^2, if the peak is really due to the κ, the apparent mass and width discrepancies must be attributed either to interference effects or statistical fluctuations (or both).

There is significant evidence, in fact, that the complete sample of Fig. 28 does not provide a "clean" $K\pi$-mass sample. We note that these data yield the wrong mass and width for the K^*. As illustrated in Fig. 29, one finds $M_{K^*}=864\pm5$ MeV/c^2 and $\Gamma_{K^*}\approx70$ MeV/c^2, in disagreement with the accepted values of 885 ± 5 MeV/c^2 and 45 ± 5 MeV/c^2, respectively. This anomaly is due to events in the smaller shoulder located at $M^2(K\pi)\cong0.685$ (BeV/c^2)^2 of Fig. 29. Further examination reveals that most of these events are situated within the Ξ^* band, as one can see from the $M^2(K\pi)$ spectrum of events in the Ξ^* band, shown[94] in Fig. 30(a). Additional evidence that the *total* $K\pi$ sample is not "clean" comes from the observation of anomalous

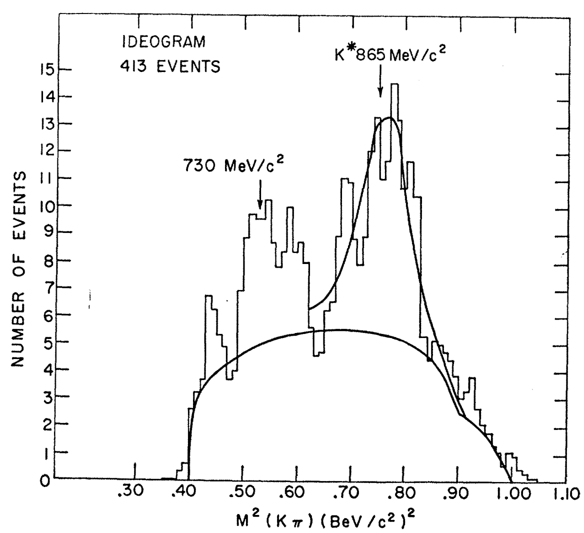

FIG. 29. $M^2(K\pi)$ ideogram for 413 $K^-p\rightarrow\Xi\pi K$ events.

[92] In support of this conclusion we have measured the branching ratio

$$Z=[(K^*)^+\rightarrow K^0+\pi^+]/[(K^{*+}\rightarrow K^0+\pi^+)+(K^{*+}\rightarrow K^++\pi^0)]$$

for events in the K^* band and find $Z=0.69\pm0.14$ in excellent agreement with the accepted ratio of $\frac{2}{3}$.

[93] This estimate does not include obvious systematic uncertainties associated with background estimation.

[94] Fig. 30 shows the densities for the visible Λ^0 sample only (368 events).

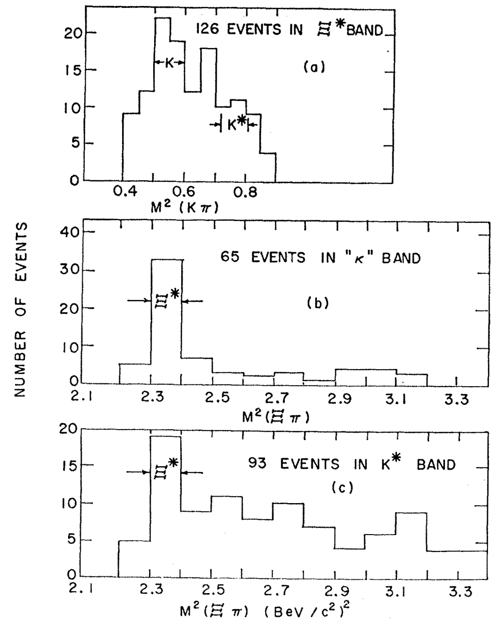

FIG. 30. (a) Projection of the 126 Ξ^* events on the $M^2(K\pi)$ axis. (b) Projection of the 65 "κ" events on the $M^2(\Xi\pi)$ axis. (c) Projection of the 93 K^* events on the $M^2(\Xi\pi)$ axis.

densities in the (Ξ^*-K^*) and (Ξ^*-730) overlap regions (see Fig. 28). From a comparison of the densities of points within the K^*, 730 and Ξ^* bands (Fig, 30), one finds a 1.5 standard deviation depletion in the (Ξ^*-K^*) overlap and a 1.5-standard-deviation excess in the (Ξ^*-730) overlap. We are unable to distinguish between possible interference effects and statistical fluctuations in the overlap regions. However, we hasten to emphasize that for present purposes, it is not the *cause* of the above-mentioned anomalies which is of interest, but only the fact that they exist and complicate the interpretation of the total $K\pi$ mass spectrum of Fig. 28.

In an attempt to obtain a $K\pi$ mass spectrum relatively free from the complications described above, we subtract all events in Ξ^* band [for this purpose, taken to be $2.3(\text{BeV}/c^2)^2\leq M^2(\Xi\pi)\leq2.4(\text{BeV}/c^2)^2$]. An ideogram of this data is shown in Fig. 31. The contrast with the total data of Fig. 29 is evident; the suspected κ enhancement is now centered nearer to the "known" κ mass and is of narrow width. One finds[95] $M(\kappa)\approx730$ MeV/c^2 and $\Gamma\lesssim15$ MeV/c^2 in reasonable agreement with the Berkeley values. Some indication of the reliability of the subtraction technique is afforded by what happens to the K^* peak in this sample. It is encouraging to note that the mass and width of the K^* ($M_{K^*}=875\pm8$ MeV/c^2, $\Gamma\cong40$ MeV/c^2) are now much closer to accepted values. We now summarize our conclusions concerning these resonances.

[95] These values are not significantly changed if one varies the width of the Ξ^* band by $\pm0.2(\text{BeV}/c^2)^2$ on either side of the central value.

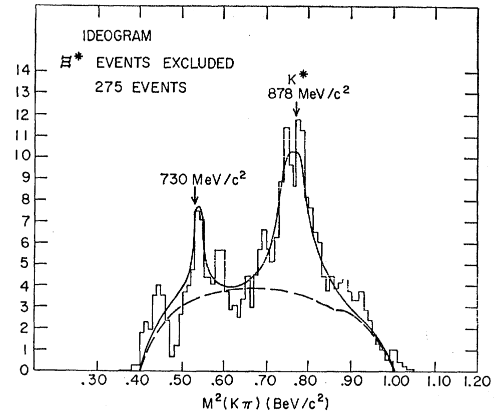

FIG. 31. $M^2(K\pi)$ ideogram for 275 $K^-p \to \Xi\pi K$ events (in arbitrary units) with Ξ^* events excluded.

First, the mass spectra clearly establish that the $\Xi^*(1530)$ exists and that it, and the $K^*(885)$, contribute significantly to the final states studied here. Second, in neither the total data nor any of the subtracted samples is there evidence for additional $\Xi\pi$ resonances. Because of the phase-space cutoffs and the dominance of the 1530 resonance, we believe this result is significant only in the mass region 1550 to 1800 MeV/c^2. In this region we can place an upper limit for Ξ^*-type resonance production of $\approx 3\%$ relative to the $\Xi^*(1530)$. Third, the subtracted mass spectrum of Fig. 31 certainly provides qualitative support[96] for the existence of the κ. However, the uncertainties involved in subtraction and estimation of phase space background make it impossible to assess our evidence quantitatively, and thus prevent any strong conclusions. At best, our results may be considered another link in a chain of observations,[97] each of which are insufficient to establish the κ, but which when taken together do provide strong support for the existence of a κ anomaly in the region of 730 MeV/c^2.[98]

2. *Properties of the* Ξ^*

In order to obtain as pure a sample as possible, from which to determine the mass and width of the $(\Xi^*)^0$ and $(\Xi^*)^-$, we use only those events with a visible Λ^0 *and* with $K\pi$ effective masses outside of the K^* and 730 MeV/c^2 bands of Fig. 28. The $(\Xi^*)^0$ sample is intrinsically better measured than the $(\Xi^*)^-$ sample, the average mass resolution being ≈ 5 MeV/c^2 versus ≈ 13 MeV/c^2. The appropriate mass histograms are shown in Fig. 32(a) and 32(b), respectively. To analyze these data, we assume a Breit-Wigner shape[99] for the resonance, fold in the resolution function and consider the mass, width and number of background events as variable parameters.[100] The χ^2 probabilities for the best $(\Xi^*)^0$ and $(\Xi^*)^-$ fits were 75% and 45%, respectively, yielding the values: $M[(\Xi^*)^0] = 1528.7 \pm 1.1$ MeV/c^2, $M[(\Xi^*)^-] = 1535.7 \pm 3.2$ MeV/c^2, $\Gamma[(\Xi)^0] = 8.5 \pm 3.5$ MeV/c^2. These values substantiate earlier estimates[89] and are in good agreement with those reported by the UCLA group.[88,101] For purposes of later comparison with theory, we note that the mean multiplet mass is 1532.2 ± 2.5 MeV/c^2 and the mass splitting is $\Delta M = M[(\Xi^*)^-] - M[(\Xi^{*0})] = +7.0 \pm 4.0$ MeV/c^2. These results are in agreement with those of the UCLA group.[101]

We turn now to the determination of the isospin (I). Direct information on I is obtained from various production and decay branching ratios. First, if one assumes

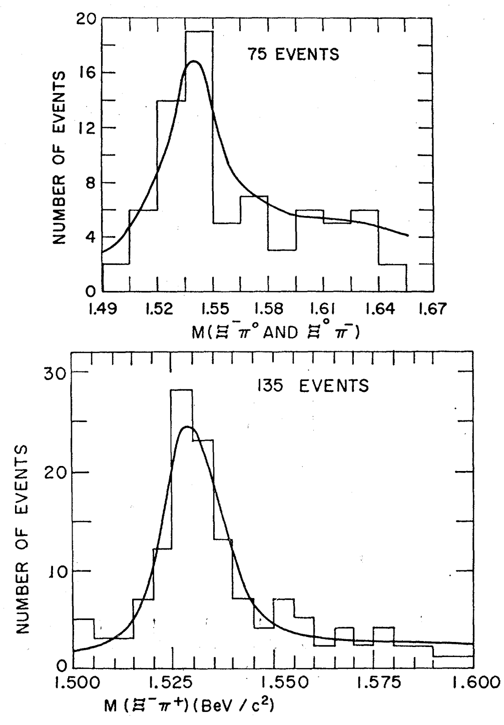

FIG. 32. (a) $(\Xi\pi)^-$-mass histogram of 75 $\Xi^-\pi^0K^+$ and $\Xi^0\pi^-K^+$ events. (b) $(\Xi\pi)^0$-mass histogram of 135 $\Xi^-\pi^+K^0$ events with best fit curve.

[96] Angular-distribution information is of no value here. There is no indication of any special production mechanism such as hyperon exchange which would produce κ's preferentially backwards. Also, mass searches in other channels such as $\bar{K}^0\pi^-p$ give no indication of the κ peak, but this may not be significant in view of the very small cross section for κ production in such channels (see Ref. 97).

[97] In addition to the π^-p experiments in Ref. 90 and 93, "κ peaks" have been seen in K^-p interactions [S. G. Wojicicki *et al.*, Phys. Letters **5**, 283 (1963)] and K^+p interactions [M. Ferro-Luzzi *et al.*, Phys. Letters **12**, 255 (1964)]. However, the original experiment of Ref. 90 has been repeated with increased statistics and the 725 MeV/c^2 peak is now of less significance than originally reported [D. Miller (private communication)].

[98] Alternative explanations of the 730 MeV/c^2 mass anomaly in terms of triangle graphs with logarithmic singularities have been proposed. See Y. F. Chang and S. F. Tuan, Phys. Rev. **136**, B741 (1964); M. Month, Phys. Rev. **139**, B1093 (1965).

[99] Because of the narrow width of Ξ^*, the effect of an angular-momentum barrier on the shape (k^5 dependence) is negligible—the peak would be shifted by less than 1 MeV/c^2.

[100] G. W. London, thesis, University of Rochester, 1964 (unpublished).

[101] G. Pjerrou *et al.*, Phys. Rev. Letters **14**, 275 (1965).

that $I=\frac{3}{2}$, then the ratio

$$R=\begin{matrix}[(\Xi^*)^0+K^0]\\ \searrow\\ \Xi^-+\pi^+\end{matrix}\Bigg/\left\{\begin{bmatrix}(\Xi^*)^0+K^0\\ \searrow\\ \Xi^-+\pi^+\end{bmatrix}+\begin{bmatrix}(\Xi^*)^-+K^+\\ \searrow\\ \Xi^-+\pi^0\end{bmatrix}\right\}$$

is completely determined since the reaction can proceed only through the isotopic spin 1 portion of the K^-p system. Ignoring small mass-difference effects, one expects $R=\frac{1}{3}$ for $I=\frac{3}{2}$, while R is undetermined for $I=\frac{1}{2}$. To obtain a pure sample, we use the following selection criteria: (i) the Λ^0 must be visible, (ii) the Ξ^* must decay into a Ξ^- [channels (30) and (31)], (iii) the $M(K\pi)$ value must be outside of the K^* and 730 MeV/c^2 bands. This sample containing a total of 76 events, yields $R=0.76\pm0.15$ which disagrees with the $I=\frac{3}{2}$ hypothesis by about three standard deviations.[102] Less accurate but significant corroborative evidence is furnished by a study of the relative Ξ^- to Ξ^0 decay rates of each charge state of the Ξ^*. Defining r_1 and r_2 by

$$r_1=\frac{(\Xi^*)^0\to\Xi^-\pi^+}{(\Xi^*)^0\to\Xi^0\pi^0}\quad\text{and}\quad r_2=\frac{(\Xi^*)^-\to\Xi^0\pi^-}{(\Xi^*)^-\to\Xi^-\pi^0},$$

we expect $r_1=r_2=2$ for $I=\frac{1}{2}$ or $r_1=r_2=\frac{1}{2}$ for $I=\frac{3}{2}$. Using the samples involved in the previous analysis along with the equivalent sample of channel (33), (after making corrections for the neutral K^0 branching ratio and rough corrections for kinematic ambiguity and relative scanning efficiencies) we find $r_1\approx3$ and $r_2\approx2$ thus verifying the $I=\frac{1}{2}$ assignment. Both isospin analyses taken together rule out $I=\frac{3}{2}$ by $\gtrsim4$ standard deviations, establishing $I=\frac{1}{2}$ in agreement with earlier conclusions[89] and other determinations.[88]

Finally, we discuss the relevant information pertinent to the Ξ^* spin J. Qualitative information concerning J is provided by the Ξ^* decay angular distributions in the Ξ^* rest frame. In a system where the z axis is taken to be the production plane normal $\hat{N}$, and the y axis is the incoming K^- direction, the distribution in spherical angles (θ,ϕ) of the decay Ξ^- must be isotropic for $J=\frac{1}{2}$, barring interference effects. For a study of this type we use the complete 132 event Ξ^* sample with visible Λ^0's, regardless of $K\pi$ mass. This is done for two reasons. First, as we have noted earlier, the majority of the events in the (Ξ^*-K^*) and/or (Ξ^*-730)MeV/c^2 overlap region are most probably Ξ^*'s. Second, for a fixed $\Xi\pi$ mass the $K\pi$ mass of each event is proportional to the cosine of decay angle with respect to the Ξ^* direction in the Ξ^* rest frame. Thus, omission of events in the overlap regions of Fig. 28 would necessarily bias the angular distribution.

The observed polar and azimuthal distributions for the 132 event sample are shown in Fig. 33. The polar distribution has a χ^2 probability for isotropy of $\approx1\%$ indicating that $J\geqslant\frac{3}{2}$. Before any conclusions can be drawn, however, one must consider the possibility that the observed anisotropy can result from a spin $\frac{1}{2}$ Ξ^* interfering with nonresonant background. Adair[103] has emphasized that such effects are possible with as little as 5–10% of nonresonant amplitude. In order to investigate this possibility, we take note of the fact that the resonant phase must vary rapidly with $M^2(\Xi\pi)$ as one passes through the resonant region, while the phase of the background amplitude is expected to be relatively constant. Under such conditions the decay-angular-distribution anisotropy would be expected to vary considerably with $M(\Xi\pi)$. Experimentally, we find no such $M(\Xi\pi)$ variation of the decay distribution data. Thus, there is no evidence of significant interference phenomena, and we conclude that $J\geqslant\frac{3}{2}$. This result is in agreement with those of the UCLA[104] and Berkeley groups,[105] who find $J^P=\frac{3}{2}^+$ using the method of Byers and Fenster.[106,107]

3. Discussion

It is well-known[108] that a $\Xi\pi$ resonance can be accommodated within a 10-fold representation of $SU(3)$, whose other members are $Y_1^*(1385)$, $N^*(1238)$ and Ω^-. Such a resonance can also be fitted into a 14-fold representation of G_2, the only other Lie group consistent with the established octet structure of the ground-state baryons and mesons.[109] In either case, if one assumes[110] that the symmetry-breaking interaction transforms like the $I=0$ member of an $SU(3)$ octet, the resulting mass formula predicts[109] the Ξ^* mass to be 1530 MeV/c^2 to within a few percent. Moreover, the spin-parity assignment is $\frac{3}{2}^+$ in both cases—the only difference is the isospin assignment: $\frac{3}{2}$ in G_2 and $\frac{1}{2}$ in $SU(3)$. Since the combined world evidence favors $I=\frac{1}{2}$ by ≈8 standard

[102] If the events in the 730 and K^* bands are included, one finds $R=0.77\pm0.11$.

[103] R. Adair, Rev. Mod. Phys. **33**, 406 (1961); R. H. Dalitz, Brookhaven National Laboratory Report 735, 1961 (unpublished).

[104] P. Schlein *et al.*, Phys. Rev. Letters **11**, 167 (1963).

[105] G. Smith (private communication).

[106] N. Byers and S. Fenster, Phys. Rev. Letters **11**, 52 (1963).

[107] We have analyzed the entire production and decay chain sequence $K^-+p\to\Xi^*+K$; $\Xi^*\to\Xi^-+\pi^+$; $\Xi^-\to\Lambda^0+\pi^-$ using the Byers-Fenster technique. A complete account of the use of the method has been given elsewhere. (M. Gundzik, Syracuse University, ONR Report 2-64, unpublished). The results of the analysis simply confirm the $J=\frac{3}{2}$ result obtained above and give no significant information on the parity.

[108] M. Gell-Mann, in *Proceedings of the International Conference on High Energy Physics, 1962*, edited by J. Prentki (CERN, Geneva, 1962), p. 805.

[109] B. d'Espagnat, in *Proceedings on the International Conference on High Energy Physics, 1962*, edited by J. Prentki (CERN, Geneva, 1962), p. 917.

[110] In the case of $SU(3)$ the formula is first order and contains 2 parameters. Thus, using the $Y_1^*(1385)$ and $N^*(1238)$ as input, both the Ξ^* and Ω^- are predicted. In the case of G_2, the formula is 2nd order and contains 4 parameters. One must therefore assume the Y_1^*, N^*, Ω^-, and $Y_0^*(1405)$ masses to "predict" the Ξ^* mass. One might note also that the predicted widths are the order of a few MeV in both cases—in agreement with observation.

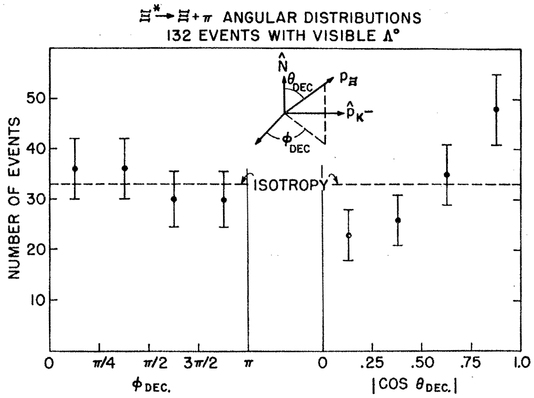

FIG. 33. Polar and azimuthal decay distributions for 132 Ξ^* events.

deviations, G_2 may be rejected with a high degree of confidence.[111]

We now consider the relevance of our data to other aspects of $SU(3)$. Several speculations concerning the existence of other $\Xi\pi$ resonances have been made. There is a suggestion of Tuan[112] that the $\Xi^*(1530)$ might generate another Ξ^* at ≈ 1750 MeV/c^2 by means of the Peierls mechanism.[113] Also, Alvarez *et al.*[114] have conjectured the existence of a $\frac{3}{2}^-$ octet (called the γ octet) incorporating the $N^*(1512)$, $Y_0^*(1520)$, $Y_1^*(1660)$ and requiring a new Ξ^* of mass ≈ 1600 MeV/c^2. As emphasized earlier, we find no evidence for any $\Xi\pi$ resonances[115] in the mass range 1550–1800 MeV/c^2, and in particular find an upper limit to the production of a $\Xi^*(1600)$ of $\lesssim 3\%$ relative to that of the $\Xi^*(1530)$. Similar results have been obtained by other groups.[104] Such null results indicate that the existence of the γ octet of Ref. 114 can only be considered a very remote possibility.[116]

Following the early success of the Okubo mass relation for supermultiplet splitting, Coleman and Glashow[117] obtained an analogous mass relation for the electromagnetic splitting within the ground-state octet. This relation, based on the assumption that the electric current transforms as an octet singlet under $SU(3)$, (in direct analogy to the Gell-Mann assumption for the symmetry-breaking strong interaction), was well verified experimentally[118] and prompted similar studies for the decuplet.[119] The result of these studies may be expressed in the form of a sum rule involving measurable mass differences as follows:

$$M[(\Xi^*)^-]-M[(\Xi^*)^0]=\tfrac{3}{4}\{M[(Y_1^*)^-]-M[(Y_1^*)^+]\}-\tfrac{1}{4}\{M[(N^*)^0]-M[(N^*)^{++}]\}.$$

Making use of available experimental results,[120] one finds an expected $M[(\Xi^*)^-]-M[(\Xi^*)^0]$ mass difference of 6 ± 2 MeV/c^2. This is in excellent agreement with the best available world average of 6.2 ± 2.5 MeV/c^2. The apparent success of the assumption of octet dominance has motivated considerable study of its origin and (at least) two specific models have been proposed which lead to additional independent predictions concerning baryon mass differences. The first of these is the tadpole model of Coleman and Glashow[121] which predicts a contribution to the $M[(\Xi^*)^-]-M[(\Xi^*)^0]$ mass difference of $+2.7$ MeV/c^2.[122] This, together with the contribution[122] ($+4.7$ MeV/c^2) from the conventional Feynman-Speisman mechanism, predicts a total mass difference of $+7.4$ MeV/c^2, in quite reasonable agreement with the observed value. In the model of Radicati *et al.*,[123] octet dominance follows from the assumption that the symmetry-breaking and electromagnetic interaction are due to ω^0-ϕ^0 mixing and ρ^0-ω^0 mixing, respectively. This model predicts "hybrid" product rules which are well satisfied for the baryon and meson octets; for the decuplet, they predict:

$$M[(\Xi^*)^0]=\{M[(Y_1^*)^-]-M[(Y_1^*)^+]\}\times\left[\frac{M(\Xi^0)-M(n)}{M(\Sigma^-)-M(\Sigma^+)}\right]+M[(N^*)^0],$$

which yields an expected mass of 1517 ± 100 MeV/c^2 in agreement with the observed value.

The $\Xi^*(1530)$ may be accommodated[124] within $SU(6)$ in much the same way as within $SU(3)$. It remains a member of a decuplet, which together with the baryon octet form the 56-dimensional representation of $SU(6)$. Mass formulas analogous to the Okubo relation have

[111] It is interesting to note that both G_2 and $SU(3)$ accommodate the Ω^- and the $\Xi^*(1530)$ equally well and in fact differ in only one point (as far as established resonances are concerned) aside from the isospin of the Ξ^*. The case in point is the J^P assignment of the $Y_0^*(1405)$ which, as a member of the $\Xi^*(1530)$ multiplet must be $\frac{3}{2}^+$ in G_2. Since the J^P value of the 1405 has not been directly measured (it is inferred to be $\frac{1}{2}^-$ from analyses of low-energy K^--p data), the Ξ^* isospin evidence provides a convincing reason for rejecting G_2.

[112] S. F. Tuan (private communication).

[113] R. Peierls, Phys. Rev. Letters **6**, 641 (1961).

[114] L. Alvarez *et al.*, Phys. Rev. Letters **10**, 192 (1962).

[115] For Ξ^* masses >1650 MeV/c^2, one might expect a significant contribution from the decay mode $\Lambda\bar{K}$. No evidence for an enhancement in this system was found (see Fig. 20, 21 in the ϕ section, Sec. IIIB). We note also that we find no significant indication of the $\Xi^*(1810)$ reported by Smith *et al.*, Phys. Rev. Letters **14**, 25 (1965). Presumably this is due to its relatively small production amplitude at our energy and its nearness to the end of the available phase space.

[116] A new version of a $\frac{3}{2}^-\gamma$ octet incorporating $Y_1^*(1660)$, $\Xi^*(1810)$, $N^*(1512)$ has been suggested by I. P. Gyuk and S. F. Tuan, Phys. Rev. Letters **14**, 121 (1965).

[117] S. Coleman and S. L. Glashow, Phys. Rev. Letters **6**, 432 (1961).

[118] R. H. Dalitz, Ann. Rev. Nucl. Sci. **13**, 424 (1963).

[119] S. P. Rosen, Phys. Rev. Letters **11**, 100 (1963); A. J. Macfarlane and E. C. G. Sudarshan, Nuvo Cimento **31**, 1176 (1964).

[120] For the N^*: M. G. Olson, Phys. Rev. Letters **14**, 118 (1965); for the Y_1^*: W. Cooper *et al.*, Phys. Letters **8**, 365 (1964); D. Huwe, University of California Radiation Laboratory Report 11291, 64 (unpublished) and our own results.

[121] S. Coleman and S. Glashow, Phys. Rev. **134**, B671 (1964).

[122] R. Socolow, Ph.D. thesis, Harvard University 1964 (unpublished). H. J. Schnitzer (private communication).

[123] L. A. Radicati, L. E. Picasso, D. P. Zanello, and J. J. Sakurai, Phys. Rev. Letters **14**, 160 (1965).

[124] T. K. Kuo and T. Yao, Phys. Rev. Letters **14**, 79 (1965).

been proposed.[125] They lead to the usual equal-spacing rule within the decuplet, but also lead to the hybrid relation

$$M(\Xi^*)=M(\Xi)-M(\Sigma)+M(Y_1^*),$$

which is well satisfied by our results. In addition, several models based upon the invariance of the mass operator under $SU(6)$ have led to new electromagnetic mass relations,[217,126,127] all of which are compatible with present results.

D. The $Y_1^*(1385)$ and $Y_0^*(1405)$

In this section we discuss the investigation of the three-body final states, $\Lambda^0\pi^+\pi^-$ and $\Sigma^\pm\pi^\mp\pi^0$, in order to study the $Y_1^*(1385)^\pm$ and $Y_0^*(1405)$. The data provide some information on the properties of the $Y_1^*(1385)$, including the spin, the $\Sigma\pi/\Lambda\pi$ branching ratio and the mass estimates for the different charge states.[128] Both resonances appear to be produced by K^* exchange. The $Y_1^*(1385)^+$ data provides an opportunity for the detailed study of the exchange model itself, which is found to be *quantitatively* accurate. As regards the $Y_0^*(1405)$, within the context of the model, there is evidence against $J^P=\frac{3}{2}^+$ and consistency with $J=\frac{1}{2}$.

1. Existence and Decay Modes

The final states of interest here are produced in the reactions:

$$K^-+p\rightarrow(\Lambda^0 \text{ or } \Sigma^0)+\pi^++\pi^-, \quad \text{(a)}$$

$$K^-+p\rightarrow\Sigma^++\pi^-+\pi^0, \quad \text{(b)}$$

$$K^-+p\rightarrow\Sigma^-+\pi^++\pi^0. \quad \text{(c)}$$

The final states (a) and (b) provide a sample of $Y_1^*(1385)^\pm$ while (b) and (c) provide a sample of $Y_0^*(1405)$. We begin by taking up the questions of identification and background for (a).

A general discussion of the $V^0+2\pi$ topology was given in Sec. IIIA. In practice, the only significant source of background for (a) is the related final state $\Lambda^0\pi^+\pi^-\pi^0$. Other possibilities, such as the kaon-induced reactions $\Lambda^0\pi^+\pi^-MM$, $\Lambda^0K^+K^-(\pi^0)$ or the pion-induced reaction $\Lambda^0K^+\pi^-(\pi^0)$, are easily distinguished on the basis of missing mass or ionization (or both). Previous studies indicate that $\Lambda^0\pi^+\pi^-\gamma$ contamination is negligible.[129] A study of the neutral missing mass of all events compatible with $\Lambda^0\pi^+\pi^-\pi^0$ indicates that the majority are in reality $\Lambda^0\pi^+\pi^-\pi^0$. Thus, for present purposes we accept only those events which are kinematically incompatible with the $\Lambda^0\pi^+\pi^-\pi^0$ hypothesis. This results in a channel (a) sample of 827 events with a probable contamination[130] bias of $\lesssim 10\%$ and an omission bias of $\approx 5\%$.

The $\Lambda^0\pi^+$, $\Lambda^0\pi^-$ mass spectra, as well as the $\pi^+\pi^-$ mass spectrum for events not in the $Y_1^*(1385)$ region, are shown in Figs. 34(a), 34(b) and 34(c), respectively. The structure of these plots reveals the presence of the $Y_1^*(1385)^+$ and indications of the $Y_1^*(1385)^-$ and the ρ^0, if reflection effects are discounted. There is no statistically significant indication of the $Y_1^*(1660)^+$. With appropriate background subtractions, we may estimate (with varying degrees of reliability) the relative proportion of various reaction channels which feed the final state (a). From Fig. 34, we find,

Channel	Relative proportion
$Y_1^*(1385)^+\pi^-$	8.8
$Y_1^*(1385)^-\pi^+$	1
$\binom{\Lambda^0}{\Sigma^0}\rho^0$	4
$\binom{\Lambda^0}{\Sigma^0}\pi^+\pi^-$	27.5

Since the $Y_1^*(1385)^+$ sample is of primary interest here, we discuss the subtraction details more fully below.

Examination of the Dalitz plot densities (not shown) with the bands corresponding to $(Y_1^*)^\pm$ and ρ^0 suggests no interference effects. The same is true of the decay angular distribution of $Y_1^*(1385)^+$, which will be discussed later. One may conclude that the mass band $M^2(\Lambda^0\pi^+)=1.80$–$2.025(\text{BeV}/c^2)^2$ consists of an incoherent mixture of $Y_1^*(1385)^+$ and $\approx 14\%$ phase-space background. Selection of an almost completely pure ($\approx 95\%$) sample is made possible by the fact that the real $Y_1^*(1385)^+$ resonance particles are produced extremely backward in the over-all center of mass (see Fig. 35), while the background $\Lambda^0\pi^+$ combinations are produced relatively isotropically. The $Y_1^*(1385)^+$ sample used for most subsequent studies is selected using both effective-mass information and the criterion: $\cos\theta_{Y^*}\leq -0.6$. This criterion selects 170 events out of the 221 event peak of Fig. 34(a). When background is subtracted, this sample is reduced to 135 events.

Next, we consider the final states (b) and (c). These consist of all events in Run I and a partial sample of Runs II and III, in which the Σ decay is observed. Be-

[125] T. K. Kuo and T. Yao, Phys. Rev. Letters **13**, 415 (1964); M. A. B. Bég and V. Singh, Phys. Rev. Letters **13**, 418 (1964).

[126] B. Sakita, Phys. Rev. Letters **13**, 643 (1964).

[127] C. H. Chan and A. Q. Sarker, Phys. Rev. Letters **13**, 731 (1964).

[128] For a summary of the evidence for $J=\frac{3}{2}^+$, see the review article of R. H. Dalitz, Ann. Rev. Nucl. Sci. **13**, 339 (1963).

[129] This was discussed in detail in Sec. IIIA in conjunction with the $\eta^*\rightarrow\rho\gamma$ decay-mode study.

[130] A study of the Y^0 mass spectrum, calculated from the K^-, π^+, and π^- of the accepted events, indicates that the $\Sigma^0\pi^+\pi^-$ contribution is small ($\lesssim 20\%$). This is consistent with the small number of unique $\Sigma^0\pi^+\pi^-$ fits observed (106). For present purposes, however, the $\Sigma^0\pi^+\pi^-$ contribution is of little consequence because it presumably does not contribute to the $(Y_1^*)^+$ peak, but appears only in the general phase-space background.

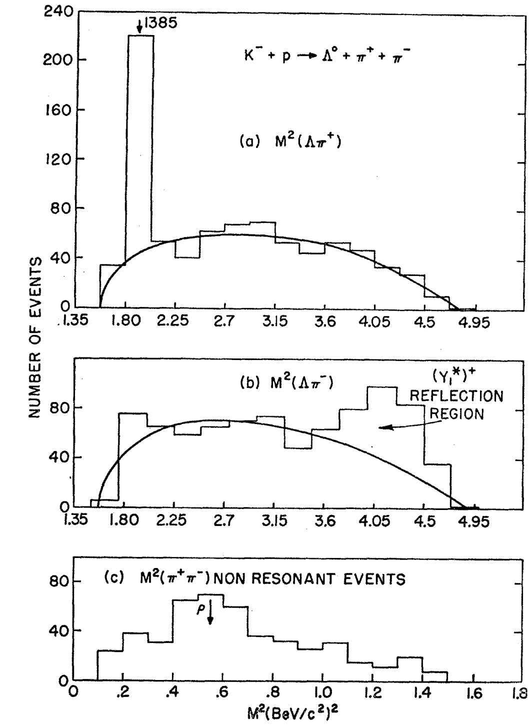

FIG. 34. (a) $M^2(\Lambda\pi^+)$ histogram for 827 $K^-p \to \Lambda\pi^+\pi^-$ events. (b) $M^2(\Lambda\pi^-)$ histogram for same sample. (c) $M^2(\pi^+\pi^-)$ histogram for same sample for events not in the $Y_1^*(1385)$ region.

cause of the poor measurement accuracy associated with short decay tracks, the kinematic overlap with other event types of the same topology is more serious here than in any other channel. Potential background-event types may be separated into subgroups, each of which can be discussed as a unit.

(i) $\Sigma^+K^-K^0$; $\Sigma^-K^+\bar{K}^0$;

(ii) $\Sigma^-K^+(\pi^0)$ (pion-induced);

(iii) $\Xi^-K^+(\pi^0)$; $\Lambda^0K^+K^-$; $K^-p(\pi^0)$ and $\Lambda^0K^+\pi^-$ (pion-induced);

(iv) $K^-N\pi^+(\pi^0)$;

(v) $\Sigma^\pm\pi^\mp$;

(vi) $\Sigma^\pm\pi^\mp MM$.

From a study of events of type (i) in which *both* the $\Sigma^\pm$ and the K^0 decayed visibly, we estimate that the total number of $\Sigma^+K^-K^0$ and $\Sigma^-K^+\bar{K}^0$ events with one charged decay are 6 and 15, respectively. Except for three or four events which were identified by ionization, this source of contamination could not be eliminated but is obviously small enough to be of no concern. Type (ii) events could not in general be separated from $\Sigma^\pm\pi^\mp\pi^0$ and are included in the sample. From the known pion background, however, we calculate that the sample contains no more than 20 such events. Events of type (iii) were easily distinguished on the basis of the general kinematic *and* ionization criteria. Type (iv) events could not be distinguished from one-constraint Σ^- fits on an event-by-event basis. However, the observed decay-time distribution of the negative decay prong from such ambiguous events clearly indicates that the vast majority of them are indeed Σ^-'s. It is this study which leads to the criterion (5) of Sec. IIC for the selection of Σ^- candidates, i.e., all type (iv) ambiguities which decay within ≈ 3 Σ^- lifetimes are accepted as Σ^- events. Type (v) ambiguities are also dealt with on a statistical basis. Because the $\Sigma^\pm\pi^\mp\pi^0$ hypothesis can be relatively easily fit with only one constraint, while the $\Sigma^\pm\pi^\mp$ hypothesis is relatively hard to fit with four constraints, all type (v) ambiguities were resolved in favor of the two-body hypothesis unless the χ^2 probability was a factor of 10 lower than the three-body hypothesis. Finally, the criterion (5) of Sec. IIC was used to resolve ambiguities of type (vi). This is worthy of special mention here because the MM resolution is particularly poor for the Σ channels, and true MM events often satisfy the loose one-constraint fit procedures. In addition to confusion with other event types, there is an ambiguity $\approx 15\%$ arising from the indistinguishability of $\Sigma^+ \to p+\pi^0$ and $\Sigma^+ \to \pi^+ + n$ decays. In all such cases, the event was accepted only if the alternative decay product assignments led to the same effective masses at production (almost all ambiguities did so).

These criteria yield $\Sigma^+\pi^-\pi^0$ and $\Sigma^-\pi^+\pi^0$ samples of 815 and 760 events, respectively, with a purity of $\approx 94\%$. Since the above selection criteria were designed to err on the side of omission rather than contamination, the resultant purity is obtained at the expense of introducing an omission bias. The latter, together with scanning bias against short Σ's and small decay angles must certainly be taken into account for *relative* comparisons with other modes. Although $\Sigma\pi$ effective-mass distributions may also be affected by such biases, the

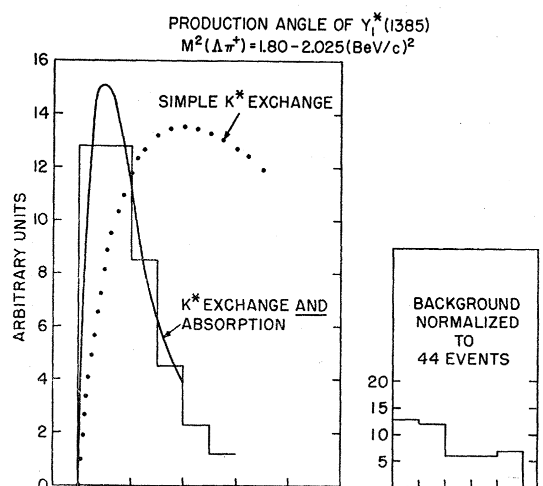

FIG. 35. Production angular distributions for $K^-p \to Y_1^{*+}\pi^-$ with background subtracted (see inset and text).

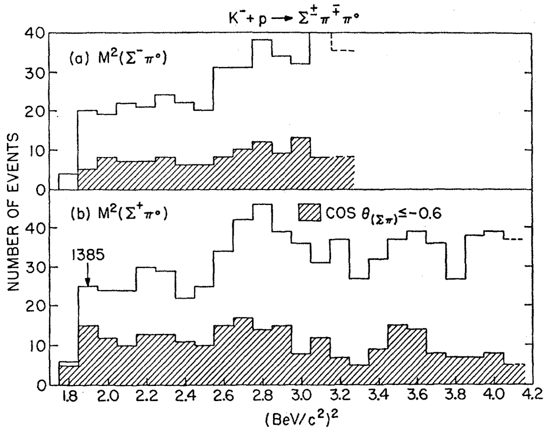

FIG. 36. (a) $M^2(\Sigma^-\pi^0)$ histogram for peripheral sample of $K^-p\to\Sigma^-\pi^+\pi^0$ events. (b) $M^2(\Sigma^+\pi^0)$ histogram for peripheral sample of $K^-p\to\Sigma^+\pi^-\pi^0$ events.

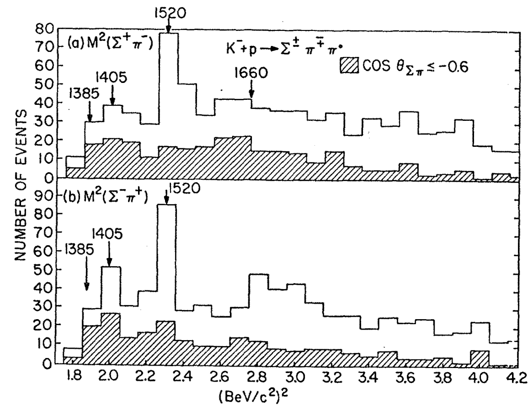

FIG. 37. (a) $M^2(\Sigma^+\pi^-)$ histogram for 815 $K^-p\to\Sigma^+\pi^-\pi^0$ events, with peripheral events shaded. (b) $M^2(\Sigma^-\pi^+)$ histogram for 760 $K^-p\to\Sigma^-\pi^+\pi^0$ events, with peripheral events shaded.

net effect should not be serious since the Σ^- and π momentum spectra are not sharply peaked and the biases concern only $\approx 15\%$ of the sample.

Those effective mass distributions which reveal the structure of the $\Sigma^\mp\pi^\pm\pi^0$ final state are shown in Figs. 36–39. A small $Y_1^*(1385)^+$ signal is indicated by the peripheral excess of Fig. 36(b) at $M^2(\Sigma^+\pi^0) \cong 1.9(\text{BeV}/c^2)^2$, and the absence of a corresponding excess in $M^2(\Sigma^-\pi^0)$ [Fig. 36(a)]. The presence of the $Y_0^*(1520)$, and a suggestion of contributions from $Y_0^*(1405)$ and/or $Y_1^*(1385)^0$ are indicated in Fig. 37. In looking at Fig. 37, one must keep in mind the poorer resolution of the Σ^+ events.

Finally, in the $\pi^\mp\pi^0$ mass spectra of the non-Y^* events shown in Fig. 38, one sees a significant ρ^- signal after imposing a peripheral selection.

To summarize, we give *rough estimates* of the relative proportions of various reaction channels which feed the $\Sigma^\pm\pi^\mp\pi^0$ final state. With appropriate background subtractions, we find for channel (b):

Channel	Relative proportion
$Y_0^*(1520)\pi^0$	8.1
$Y_0^*(1405)\pi^0+Y_1^*(1385)^0\pi^0$	3.1
$Y_1^*(1385)^+\pi^-$	1.0
$\Sigma^+\rho^-$	7.5
$\Sigma^+\pi^-\pi^0$	82.0

and for channel (c):

Channel	Relative proportion
$Y_0^*(1520)\pi^0$	3.7
$Y_0^*(1405)\pi^0+Y_1^*(1385)^0\pi^0$	2.7
$\Sigma^-\rho^+$	1.0
$\Sigma^-\pi^+\pi^0$	43.3

In order to elucidate the criteria used to isolate the $\Sigma^+\pi^0$ and $\Sigma^\pm\pi^\mp$ samples used to study the $Y_1^*(1385)^+$, $Y_1^*(1385)^0$ and $Y_0^*(1405)$, we call attention to the detailed comparison of $M^2(\Sigma^\pm\pi^\mp)$ versus $M^2(\Sigma^+\pi^0)$ shown in Fig. 39. To begin with, we associate the small $(\Sigma^+\pi^0)$ excess near the low end of phase space with the $Y_1^*(1385)^+$. Note that this excess is peripheral, just as the $\Lambda^0\pi^+$ sample of Fig. 34(a). The apparent mass shift between the $\Sigma^+\pi^0$ peak and the wide $\Sigma^\pm\pi^\mp$ peak centered at $\approx 2.0(\text{BeV}/c^2)^2$, indicates that the latter must be due primarily to the $Y_0^*(1405)$ rather than the $Y_1^*(1385)^0$. In fact, the value $M^2(\Sigma^\pm\pi^\mp)=1.96(\text{BeV}/c^2)^2$ serves as a rough cutoff to separate the two neutral resonance contributions. This procedure for mass separation is obviously crude.[131] We emphasize, however, that for present purposes, it is not the absolute number of $Y_0^*(1405)$ events which is of interest, but only their existence. Moreover, the cutoff selects the 1405 sample conservatively. (While the statistics are too limited to warrant anything but a qualitative check, it is gratifying to note that both the production and the azimuthal-angular-decay distributions of the $(\Sigma^+\pi^0+\Sigma^+\pi^-)$ $Y_1^*(1385)$ samples (not shown) are consistent with the corresponding distributions for the $(\Lambda^0\pi^+)$ $Y_1^*(1385)$ sample.)

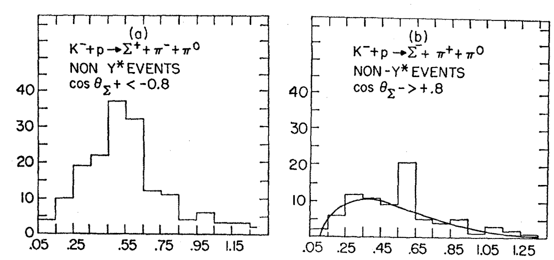

FIG. 38. (a) $M^2(\pi^-\pi^0)$ histogram for peripheral sample of $K^-p\to\Sigma^+\pi^-\pi^0$ events with $Y_1^*(1385)$ events subtracted. (b) $M^2(\pi^+\pi^0)$ histogram for peripheral sample of $K^-p\to\Sigma^-\pi^+\pi^0$ events with $Y_1^*(1385)$ events subtracted.

[131] This criterion cannot be improved because the production angular distributions of the $Y_1^*(1385)^0$ and $Y_0^*(1405)^0$ contributions are identical (see Fig. 44).

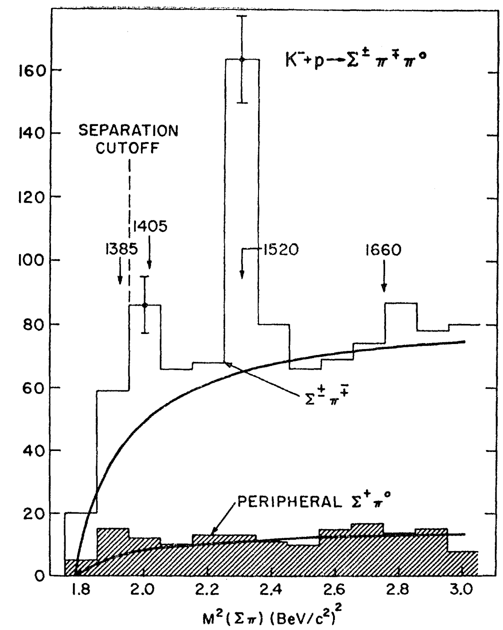

FIG. 39. $M^2(\Sigma^\pm\pi^\mp)$ histogram for 1575 $K^-p\to\Sigma^\pm\pi^\mp\pi^0$ events, compared to $M^2(\Sigma^+\pi^0)$ histogram for peripheral $K^-p\to\Sigma^+\pi^-\pi^0$ events.

On the basis of the above considerations, making subtractions using a smooth background curve *and* production-angular-distribution information, we find that the raw data of Fig. 39 provide a sample of $\approx 50 Y_0^*(1405)$ events and 8 ± 4 examples of

$$Y_1^*(1385)^+\to\Sigma^+\pi^0.$$

For the determination of the branching ratio,

$$r_1=[(Y_1^*)^+\to\Sigma^+\pi^0]/[(Y_1^*)^+\to\Lambda^0\pi^+],$$

the raw data of Figs. 34 and 39 must be corrected to account for many differences between the $\Lambda^0\pi^+$ and $\Sigma^+\pi^0$ samples and the unobserved $\Sigma^0\pi^+$ decay mode. With these corrections,[132] one finds $r_1=(8\pm6)\%$ where the error has contributions from both statistical and systematic sources. This result is in agreement with the world average value of $(9\pm4)\%$ given by Rosenfeld *et al.*[133]

2. *Properties of the* $Y_1^*(1385)$

One of the first unambiguous indications of spin $J\geqslant\frac{3}{2}$ came from preliminary results[134] of this experiment, which we now update. The $[Y_1^*(1385)]^+$ sample available from the $\Lambda^0\pi^+\pi^-$ final state is especially suitable for a study of angular correlations relevant to spin determination. As indicated above, aside from its inherent purity, there are no indications of interference with other resonant channels. Moreover, the Y_1^* velocity is high so that dynamical interference between the final state pions should be negligible.

Information on J comes from a study of the angular distribution of the decay π^+ from $[Y_1^*(1385)]^+$ with respect to the production plane normal $(\hat{N})$ in the Y_1^* rest frame. This distribution must be isotropic for $J=\frac{1}{2}$ and of the form $1+A(\hat{N}\cdot\hat{p}_{\pi^+})^2$ for $J=\frac{3}{2}$. The observed distribution in $(\hat{N}\cdot\hat{p}_{\pi^+})$ for our selected peripheral Y_1^* sample (135 events after removal of background) is shown in Fig. 40(a). The best fitted curve is given by

$$1+(0.0\pm0.4)\hat{N}\cdot\hat{p}_{\pi^+}+(4.7\pm1.8)(\hat{N}\cdot\hat{p}_{\pi^+})^2 \qquad (38)$$

all higher terms being consistent with zero. The distribution is in disagreement with isotropy by about three standard deviations, providing strong evidence for $J\geqslant\frac{3}{2}$.

The small size of the linear term in (38) is consistent with the absence of dynamical interference effects. The strong $(\hat{N}\cdot\hat{p}_{\pi^+})^2$ ansiotropy cannot be attributed to unknown systematic effects because a similar investigation[134] on 200 nonresonant $\Lambda^0\pi^+\pi^-$ events showed no such anisotropy. However, there does exist the possibility that the latter might be due to interference between a $J=\frac{1}{2}$ Y_1^* and a D-wave nonresonant background amplitude (15% is required). The important characteristic of such an hypothesis is that the nonresonant background amplitude is expected to change slowly with energy while the resonant amplitude, by definition, changes rapidly with energy.[135] This inter-

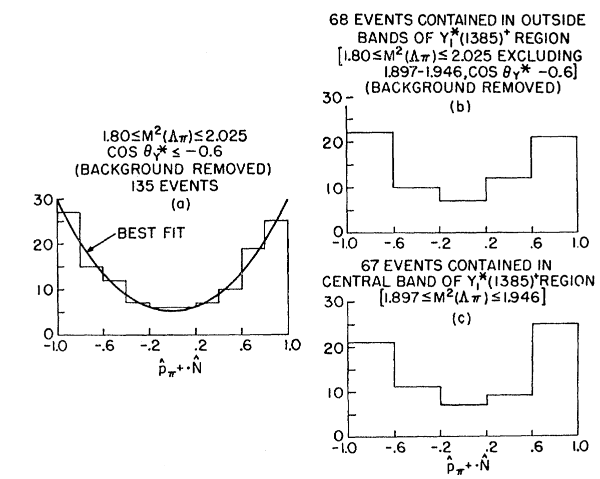

FIG. 40. (a) Polar decay angular distribution of 135 $Y_1^*(1385)$ events with background subtracted (see text). (b) Polar decay angular distribution of 68 $Y_1^*(1385)$ events in wings of peak, $1.80\leqslant M^2\leqslant 2.025$, excluding $1.897\leqslant M^2\leqslant 1.946$. (c) Polar decay angular distribution of 67 $Y_1^*(1385)$ events in center of peak, $1.897\leqslant M^2\leqslant 1.946$.

[132] The corrections arise from differences in: (i) sample size; (ii) Σ decay losses; (iii) ambiguities; (iv) background; (v) geometrical detection efficiency; (vi) scanning efficiencies; (vii) unobserved decays; and (viii) omission biases for Σ^+ events.

[133] A summary of references is given in A. H. Rosenfeld *et al.*, Rev. Mod. Phys. **36**, 996 (1965).

[134] L. Bertanza *et al.*, Phys. Rev. Letters **10**, 176 (1963). This paper summarizes the experiments bearing on J.

[135] R. H. Dalitz, Brookhaven National Laboratory Report BNL-735(T-264) (unpublished).

ference effect should therefore vary with the Y_1^* mass. To investigate this, we have divided the Y_1^* sample into two mass regions: (1) $1.86 \leq M^2(\Lambda^0\pi^+) \leq 1.94$; (2) $1.94 < M^2(\Lambda^0\pi^+) < 2.02$ *and* $1.80 \leq M^2(\Lambda^0\pi^+) \leq 1.86$ (in units of $(\text{BeV}/c^2)^2$. The $(\hat{N}\cdot\hat{p}_{\pi^+})$ distributions corresponding to these intervals are shown in Figs. 40(b) and 40(c). Now, the similarity between the shapes of these curves can be attributed either to the absence of any interference or to the remote possibility that the background amplitude just happens to vary as rapidly as that of the resonance in our energy region. The latter is extremely unlikely because Ely *et al.*[136] have observed a similar mass-independent behavior at a considerably different energy. We conclude that $J \geqslant \frac{3}{2}$. Indeed, the vanishing of all terms in $(\hat{N}\cdot\hat{p}_{\pi^+})^l$ for $l > 2$ suggests $J = \frac{3}{2}$. Our results thus provide confirmation of the accepted[128] assignment $J = \frac{3}{2}$ for the $Y_1^*(1385)$, and we shall assume this J assignment as well as positive parity in further analysis.

We now discuss the difference in mass between the $Y_1^*(1385)^-$ and the $Y_1^*(1385)^+$, which we designate ΔM_{1385}. Previous measurements of ΔM_{1385} ($+17\pm7$ MeV/c^2 by Cooper *et al.*,[120] and $+4\pm2$ MeV/c^2 by Huwe *et al.*[120]) have been carried out at relatively low energies where the peripheral mechanism cannot aid in the identification of the Y_1^* samples and where the general background level is high. On the other hand, in the present experiment both the $(Y_1^*)^+$ and $(Y_1^*)^-$ can be identified on the basis of characteristic production angular distribution, with concomitant decrease in background. Thus, in spite of the small sample of $(Y_1^*)^-$ available, there is reason to attempt an estimate

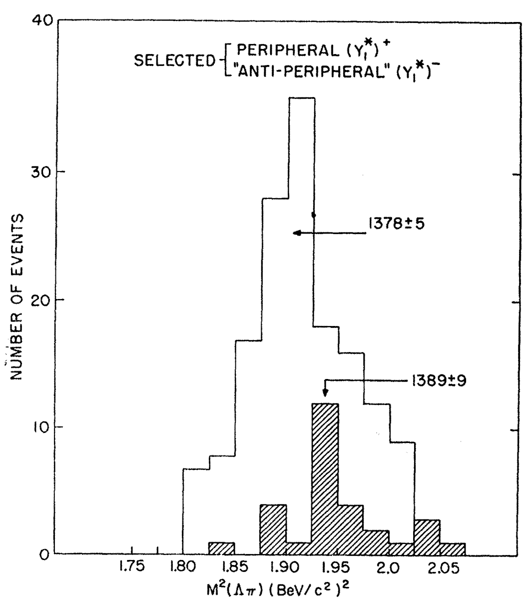

FIG. 41. $M^2(\Lambda\pi^\pm)$ histograms in mass region $1.75 \leqslant M^2 \leqslant 2.05$ for peripheral $K^-p \to \Lambda\pi^+\pi^-$ events.

[136] R. P. Ely *et al.*, Phys. Rev. Letters **7**, 461 (1961).

of ΔM_{1385}. The $(Y_1^*)^+$ and $(Y_1^*)^-$ excesses of Figs. 34(a) and 34(b), respectively, are essentially contained within the production angular regions $\cos\theta_{(\Lambda^0\pi^+)} \leq -0.6$ and $\cos\theta_{(\Lambda^0\pi^-)} \geqslant +0.6$. The histograms of events in the mass region $M^2(\Lambda^0\pi^\pm) = 1.75 - 2.05$ $(\text{BeV}/c^2)^2$ with their respective angular cutoffs are compared in Fig. 41 on an expanded mass scale. The relative displacement of the $(Y_1^*)^+$ and $(Y_1^*)^-$ peaks is evident and yields the estimate $\Delta M_{1385} \approx +11\pm9$ MeV/c^2, in rather good agreement with previous estimates, considering the statistical limitations of the present result and potential systematic uncertainties in other determinations.[137]

3. *Production Characteristics*

The dominant features of $Y_1^*(1385)$ production in the $\Lambda^0\pi^+\pi^-$ final state are the large $(Y_1^*)^+$ to $(Y_1^*)^-$ ratio and the peripherality of the positively charged sample. Both these features suggest the importance of one-meson exchange, which for this reaction must be K^* exchange. In fact, of all the reactions observed in this experiment which appear to proceed by means of K^* exchange, $(Y_1^*)^+$ production is the most suitable for detailed study of the exchange mechanism both because of the purity of the sample and because the decay angular correlations supply significant information.

It is well known[138,139] that the *simple* vector exchange model is inadequate to describe high-energy quasi-two-body interactions. There is universal disagreement in the observed and calculated momentum-transfer dependence. Channel (a) is no exception. Figure 35 shows the production angle distribution of all events in the mass band $1.80(\text{BeV}/c^2)^2 \leq M^2(\Lambda^0\pi^+) \leq 2.025(\text{BeV}/c^2)^2$ after appropriate background subtraction. The angular distribution of the background was estimated as follows. First, the angular distribution of all events outside the Y^* peak was studied for variation with $\Lambda\pi$ mass. Since none was found, all events were lumped to give the *shape* of the control distribution. The absolute number of background events (44) is obtained from the peak area under the phase-space curve of Fig. 34. The net background shown as the insert of Fig. 35 amounts to 25 events in the region $\cos\theta_{\Lambda^0\pi^+} \leqslant -0.6$. The data of Fig. 35 are in complete disagreement with the simple model. It has long been believed[140] that such discrepancies are due to the omission of absorptive effects. Recently, considerable theoretical work has been done

[137] Another estimate of ΔM_{1385} was made from the $(Y_1^*)^+$ and $(Y_1^*)^+$ samples available in the $\Lambda^0\pi^+\pi^-\pi^0$ final state which is discussed in detail in Sec. IIIE. The relevant $\Lambda\pi$ mass spectra are shown in Fig. 48. Fitting to the peak events yields a mass difference of $\Delta M = +9\pm6$ MeV/c^2. Since systematics are more important than statistics here, the error is assigned to encompass the variation which results when the bin size is changed, etc. It is encouraging to note that this determination (which shares the same systematic uncertainties as those at lower energy), is consistent with the estimate obtained from the $\Lambda^0\pi^+\pi^-(Y_1^*)$ samples.

[138] For a complete discussion with appropriate references, see J. D. Jackson and H. Pilkuhn, CERN Report 8379 (unpublished).

[139] J. D. Jackson [Rev. Mod. Phys. (to be published)].

[140] N. J. Sopkovich, Nuovo Cimento **26**, 186 (1962).

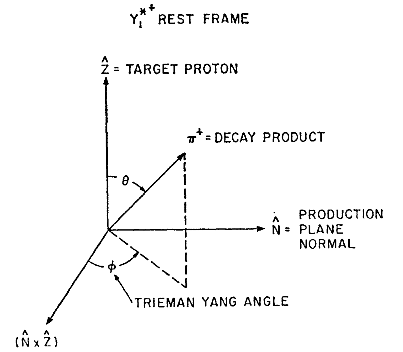

FIG. 42. Definition of polar and azimuthal decay angles.

toward understanding the essential role of absorption. It has been shown,[141] in fact, that good qualitative agreement with experiment can be obtained on the basis of a distorted-wave Born approximation. In particular, Gottfried and Jackson[142,143] have given a specific recipe for the absorptive factor A (which multiplies the usual matrix element) in terms of 4 parameters. In the notation of Ref. 143,

$$A \approx \{[1-C_1 e^{-\gamma_1(x-1/2)^2}][1-C_2 e^{-\gamma_2(x-1/2)^2}]\}^{1/2}. \quad (39)$$

Here the initial-state interaction parameters C_1, γ_1 can be obtained from K^-p elastic scattering and the final-state interaction parameters C_2, γ_2 are free. In our case for $C_1=0.9$, $C_2=1$, $\gamma_1=0.077$, and $\gamma_2=\frac{3}{4}\gamma_1$, one finds[144] reasonable quantitative agreement between theory and experiment as shown in Fig. 35. A study of the sensitivity to variation of the final state interaction parameters[144] shows that the agreement between theory and experiment is not significantly altered for values of the parameters consistent with the known [elastic/total] cross-section ratio. It should be noted that exact partial-wave sums were used in the evaluation of absorptive effects. Further evidence of the validity of the model comes from the study of Y_1^* decay.

In the Y_1^* rest frame, the decay angular distribution in terms of polar and azimuthal angles defined in Fig. 42 is given by[138]

$$W(\theta,\phi)=\frac{3}{4\pi}\left\{\rho_{33}\sin^2\theta+(\tfrac{1}{2}-\rho_{33})(\tfrac{1}{3}+\cos^2\theta) -\frac{2}{\sqrt{3}}\operatorname{Re}\rho_{3,-1}\sin^2\theta\cos2\phi-\frac{2}{\sqrt{3}}\operatorname{Re}\rho_{3,1}\sin2\theta\cos\phi\right\} \times d\phi d(\cos\theta), \quad (40)$$

which implies the integrated distributions;

$$W_1(\theta)\approx 1-3\left[\frac{4\rho_{33}-1}{4\rho_{33}+1}\right]\cos^2\theta \quad (41)$$

and

$$W_2(\phi)\approx 1-[(4/\sqrt{3})\operatorname{Re}\rho_{3,-1}]\cos2\phi, \quad (42)$$

where ρ_{ij} are the standard density matrix elements. The assumption of K^* exchange leads to *no* restrictions on the form of $W(\theta,\phi)$. However, as was first pointed out by Stodolsky and Sakurai,[145] the *additional* assumption that the vector exchange is dominated by the magnetic dipole matrix element, does lead to unique and striking decay correlations. We shall call this model M_1D, for magnetic-dipole dominance. In terms of the density matrix elements defined in the coordinate system of Fig. 42, the M_1D model requirements are listed in Table IX. Also listed in Table IX are the expected values of ρ_{ij} if one includes absorption effects in addition to the M_1D model. The predicted polar and azimuthal distributions (41), (42), are compared with the experimental data in Fig. 43. It is interesting to note that absorption does not materially effect the expected decay correlations. The agreement between the predictions of the M_1D model and our experimental data is *quantitively* good. This model has also been shown[139] to give an accurate description of $N^*(1238)$

TABLE IX. Magnetic dipole model predictions for $Y_1^*(1385)$ decay compared with experiment.

	$\rho_{3,3}$	$\operatorname{Re}\rho_{3,-1}$	$\operatorname{Re}\rho_{3,+1}$
Expt.	0.31 ± 0.05	0.27 ± 0.04	0.032 ± 0.038
Magnetic dipole model	0.38	0.22	0
Magnetic dipole with absorption	0.25	0.15	-0.14

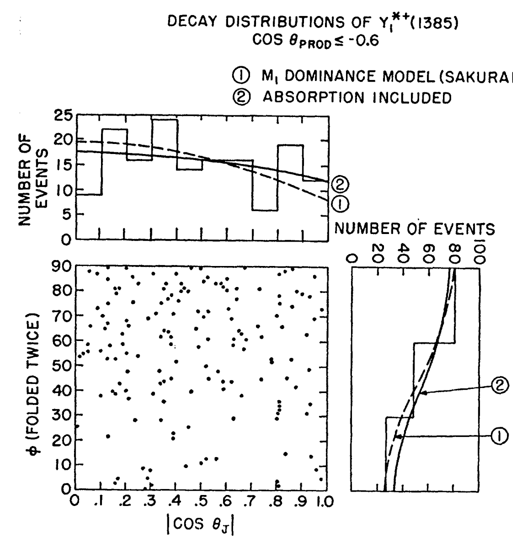

FIG. 43. $Y_1^*(1385)$ polar- and azimuthal-decay angular distributions compared to theoretical modified K^*-exchange model (see text).

[141] A. Dar *et al.*, Phys. Rev. Letters **12**, 82 (1964); also **13**, 91 (1964). L. Durand and Y. T. Chiu, *ibid.* **12**, 399 (1964); M. H. Ross and G. L. Shaw, *ibid.* **12**, 627 (1964).

[142] K. Gottfried and J. D. Jackson, Nuovo Cimento **34**, 735 (1964).

[143] J. D. Jackson *et al.*, Phys. Rev. **139**, B428 (1965).

[144] We wish to thank Prof. Jackson for the numerical evaluation at our energy.

[145] L. Stodolsky and J. J. Sakurai, Phys. Rev. Letters **11**, 90 (1963).

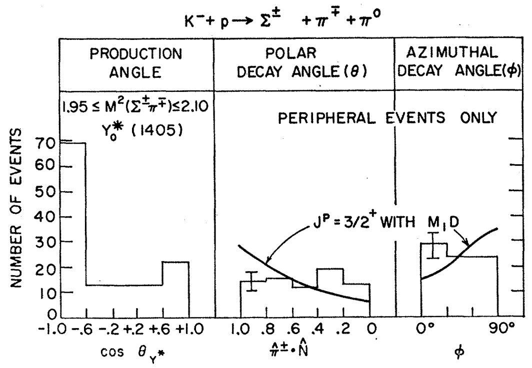

FIG. 44. $Y_0^*(1405)$- production and decay angular distributions for 130 $K^-p \rightarrow Y_0^*(1405)\,\pi^0$ events.
$\searrow \Sigma^{\pm}\pi^{\mp}$

production at similar energies. After correction for neutral decay, scanning and geometrical efficiency, background contamination and omission due to selection criteria, we find that the total $(Y^*)^+\pi^-$ cross section is $\sigma = 207 \pm 25\mu$b. (See Sec. VI.) The contribution of the peripheral sample ($\cos\theta_{Y^*} \leq -0.6$) is $\sim 187\ \mu$b. This leads to a Y^*K^*p coupling constant $g^2/4\pi = 40$–50, which is a factor of ≈ 2 larger than expected[143] on the basis of the N^*K^*p coupling with SU_3 coefficients.

The production angular distribution of the $Y_0^*(1405)$ shown in Fig. 44 is clearly the same as that of the $Y_1^*(1385)$, and so is consistent with the production requirements of the K^*-exchange model (for the same absorption parameters). *Within the context of this model*, any difference in the decay angular distributions of the two resonances would be indicative of different spin-alignment properties. From Fig. 44 one sees that the $Y_0^*(1405)$ decay distributions are consistent with isotropy and have only a $\sim\frac{1}{2}\%$ probability of agreement with the model-dependent $J^P = \frac{3}{2}^+$ assignment. To this extent, the data suggest $J = \frac{1}{2}$ for the $Y_0^*(1405)$, in agreement with the detailed analysis of the K^-p absorption data.[146]

E. The $Y_1^*(1660)$

In this section we consider evidence pertinent to the existence and properties of the $Y_1^*(1660)$ hyperon. It is found that the $Y_1^*(1660)^+$ is peripherally produced and subsequently decays (predominantly) into $Y_0^*(1405)$ $+\pi^+$, in agreement with our preliminary results and the recent observations of Eberhard *et al.*[147] A small $\Sigma^+\pi^0$ decay mode is detected but there is no significant indication of other modes, in particular $\Lambda\pi^+\pi^0$. The Dalitz plot provides no information on the spin-parity. However, if the K^*-exchange model is assumed, a study of the decay angular distributions provides some evidence against $J^P = \frac{3}{2}^+$.

[146] M. Sakitt, University of Maryland Tech. Report 410 (1964) and Y. Kim, Phys. Rev. Letters **14**, 29 (1965).
[147] J. Leitner *et al.*, Bull. Am. Phys. Soc. **10**, 517 (1965); P. Eberhard *et al.*, Phys. Rev. Letters **14**, 466 (1965).

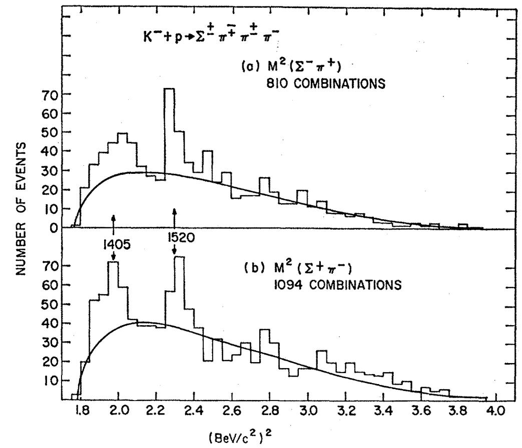

FIG. 45. (a) $M^2(\Sigma^-\pi^+)$ histogram for 405 $K^-p \rightarrow \Sigma^-\pi^+\pi^-\pi^+$ events, each event plotted twice. (b) $M^2(\Sigma^+\pi^-)$ histogram for 547 $K^-p \rightarrow \Sigma^+\pi^-\pi^+\pi^-$ events, each event plotted twice.

1. Existence

The final states of interest here are

$$\Sigma^+\pi^-\pi^+\pi^- \tag{43}$$

and

$$\Sigma^-\pi^+\pi^+\pi^-. \tag{44}$$

Application of the general acceptance criteria of Sec. II C results in the elimination of ambiguities with all background reactions [viz. $K^-p\pi^+\pi^-(\pi^0)$, $K^-N\pi^+\pi^-\pi^+$, $\Xi^-K^+\pi^+\pi^-$], except $\Sigma^{\pm}\pi^{\mp}\pi^+\pi^-\pi^0$. Ambiguous events, amounting to only $\sim 5\%$ of all candidates, are omitted from the sample, leaving 547 $\Sigma^+\pi^-\pi^+\pi^-$ and 405

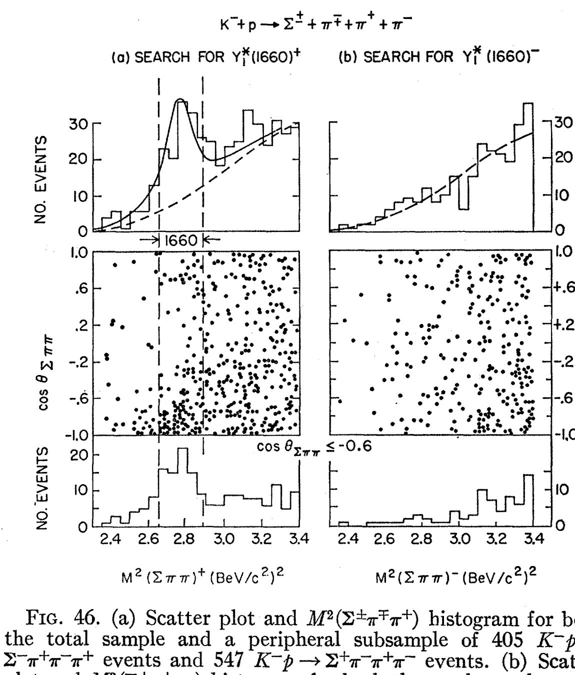

FIG. 46. (a) Scatter plot and $M^2(\Sigma^{\pm}\pi^{\mp}\pi^+)$ histogram for both the total sample and a peripheral subsample of 405 $K^-p \rightarrow \Sigma^-\pi^+\pi^-\pi^+$ events and 547 $K^-p \rightarrow \Sigma^+\pi^-\pi^+\pi^-$ events. (b) Scatter plot and $M^2(\Sigma^{\pm}\pi^{\pm}\pi^-)$ histogram for both the total sample and a peripheral subsample of $K^-p \rightarrow \Sigma^{\pm}\pi^{\mp}\pi^-\pi^+$ events.

$\Sigma^-\pi^+\pi^+\pi^-$ events for further study. (These are from incomplete samples in all three runs.)

In order to distinguish the various resonance contributions to the final states (43), (44), we examine the effective-mass combinations shown in Figs. 45(a) and 45(b). The $Y_0^*(1405)$ and $Y_0^*(1520)$ contributions are evident. Using the phase-space shape to roughly estimate background, and noting that there are two mass combinations per event, one finds that each of the resonances comprise $\sim 15\%$ of (43) and (44). A similar study of pion effective-mass plots gives no indication of ρ production or any 3-pion mass enhancement.

Figures 46(a) and 46(b) show the three-body $\Sigma\pi\pi$ mass distributions. We exhibit only a small part of the total $\Sigma\pi\pi$ spectrum near 1660 MeV/c^2; the remainder of the spectrum shows no anomalies. The $(\Sigma\pi\pi)^-$ mass distribution is nicely fit by phase space, while the $(\Sigma\pi\pi)^+$ distribution exhibits a prominent enhancement at $\sim$1660 MeV/c^2. The solid curve, representing the sum of phase space[148] plus a Breit-Wigner amplitude for $M(\Sigma\pi\pi)=1660$ MeV/c^2 and $\Gamma=50$ MeV/c^2, is seen to give an adequate fit. In addition, the production angle scatter plot clearly shows that $(\Sigma\pi\pi)^+$ enhancement is produced peripherally. The above circumstances establish the existence of the reaction:

$$K^-+p\to Y_1^*(1660)^++\pi^- \tag{45}$$

and indicate that it proceeds by means of a one-meson-exchange mechanism. From the data of Fig. 46(a), one sees that a $Y_1^*(1660)^+$ sample of high purity may be obtained from the selection criteria:

$$\left\{\begin{matrix} 2.65\,(\mathrm{BeV}/c^2)^2\leq M^2(\Sigma\pi\pi)^+\leq 2.87\,(\mathrm{BeV}/c^2)^2 \\ \cos\theta_{(\Sigma\pi\pi)^+}\leq -0.6 \end{matrix}\right\}. \tag{46}$$

Application of these criteria results in a sample of 73 events, of which $\lesssim 15$ are estimated to be due to background. This sample is used for most subsequent studies.

2. Decay Modes

We investigate the nature of the $(\Sigma\pi\pi)^+$ decay, by a study of the $\Sigma\pi$ effective masses of the $(1660)^+$ sample defined in (46). Because of inherent differences between the $\Sigma^+\pi^-\pi^+$ and $\Sigma^-\pi^+\pi^+$ configurations, we exhibit the $\Sigma^+\pi^-$ and $\Sigma^-\pi^+$ spectra separately, in Figs. 47(a) and 47(c) respectively.[149] The $\Sigma^+\pi^-$ distribution clearly disagrees with the phase-space spectrum which is indicated by the dashed curve of Fig. 47(a). The obvious enhancement at $\sim$1405 MeV/c^2 is well accounted for[150]

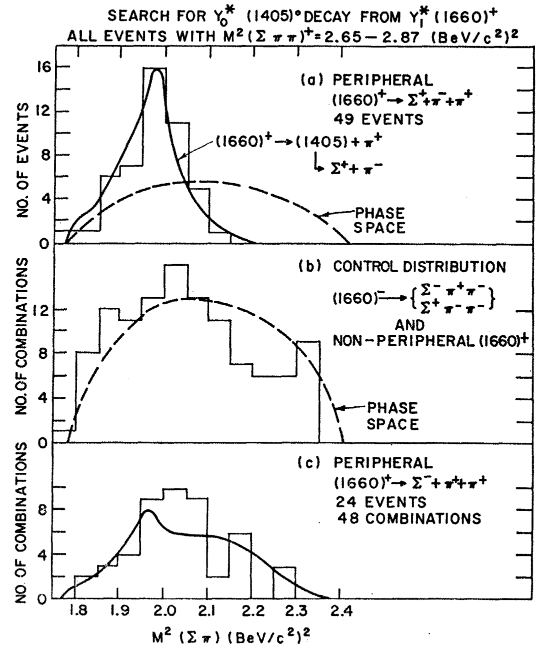

FIG. 47. (a) $M^2(\Sigma^+\pi^-)$ histogram for 49 peripheral

$$K^-p\to\pi^-Y_1^*(1660)^+ \searrow \Sigma^+\pi^-\pi^+$$

events. (b) $M^2(\Sigma^\pm\pi^\mp)$ histogram for $K^-p\to\Sigma^\pm\pi^\mp\pi^+\pi^-$ events in which either $M(\Sigma^\pm\pi^\mp\pi^+)$ is consistent with 1660 MeV/c^2 and non-peripheral *or* $M(\Sigma^\pm\pi^\mp\pi^-)$ is consistent with 1660 MeV/c^2. (c) $M^2(\Sigma^-\pi^+)$ histogram for 24 peripheral

$$K^-p\to\pi^-Y_1^*(1660)^+ \searrow \Sigma^-\pi^+\pi^+$$

events.

by the solid curve which represents the $\Sigma^+\pi^-$ spectrum[151] from the decay chain:

$$Y_1^*(1660)^+\to Y_0^*(1405)+\pi^+\to\Sigma^++\pi^-+\pi^+. \tag{47}$$

The $\Sigma^-\pi^+$ mass subspectrum of Fig. 47(c) is also consistent with the hypothesis that the 1660 decay proceeds through a $Y_0^*(1405)$ intermediate state. To illustrate this, we show the solid curve representing the $\Sigma^-\pi^+$ spectrum[152] from the chain:

$$Y_1^*(1660)^+\to Y_0^*(1405)+\pi_2^+\to\Sigma^-+\pi_1^++\pi_2^+. \tag{48}$$

A similar effective-mass study of a suitable control sample indicates that the behavior described above is not the result of systematic and/or kinematic biases. The control sample consists of all $(\Sigma\pi\pi)^-$ and all non-peripheral $(\Sigma\pi\pi)^+$ combinations with effective masses of 1660 ± 40 MeV/c^2. The $\Sigma\pi$ mass subspectrum from this control sample, shown in Fig. 47(b), is fit rather well by phase space, as expected.

The spectra of Fig. 47(a) and 47(c) are consistent

---

[148] The normalization of the $(\Sigma\pi\pi)$ phase-space curve was determined from the $(\Sigma\pi\pi)^-$ sample [of Fig. 47(b)] which serves as a control distribution. However, in using this normalization for the $(\Sigma\pi\pi)^+$ sample, a 10% adjustment was made in order to account for the larger number of mass combinations of net positive charge.

[149] No background subtraction has been made in these plots.

[150] There is, of course, a remote possibility that the peak of Fig. 47(a) represents the $\sim 5\%\Sigma\pi$ decay of the uncharged $Y_1^*(1385)$. This is easily disposed of on the grounds that it leads one to expect the order of 600 $Y_1^*(1660)^+$ events in the $\Lambda 3\pi$ final state, and as we shall see later, there are less than $\sim$20 such events (with 90% confidence).

[151] This spectrum is calculated using the $\frac{3}{2}^-$ matrix element. The shape is quite representative, being entirely insensitive to the particular choice of l. The finite width of both the 1660 and 1405 MeV/c^2 resonances is taken into account here.

[152] This spectrum is calculated using the symmetrized $\frac{3}{2}^-$ matrix element. [See Eq. (50)].

with the hypothesis that *all* of the $Y_1^*(1660)$ decays result from the chains (47) and (48). However, as a result of statistical and systematic uncertainties, one cannot exclude about 20% contribution from direct $1660 \to \Sigma\pi\pi$ decay. This is consistent with the conclusions of the Lawrence Radiation Laboratory-University of Illinois experiment.[147] Thus, for purposes of further discussion, we shall assume that the $\Sigma\pi\pi$ decay of the $Y_1^*(1660)$ proceeds *entirely* through the $Y_0^*(1405)$ intermediate state.[153] Then, in the absence of interference effects, one expects the ratio $\gamma_\pm$, defined by

$$\gamma_\pm = \frac{(1660)^+ \to \Sigma^+ + \pi^- + \pi^+}{(1660)^+ \to \Sigma^- + \pi^+ + \pi^+},$$

to be unity. After correction for geometrical detection efficiency, the observed ratio of 49/24 yields the value[154] $\gamma_\pm = 2.0 \pm 0.75$, which differs from unity by 1.3 standard deviations. Departures from unity are to be expected in view of Bose-symmetry effects[155] in the $\Sigma^-\pi^+\pi^+$ final state. Indeed, from a qualitative point of view, one might expect this effect to be sizeable because the 1405 MeV/c^2 overlap region ($\Sigma^-\pi_1^+$ versus $\Sigma^-\pi_2^+$) covers a large portion of the decay Dalitz plot (see Fig. 55). However, a direct numerical integration of the symmetrized decay amplitude for the chain (48) [see Eq. (51)] shows that Bose symmetry cannot account for a significant departure from unity. Thus the observed ratio must be considered the result of either a statistical fluctuation or of interference with the background.[156] The latter possibility would complicate further interpretation of the data and must be kept in mind in assessing the significance of later results.

Thus far we have considered only the detectable final states of $Y_1^*(1660)^+ \to \Sigma\pi\pi$ decay. In order to give branching ratios in standard form, we must make several assumptions concerning the undetectable modes $\Sigma^0\pi^0\pi^+$ and $\Sigma^+\pi^0\pi^0$ (from the final states $\Sigma^0\pi^+\pi^-\pi^0$ and $\Sigma^+\pi^-\pi^0\pi^0$, respectively). We shall assume that $\Sigma^0\pi^0\pi^+$ is identical to $\Sigma^+\pi^-\pi^+$ because in both cases the $Y_0^*(1405)$ can be formed and the final-state pions are not identical. On the other hand, we shall assume that the $\Sigma^+\pi^0\pi^0$ rate is negligible because it cannot proceed through the $Y_0^*(1405)$ intermediate state. With these assumptions, we find that the number of $Y_0^*(1405)+\pi^+$

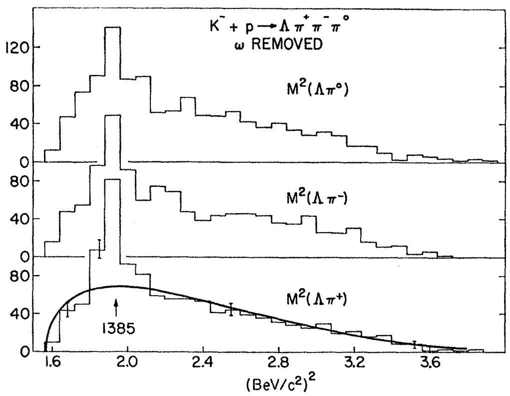

FIG. 48. Histograms of $M^2(^0\pi^+)$, $M^2(\Lambda^0\pi^-)$, and $M^2(\Lambda\pi^0)$ for non-ω $K^-p \to \Lambda^0\pi^+\pi^-\pi^0$ events.

decays of the $(1660)^+$ in a completely analyzed sample from data runs I and II, is 82 ± 15.[157]

We now search for other allowed decay modes of the positively charged[158] $Y_1^*(1660)$ beginning with the $\Lambda^0\pi^+\pi^0$ mode contained within the final state $\Lambda^0\pi^+\pi^-\pi^0$. A detailed discussion of identification problems for this final state has already been given in Sec. III A. The sample chosen here consists of 1654 uniquely identified events of which 335 have $(\pi^+\pi^-\pi^0)$ masses which correspond to the ω^0. The two-body mass distribution $M^2(\Lambda^0\pi^{\pm,0})$ of the events outside of this ω^0-mass band are shown in Figs. 48(a), 48(b), and 48(c). The approximate equal frequency of production of $Y_1^*(1385)$'s in the

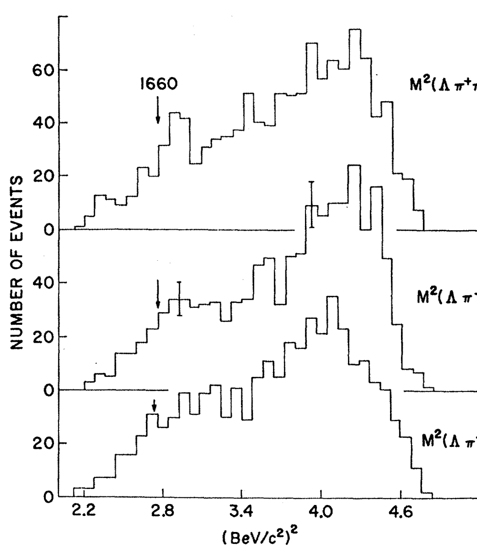

FIG. 49. Histograms of $M^2(\Lambda^0\pi^+\pi^0)$, $M^2(\Lambda^0\pi^-\pi^0)$, and $M^2(\Lambda^0\pi^+\pi^-)$ for non-ω $K^-p \to \Lambda\pi^+\pi^-\pi^0$ events.

[153] It is worthwhile to note that the existence of any amount of $Y_0^*(1405)+\pi$ decay implies that the $Y_1^*(1660)$ is a member of an octet, if the $Y_0^*(1405)$ is assumed to be a unitary singlet.

[154] The error in this determination includes both statistical and systematic uncertainties.

[155] For a discussion of similar effects in the $\Lambda\pi^+\pi^-$ final state, see R. H. Dalitz and D. Miller, Phys. Rev. Letters **6**, 562 (1961).

[156] In this connection, it is interesting to note that the Lawrence Radiation Laboratory (LRL)—University of Illinois Collaboration also observes a ratio $\gamma_\pm$ which is greater than unity for incoming K^- momenta in the range 2.45–2.7 BeV/c. (The unpublished value of ~2 is superseded by the value ~1.5 ± 0.2 reported at the 1965 Washington APS Meeting. On the other hand, Leveque *et al.* observe a ratio of ~1 at 3 BeV/c (private communication to P. Everhard). All observations ranging from 2.24 to 3 BeV/c are consistent with the pattern expected from interference which disappears as the 1660 velocity increases. However, the statistical accuracy at 2.24 and 3 BeV/c is too poor to draw firm conclusions.

[157] This includes $\Sigma^\pm$ detection efficiencies, scanning efficiencies, etc., as well as background subtraction.

[158] It is worth noting that the *neutral* $Y_1^*(1660)^0$ may also be made here. In fact, the reaction $K^- + p \to Y_1^*(1660)^0 + \pi^0$ would be expected to proceed via K^* exchange just like its charged counterpart. Unfortunately, the $Y_1^*(1660)^0$ has no detectable $(\Sigma\pi\pi)^0$ decay mode. However, the $\Lambda\pi^+\pi^-$ mode can be detected and is discussed together with the search for $\Lambda\pi^+\pi^0$ from $(1660)^+$.

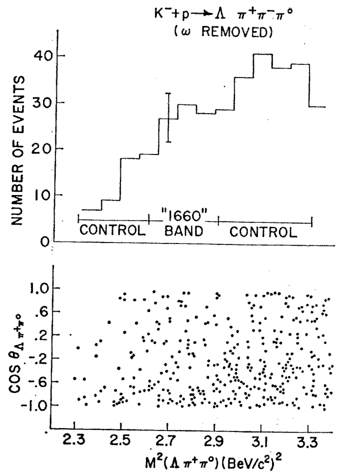

FIG. 50. Scatter plot of $M^2(\Lambda\pi^+\pi^0)$ versus production angle of π^- for non-ω $K^-p \to \Lambda\pi^+\pi^-\pi^0$ events.

three charge states is evident and is important to note for further analysis. The three-body mass distributions $M^2(\Lambda\pi\pi)$ of net charge $+$, $-$ and 0 are shown in Figs. 49(a), 49(b) and 49(c), respectively. There are no obvious enhancements in the 1660 region, and in fact the shapes of the curves may be fitted with an appropriate (7:3) combination of $(\Lambda\pi\pi)$ phase space from $K^-+p \to \Lambda^0+\pi^++\pi^-+\pi^0$ and $(Y_1{}^*\pi)$ phase space from $K^-+p \to Y_1{}^*+\pi+\pi$. We further examine the 1660 region by observing the mass versus production-angle scatter plot for $(\Lambda^0\pi^+\pi^0)$ of Fig. 50. Assuming that any real $Y_1{}^*(1660)$ contribution will be contained within the mass band 2.65–2.9(BeV/c^2)^2 (based upon the $\Sigma\pi$ study, appropriately adjusted for the poorer resolution in this channel), we compare the angular distribution of this band with that from neighboring control regions normalized to the number of events *outside* of the peripheral region. The results are shown in Fig. 51(a). The excess of "1660" over background in the peripheral region, $\cos\theta_{\Lambda\pi\pi^-} \leq -0.6$, is only 11 ± 8 events, quite consistent with zero. This study was repeated using a complete Run I+Run II sample of 1950 $\Lambda^0\pi^+\pi^-\pi^0$ final states, and yielded a 1660 signal of 2 ± 12 events. In short, the $(\Lambda\pi\pi)^+$ signal seems insignificant. Similar remarks apply to the $(\Lambda\pi\pi)^0$ signal, as indicated in Fig. 51(b). The $(\Lambda\pi\pi)^-$ spectrum, shown in Fig. 51(c) serves as a control since the $Y_1{}^*(1660)^-$ is known not to occur in this channel.

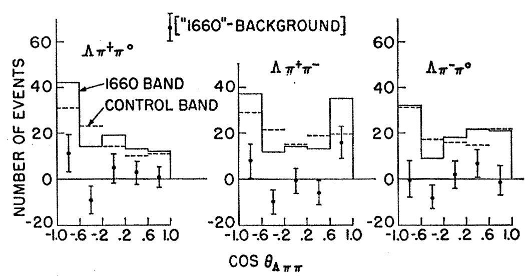

FIG. 51. Production angular distribution of "$Y_1{}^*$" band, $2.65 \leq M^2 \leq 2.90$ (BeV/c^2)^2, compared to control region for $M^2(\Lambda\pi^+\pi^0)$, $M^2(\Lambda\pi^+\pi^-)$, and $M^2(\Lambda\pi^-\pi^0)$.

The above indication of little or no $\Lambda^0\pi^+\pi^0$ decay is borne out by further investigation. Since one might expect the latter to be dominated by the $Y_1{}^*(1385)+\pi$ intermediate state, we have examined the $\Lambda\pi$ mass subspectra from peripheral events with $M(\Lambda^0\pi^+\pi^0)=1660 \pm 50$ MeV/c^2 as shown in Fig. 52(a). Comparison with the corresponding study for $(\Lambda\pi\pi)$ *control* events, shown in Fig. 52(b), indicates that the background is too high to draw any significant conclusions. It is important to note that the preference for $M(\Lambda\pi)\approx 1385$ is primarily a kinematical effect. It happens that the intersection of the two (1385) mass bands covers about 50% of the 1660 decay Dalitz Plot at our energy. Thus the $\Lambda\pi$ subspectrum of $M(\Lambda\pi\pi)\cong 1660$ MeV/c^2 events is *kinematically* constrained to contain a large proportion of $Y_1{}^*(1385)$ events which are unassociated with $Y_1{}^*(1660)$ decay. That this effect happens to be so large is a consequence of the strong $Y_1{}^*(1385)$ production of all signs of charge. We conclude that there is no significant evidence for a $\Lambda\pi\pi$ decay mode. An upper limit is given in Table X.

We have searched (within the final states listed in Table X) for the $\Sigma^+\pi^0$, $\Sigma^0\pi^+$, $\Lambda\pi^+$ and $\bar{K}^0p$ decay modes, using techniques[159] similar to those used in the $\Lambda\pi\pi$ search. The relevant data are shown in Figs. 53(a) through 53(d). Of these modes only the $\Sigma^+\pi^0$ produces a signal greater than one standard deviation. The results of the search are given in Table X.

The crude upper limits are calculated by taking two standard deviations from zero as the numerator and the total $[Y_0{}^*(1405)\pi]$ plus $(\Sigma^+\pi^0)$ contribution (109 events) as the denominator. Our results are compared with rough estimates from several Berkeley experiments[160,161] and the latest compiled values of the 1660 branching ratios.[162]

Our $\Sigma\pi/\Sigma\pi\pi$ decay ratio (0.3 ± 0.15) appears to be in disagreement with earlier estimates of ~ 1 based on very low energy K^-p data. There is no question that our result cannot be made consistent with the ratio 1.8 ± 0.05 observed in the 1.5-BeV/c data. The discrepancy may, of course, be due to interference effects which are expected to be strongest at the lower energies. To some extent than our results cast doubt on the validity of the $Y_1{}^*(1660)$ branching-ratio measurements at low energies.

3. *Properties*

In principle, information on the spin and parity of the $Y_1{}^*(1660)$ can be obtained from a study of the decay

[159] The "1660" mass band is adjusted differently in each case to reflect the appropriate mass resolution. Also, because of the dominance of $K^*(880)$ in the $\bar{K}^0\pi^-p$ sample, K^* events were removed before the 1660 search was made.

[160] L. W. Alvarez *et al.*, Phys. Rev. Letters **10**, 184 (1963).

[161] P. L. Bastien and J. P. Berge, Phys. Rev. Letters **10**, 188 (1963), and private communication from A. Barbaro-Galtieri based on K^-p data at 1.5 BeV/c.

[162] A. H. Rosenfeld *et al.*, University of California, Lawrence Radiation Laboratory Report 8030, 1965 (unpublished).

TABLE X. Branching ratios of the $Y_1^*(1660)$.

Mode	Final state used	Raw I+II sample	Fully corr. No.	Branching ratios: This experiment	Alvarez *et al.* (160)	Bastien *et al.* (161)	UCRL 8030 (162)	Eberhard *et al.* (147)	Barbaro-Galtieri *et al.* (161)
$Y_0^*(1405)\pi^+$	$\Sigma^\pm\pi^\mp\pi^+\pi^-$	50 ± 10	82 ± 14	0.75 ± 0.25	~0.18	0.28	~0.30	$\Sigma\pi\pi/\Lambda\pi\pi>0.8$	$\Sigma\pi/\Sigma\pi\pi=1.8\pm0.05$
$(\Sigma\pi)^+$	$\Sigma^+\pi^-\pi^0$, $\Sigma^0\pi^+\pi^-$	20 ± 11	27 ± 14	0.25 ± 0.15	0.27	0.26	0.30	⋯	⋯
$(\Lambda\pi\pi)_+$	$\Lambda^0\pi^+\pi^-\pi^0$	$\begin{Bmatrix}11\pm8\\2\pm12\end{Bmatrix}$	$\sim7\pm10$	$\lesssim0.2$	0.18	0.19	0.20	⋯	⋯
$(\Lambda\pi)^+$	$\Lambda^0\pi^+\pi^-$	3 ± 6	5 ± 10	<0.2	0.32	0.07	0.05	⋯	⋯
$(\bar{K}^0p)$	$\bar{K}^0p\pi^-$	0 ± 3	0 ± 9	<0.2	<0.05	0.18	0.15	⋯	⋯ %

chains (47) and (48). Two independent methods may be used. The first of these is a Dalitz plot analysis of the final states $\Sigma^+\pi^-\pi^+$ and $\Sigma^-\pi^+\pi^+$. The second is an analysis of the $Y_0^*(1405)+\pi$ angular correlations, assuming that $Y_1^*(1660)$ production is adequately described by the K^* exchange model. In both of these methods, the $Y_0^*(1405)$ is assumed[146] to have spin-parity of $\frac{1}{2}^-$ and interference with the background is ignored.

Even though the Dalitz plot information is insufficient to rule out any permissible J^P value, we present details of the analysis because it may be useful in a later compilation of the data. In addition, it is important to note that our conclusions do not agree with those reached by Leveque *et al.*[163] who carried out a similar analysis on the basis of a sample comparable to that used here.

The Dalitz plot for 49 $\Sigma^+\pi^-\pi^+$ events from this experiment and 45 from Eberhard *et al.*[147] is shown in Fig. 54, along with $\Sigma^+\pi^-$ and $\Sigma^+\pi^+$ mass projections. The solid curves represent the results of numerical integration of a typical $(\frac{3}{2}^-)$ matrix element describing the decay chain (47), taking into account the finite width[164] of the $Y_1^*(1660)$ and $Y_1^*(1405)$. As one can see, the theoretical $\Sigma^+\pi^-$ spectrum is dominated by the Breit-Wigner shape of the 1405; the peaking in $\Sigma^+\pi^+$ at 1450

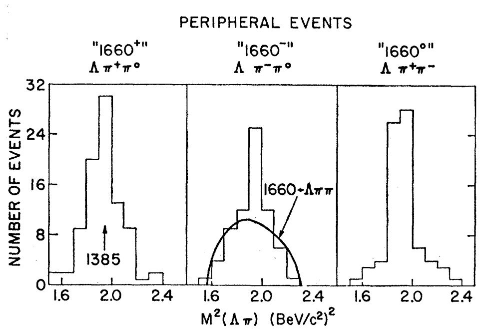

FIG. 52. $M^2(\Lambda\pi)$ histogram for $K^-p\to\Lambda\pi^+\pi^-\pi^0$ events with ω removed *and* $M(\Lambda\pi\pi)=1660\pm50$ MeV/c^2 for $M(\Lambda^0\pi^+\pi^0)$, $M(\Lambda^0\pi^-\pi^0)$ and $M(\Lambda^0\pi^+\pi^-)$.

[163] A. Leveque *et al.*, Phys. Letters **18**, 69 (1965).

[164] We use $\Gamma_{1660}=50$ MeV/c^2, $\Gamma_{1405}=40$ MeV/c^2. Resolution broadening is ignored because the $(\Sigma\pi\pi)$ mass resolution is ±10 MeV/c^2, and the $\Sigma\pi$ mass resolution is ±5 MeV/c^2.

MeV/c^2 is the result of kinematic reflection. The spin-parity dependence of the matrix element is negligible. The observed agreement simply reinforces the conclusion that the decay proceeds via the $Y_0^*(1405)$ intermediate state, and one sees no evidence of interference effects.

Before we consider the $\Sigma^-\pi^+\pi^+$ final state, it is profitable to discuss the matrix elements in more detail. The final state $\Sigma^+\pi_1^-\pi_2^+$ may be described by means of the variables $\mathbf{p}_1$, $\mathbf{p}_2$, the momenta of the pions in the 1660 rest frame, and l, L, the orbital angular momentum of the π_2 and $(\Sigma\pi_1)$ systems, respectively. Straightforward application of the conservation laws gives a single value of l for every possible J^P value of the 1660 because the $Y_0^*(1405)$ is assumed to be $\frac{1}{2}^-$, i.e. $L=0$. The nonrelativistic matrix elements are then determined by the following requirements: (i) they have the spatial transformation properties corresponding to a $\mathbf{J}=\mathbf{l}+\frac{1}{2}$, $P=(-1)^{l+1}$ transition; (ii) momentum dependence $p_2{}^l$; and (iii) a $(\Sigma\pi_1)$ resonance line shape[155] of the form

$$G(1)=G(p_1)=\left\{[M(\Sigma\pi_1)-(1405)]+i\left(\frac{40}{2}\right)\right\}^{-1}\times(M\text{eV}/c^2)^{-1}. \quad (49)$$

$G(2)$ is the same equation with π_2 substituted for π_1. The resultant matrix elements $\mathfrak{M}_l$ are given in Table XI. When averaged over the spin of the final state Σ,

TABLE XI. Matrix elements for $Y_1^*(1660)\to Y_0^*(1405)+\pi_2^+\to\Sigma^++\pi_1^-+\pi_2^+$. $J^P\to\frac{1}{2}^-+0^-$.

J^P	l	$\mathfrak{M}_l(\Sigma^+,\pi_1^-,\pi_2^+)$
$\frac{1}{2}^+$	0	$G(2)$
$\frac{1}{2}^-$	1	$[\boldsymbol{\sigma}\cdot\mathbf{p}_1]G(2)$
$\frac{3}{2}^-$	1	$[\boldsymbol{\sigma}\times\mathbf{p}_1]G(2)$
$\frac{3}{2}^+$	2	$(\boldsymbol{\sigma}\cdot\mathbf{p}_1)(\boldsymbol{\sigma}\times\mathbf{p}_1)G(2)$
$\frac{5}{2}^+$	2	$[p_1{}^\alpha p_1{}^\beta-\frac{1}{3}\delta^{\alpha\beta}p_1{}^2]G(2)$
$\frac{5}{2}^-$	3	$\{p_1{}^\alpha p_1{}^\beta p_1{}^\gamma-\frac{1}{5}(\delta^{\alpha\beta}p_1{}^\gamma+\delta^{\beta\gamma}p_1{}^\alpha+\delta^{\alpha\gamma}p_1{}^\beta)\}G(2)$

the square of the matrix element $|\mathfrak{M}_l|^2$ is of the form[165]

$$|\mathfrak{M}_l(\Sigma^+\pi^+\pi^-)|^2\approx p_2{}^{2l}|G(1)|^2. \quad (50)$$

[165] After obtaining these results, we were informed of prior and independent derivations by R. H. Dalitz and J. D. Jackson. We thank Professor Jackson for bringing this to our attention.

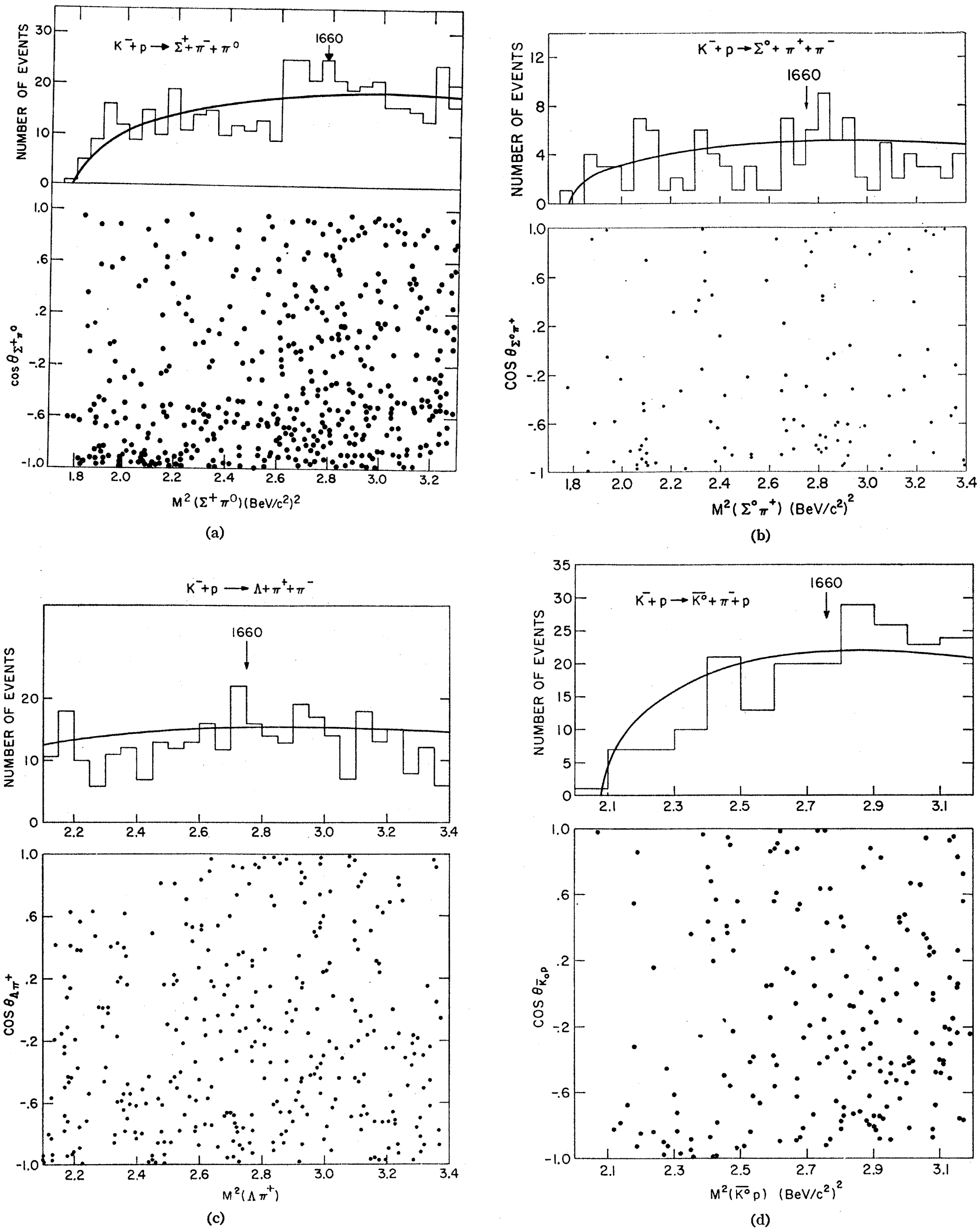

FIG. 53. (a) $M^2(\Sigma^+\pi^0)$ histogram and scatter plot for $K^-p \to \Sigma^+\pi^-\pi^0$ events. (b) $M^2(\Sigma^0\pi^+)$ histogram and scatter plot for $K^-p \to \Sigma^0\pi^+\pi^-$ events. (c) $M^2(\Lambda\pi^+)$ histogram and scatter plot for $K^-p \to \Lambda\pi^+\pi^-$ events. (d) $M^2(\bar{K}^0p)$ histogram and scatter plot for $K^-p \to \bar{K}^0p\pi^-$ events.

Similar remarks apply to the analysis of the $\Sigma^-\pi_1^+\pi_2^+$ final state. The only difference here is that one must symmetrize the amplitude between the pions 1 and 2 because of Bose symmetry. One then obtains the spin averaged result[165]

$$|\mathfrak{M}_l(\Sigma^-\pi^+\pi^+)|^2 \simeq \tfrac{1}{2}\{p_2^{2l}|G(1)|^2+p_1^{2l}|G(2)|^2 +2p_1^l p_2^l[\mathrm{Re}G^*(1)G(2)]P_l(\theta_{12})\}, \quad (51)$$

where $P_l(\theta_{12})$ is an lth order Legendre polynomial of the angle θ_{12} between $\mathbf{p}_1$ and $\mathbf{p}_2$. This expression has been numerically integrated over the 1660 decay region, and the results are compared with the experimental data[166]

[166] The data consist of 24 $\Sigma^-\pi^+\pi^+$ events from this experiment and 26 events from the LRL—Illinois experiment. Each event has two $\Sigma^-\pi^+$ combinations, and each is plotted twice, once as $\Sigma^-\pi_1^+$ and once as $\Sigma^-\pi_2^+$, so the plot contains 100 points.

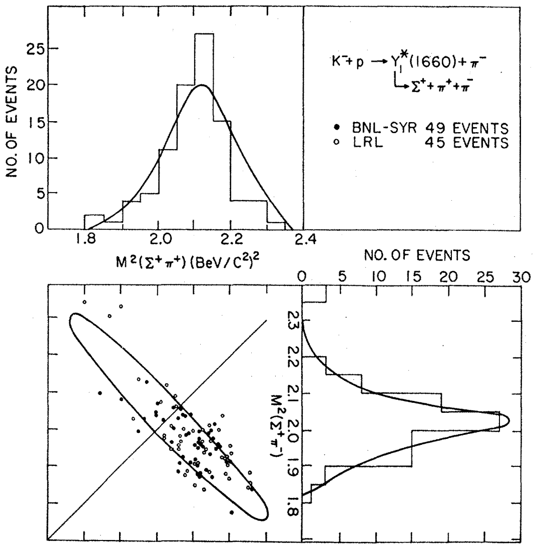

FIG. 54. Dalitz plot for 94 $\Sigma^+\pi^-\pi^+$ events, with $M^2(\Sigma^+\pi^-)$ and $M^2(\Sigma^+\pi^+)$ projections, with prediction of $\frac{3}{2}^-$ matrix element.

in Fig. 55 for $l=0$, 1 and 2. Although the sensitivity to the assumed J^P value of the 1660 is greater in this case than in the $\Sigma^+\pi^+\pi^-$ case, it is clear that no J^P value may be eliminated. We have reanalyzed our own 24 event sample using *normalized* Dalitz coordinates to avoid complications due to the finite width of the 1660, and find no change in the results. Also, we note that the Σ^- kinetic-energy spectrum (not shown) does not peak near zero energy in contrast to the results of Leveque *et al.*[163] We conclude that there is no evidence favoring $J^P=\frac{3}{2}^+$ from this analysis. Finally, we note that our results do not disagree with (nor of course do they confirm) the recent[167] Lawrence Radiation Laboratory-Illinois results which favor $\frac{3}{2}^-$; the latter analysis is carried out using a *selected* region of the Dalitz plot and uses considerably more data than our analysis.

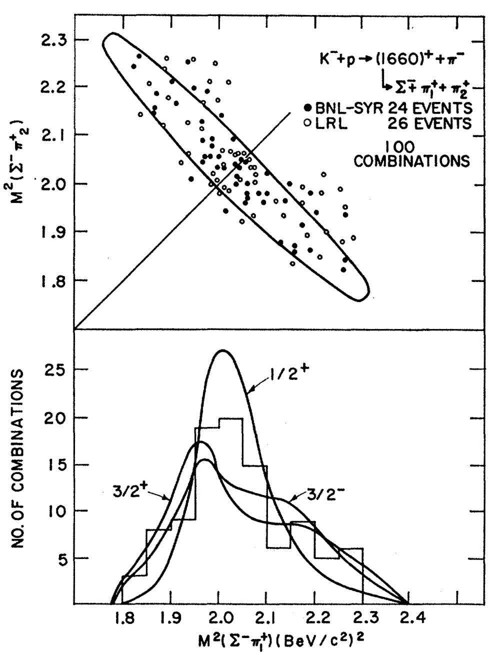

FIG. 55. Dalitz plot for 50 $\Sigma^-\pi^+\pi^+$ events, plotted twice, with $M^2(\Sigma^-\pi^+)$ projection, with predictions for $l=0$, 1, 2 (see text).

We now study the angular distributions of the $Y_0^*(1405)$ from the decay of the $Y_1^*(1660)$. As emphasized earlier, the extreme peripherality of $Y_1^*(1660)^+$ production and the absence of $Y_1^*(1660)^-$ production, indicate the operation of the K^*-exchange mechanism. A quantitative test of the latter is illustrated in Fig. 56. Here the observed production angular distribution[168] of the $Y_1^*(1660)$ is compared with a typical[169] prediction in which absorption effects are included. The agreement is entirely adequate.

The decay angular distributions for our sample of 45 $Y_1^*(1660)^+ \to Y_0^*(1405)+\pi^+ \to \Sigma^++\pi^-+\pi^+$ decays,[170]

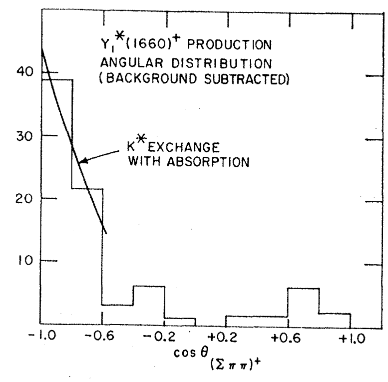

FIG. 56. $Y_1^*(1660)^+$ production angular distribution for

$$K^-p \to \pi^- Y_1^{*+} \searrow \Sigma^\pm\pi^\mp\pi^+$$

events, with background subtracted, compared to prediction of K^* exchange model with absorption effects.

are given in Fig. 57(a) and 57(b). The coordinate system illustrated in Fig. 57(c) is chosen because it is known that $\frac{3}{2}^+$ resonances, if produced via $M2$ dominant K^* exchange, decay in a strikingly anisotropic fashion when observed in this system. A prime example is the $Y_1^*(1385)^+$, whose decay distributions are shown in Figs. 41 and 44 of Sec. III D. The predictions of the magnetic dipole dominance version[171] of the K^* ex-

[167] At the 1965 Washington American Physical Society meeting, P. Eberhard reported strong evidence for $\frac{3}{2}^-$ on the basis of a somewhat different analysis of the Dalitz plot information concerning a 99-event $\Sigma^-\pi^+\pi^+$ sample from the LRL—Illinois experiment.

[168] A background subtraction has been made using the same techniques as those employed in the case of the $Y_1^*(1385)$. See Sec. IIID for details.

[169] The curve shown in Fig. 56 corresponds to an electric dipole (E_1) dominance model which is consistent with $J^P=\frac{3}{2}^-$. This assumption is of little significance, however, inasmuch as the observed peripherality is primarily due to the effects of absorption rather than the particular form of the matrix element. In fact, the $\frac{3}{2}^+$ magnetic-dipole model prediction fits almost as well.

[170] The $\Sigma^-\pi^+\pi^+$ sample is not useful because of the indistinguishability of final-state pions.

[171] A complete discussion of this model is given in our analysis of the $Y_1^*(1385)$ hyperon. See Sec. IIID for details and references.

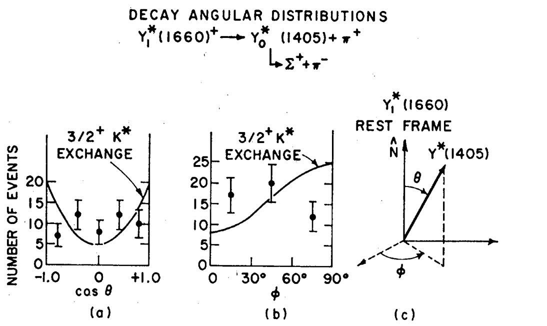

FIG. 57. (a) $Y_1^*(1660)$ polar-decay angular distribution. (b) $Y_1^*(1660)$ azimuthal-decay angular distribution. (c) Definition of coordinate system.

change model,[172] appropriate for $\frac{3}{2}^+$ hyperon decay are

$$W(\theta)\approx(1+3\cos^2\theta)d(\cos\theta)$$
$$W(\varphi)\approx(1-\tfrac{2}{3}\cos^2\varphi)d\varphi.$$

These distributions are shown as the solid curves of Figs. 57(a) and 57(b). The disagreement with experiment is evident; the over-all χ^2 probability for a fit, based upon statistical errors only, is less than 0.2%. Uncertainties due to the size of the background, possible interference effects, etc., have been ignored. Although the above evidence strongly suggests that $J^P\neq\frac{3}{2}^+$, it cannot be considered conclusive. Nevertheless, we believe that it is sufficient to nullify previous (weak) evidence[163,173] favoring $\frac{3}{2}^+$. Indeed, as mentioned above, recent evidence[167,174] appears to favor $\frac{3}{2}^-$. In this connection, it is relevant to note that the $M2$-dominance model does not make unique predictions[175] for $\frac{3}{2}^-$ decay. For this reason we have not attempted a quantitative test of the $\frac{3}{2}^-$ hypothesis.

IV. TWO AND THREE-BODY REACTIONS

In this section we present data concerning those identifiable reactions not considered elsewhere. The $\bar{K}^0N$ and $(K^*)^-p$ reactions are discussed in some detail while the other two- and three-body reactions are considered qualitatively. Most of the 20 two-body reactions appear to be produced predominantly by means of meson or baryon exchange. The two (apparent) exceptions are $\Lambda+\omega$ and $Y_0^*(1520)+\pi^0$. Three-body reactions which contribute to 4- and 5-body final states are discussed.

A. Two-Body Reactions

The reactions of interest here are listed in Table XII. Pertinent information concerning these reactions is described in this table. This includes: (i) the final states from which the samples are selected; (ii) the criteria used to select the samples; (iii) background subtraction information; and (iv) the net number of events after background subtraction and other items. This information is a summary of details discussed elsewhere; references to the original discussions are given in Table XII. The two final states not previously considered, namely, $\bar{K}^0n$ and $\bar{K}^0\pi^-p$ are discussed below.

1. Charge Exchange

The final state $\bar{K}^0$+MM is separated from the "V^0+MM" topology with virtually no ambiguity. Of the single V^0 candidates, only about 3% are ambiguous between $\bar{K}^0$ and Λ^0, and these are omitted from the sample. The pion-induced contamination from $\Lambda^0K^0(\pi^0)$, as ascertained from an analysis of events in which both the Λ^0 and K^0 decay visibly,[176] is negligibly small ($\approx$20 events). The same is true of contamination from the very rare modes[176] Ξ^0K^0, $\Lambda K^0\bar{K}^0$ and $\Sigma^0K^0\bar{K}^0$.

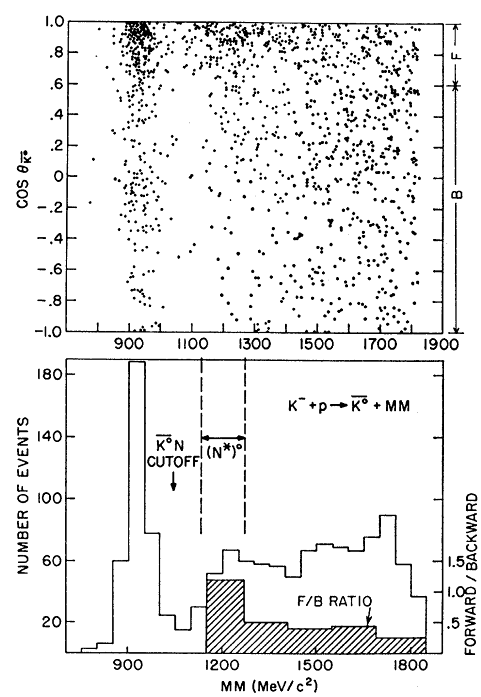

FIG. 58. Scattergram of (MM) as a function of $\bar{K}^0$ center of mass production angle, with (MM) production and forward-backward ratio (see text) as a function of (MM) for 1178 $K^-p\rightarrow\bar{K}^0$+neutrals events.

[172] Absorption is ignored here. Calculations carried out for the $Y_1^*(1385)$ hyperon show that decay distributions are trivially altered by absorption effects at our energy.

[173] M. Taher-Zadeh *et al.*, Phys. Rev. Letters **11**, 470 (1963).

[174] D. Berley *et al.*, *Proceedings of the 12th Annual International Conference on High Energy Physics, Dubna, 1964* (Atomizdat, Moscow, 1965).

[175] In the case of $\frac{3}{2}^+$ decay, in addition to K^* exchange, the $\rho-K^*$-photon analogy is used as a basis for the assumption of M_1 dominance. This leads to unique predictions. In the case of $\frac{3}{2}^-$ decay, there is no basis for any analogous simplifying assumptions. Of course, other theories may well offer predictions concerning the relative contributions of electric, magnetic and longitudinal matrix elements. One such is the $SU(6)_W$ theory of H. Lipkin *et al.* [Phys. Rev. Letters **14**, 670 (1965)] and Carter *et al.* (to be published). It appears to us that the uncertain status of such theories does not warrant their use in spin-parity determinations.

[176] See discussion in Sec. IIIA.

TABLE XII. Definition of samples of two-body final states. See text.

Reaction	Final state	Discussion of final state	Selection criteria: Effective mass (BeV/c^2)^2	Selection criteria: "Background" subtractions	Events[a] in sample after background subtraction and geometrical loss	% Estimated purity of sample
$\Sigma^-\pi^+$	$\Sigma^-\pi^+$	III D	···	···	123	$>90\%$
$\Sigma^+\pi^-$	$\Sigma^+\pi^-$	III D	···	···	464	$>90\%$
$\Sigma^+\rho^-$	$\Sigma^+\pi^-\pi^0$	III D	$M^2(\pi^-\pi^0)=0.45-0.65$	$\{Y_1^*(1385)$, $Y_0^*(1405)$	129	$\gtrsim 80\%$
$\Sigma^-\rho^+$	$\Sigma^-\pi^+\pi^0$	III D	$M^2(\pi^+\pi^0)=0.45-0.65$	$Y_0^*(1520)$ and C.R.*$\}$	56	$\sim 70\%$
$Y^*(1520)\pi^0$	$\Sigma^\pm\pi^\mp\pi^0$	III D	$M^2(\Sigma^\pm\pi^\mp)=0.225-0.235$	C.R.	134	$\gtrsim 85\%$
$\Lambda\pi^0$	ΛMM	III A	$(MM)^2=\leq 0.12$	···	363	$\approx 95\%$
$\Lambda\eta^0$	$\{\Lambda MM$, $\Lambda\pi^+\pi^-\pi^0$	III A, III D	$MM^2=0.50-0.60$	C.R.	30	$>70\%$
$\Lambda\rho^0$	$\Lambda\pi^+\pi^-$	III D	$M^2(\pi^+\pi^-)=0.45-0.65$	C.R. and $Y_1^*(1385)^\pm$	58	$\gtrsim 60\%$
$\Lambda\omega$	$\Lambda\pi^+\pi^-\pi^0$	III A, III D	$M^2(\pi^+\pi^-\pi^0)=0.56-0.70$	···	261	$>85\%$
$\bar{K}^0N$	$\bar{K}^0MM$	IV	$MM\leq 1.02$	···	411	$\gtrsim 98\%$
$K^{*-}p$	$K^0\pi^-p$	IV	$M^2(K\pi)=0.72-0.88$	Non-K^* events	263 $\cos\theta_{K^*}>0.6$	$\gtrsim 95\%$
Ξ^-K^+	Ξ^-K^+	V	···	···	244	$\gtrsim 95\%$
Ξ^-K^{*+}	$\{\Xi^-\pi^+K^0$, $\Xi^-\pi^0K^+$	III C	$M^2(K\pi)=0.72-0.90$	···	240*	$\gtrapprox 80\%$
$(\Xi^*)^0K^0$	$\Xi^-\pi^+K^0$	III C	$M^2(\Xi\pi)=0.23-0.24$	···	199*	$\gtrapprox 85\%$

[a] Control-region shape, normalized to events in background.

Figure 58 shows the MM as a function of $\bar{K}^0$(c.m.) production angle for an 1178 event sample. One sees that the charge-exchange reaction is a major contributor to the final state. There is an indication of a peripheral excess in the neighborhood[177] of the $N^*(1238)^0$ mass, but no significant trace of higher nuclear resonances. The peripherality of the N^* peak is indicated by the forward to backward ratio ($F\rightarrow\cos\theta_{K^0}\geq 0.7$, $B\rightarrow\cos\theta_{K^0}<0.7$) shown under the mass projection. From Fig. 58, we estimate the relative contributions to the $\bar{K}^0$MM final state as follows:

Channel	Relative proportion
$\bar{K}^0N$	9
$\bar{K}^0N^*(1238)^0$	1
$\bar{K}^0N(n\pi)+\bar{K}^{*0}N$	21.

Because of the excellent mass separation, we adopt the criterion 850 MeV/$c^2\leq$MM$\leq$1020 MeV/c^2 for the selection of the $\bar{K}^0N$ sample, resulting in a sample of 333 events. The angular distribution of these events, after correction for geometrical detection efficiencies[178] is shown in Fig. 59. There is no indication of a relative depletion near 0°, an effect which has been observed[179,180] at the neighboring momenta of 1.8 BeV/c and 2.45 BeV/c. Since potential biases in the forward hemisphere are in the direction of producing such a forward dip, we believe its absence here is significant. To compare the data with that at other energies, it has been fit with the standard Legendre polynomial expansion

$$f(\theta)=\sum_{l=0}^{l_{\max}} B_nP_n(\cos\theta).$$

The results of the fits for $l_{\max}=1$, 2, 3 are summarized in Table XIII. Both the $l_{\max}=2$ and 3 fits are adequate, indicating the importance of partial waves with $L\geq 2$. This is in agreement with the results at 2.45 BeV/c, and may be contrasted with the need for $L\geq 5$ at 1.8 BeV/c.

TABLE XIII. Results of best fits to production angular distributions for charge exchange.

	S-P fit	S, P, D	S, P, D, F
B_0	9.5±0.6	11.2±0.63	11.3±0.63
B_1	15.5±1.3	20.1±1.6	19.9±1.6
B_2	8.0±1.2	14.1±1.6	13.3±1.7
B_3	···	8.6±1.4	8.6±1.5
B_4	···	6.8±1.2	5.7±1.6
B_5	···	···	−0.75±1.5
B_6	···	···	−0.25±1.2

The forward peaking is consistent with ρ-exchange dominance in the small-momentum-transfer region.

2. The $(K^*)^-p$ Reaction

Owing to the small Λ^0, K^0 ambiguity and the marked ionization difference between a π^+ and p of momentum $\lesssim$1 BeV/c, the $\bar{K}^0\pi^-p$ final state is well separated from

[177] The center of the peripheral enhancement appears at $\approx$1200 MeV. It is well known that the apparent mass of a broad resonance like the N^* is displaced downward from its true mass.

[178] Two corrections are applied: (1) the "escape" correction for forward K^0's ($\approx$12%); and (2) the "lifetime" correction for backward K^0's ($\sim$2%).

[179] P. M. Dauber, Phys. Rev. 134, B1370 (1964).

[180] A. Barbaro-Galtieri and R. Tripp, Lawrence Radiation Laboratory, University of California Report No. UCRL 11429 (unpublished).

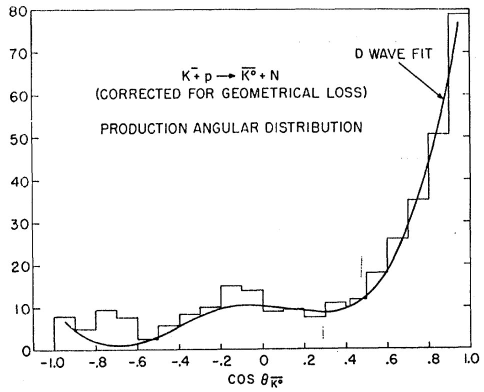

FIG. 59. $\bar{K}^0$-production angular distribution, corrected for geometrical losses, for 333 $K^-p \rightarrow \bar{K}^0+N$ events, fitted with s, p and d waves.

all "2 prong$+V^0$" candidates. The only source of background is the associated one-constraint fit $\bar{K}^0\pi^-p\pi^0$. The 23 ambiguous events of this type are omitted from the 652-event sample.

The $M^2(\bar{K}^0\pi^-)$ plot of Fig. 60 shows that the $(K^*)^-p$ reaction dominates the final state. The associated $M^2(\pi^-p)$ distribution (not shown) and $M^2(\bar{K}^0p)$ distribution [Fig. 53(d) of Sec. III E] indicate no significant $N^*(1238)$ or $Y_1^*(1660)$ production. From Fig. 60(a), we estimate that the 346-event mass band defined by 0.72 $(\mathrm{BeV}/c^2)^2 \leq M^2(\bar{K}^0\pi^-) \leq 0.88$ $(\mathrm{BeV}/c^2)^2$ contains 64 background events. The production angular distribution of this mass band is shown in Fig. 60(b). It is compared with the angular distribution of events well outside the K^* band, which is seen to be roughly isotropic. The contribution of the background in the region $\cos\theta_{K^*} \geq +0.6$ is only $\sim$12 events, as indicated by

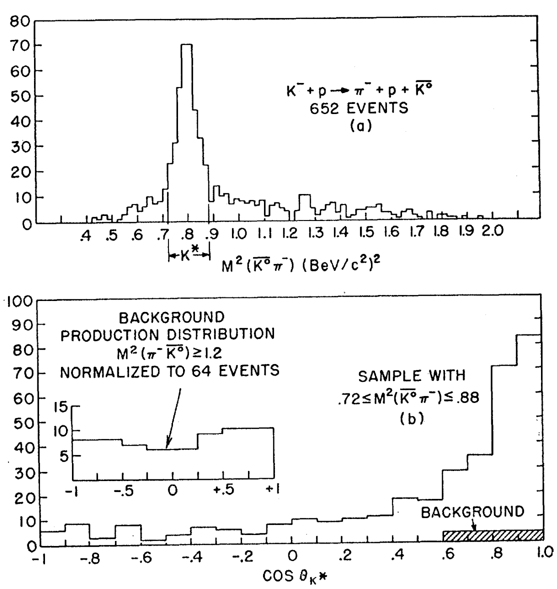

FIG. 60. (a) $M^2(\bar{K}^0\pi^-)$ histogram for 652 $K^-p \rightarrow \bar{K}^0\pi^-p$ events. (b) K^*-production angular distribution for 346 $K^-p \rightarrow K^{*-}p$ events compared to control region outside K^* band.

the shaded area under the peak. The corrected production angular distribution is shown in Fig. 61.

The peripherality of the K^* distribution is undoubtedly a reflection of one-meson exchange. For this reaction any or all of π, ρ, ω, or ϕ exchange are permitted. In view of the possible complexity of the exchange process, it is necessary to make use of information obtained from K^* production obtained in K^--deuterium reactions which have been studied by Goldhaber *et al.*[181] Jackson[139] has found that the K^--d experiments may be fitted if both π and vector (ϕ and ω, not ρ) exchange are invoked. In fact, he finds two solutions for the vector couplings, one corresponding to constructive interference in the π- and vector-exchange amplitudes and a nonzero tensor/vector

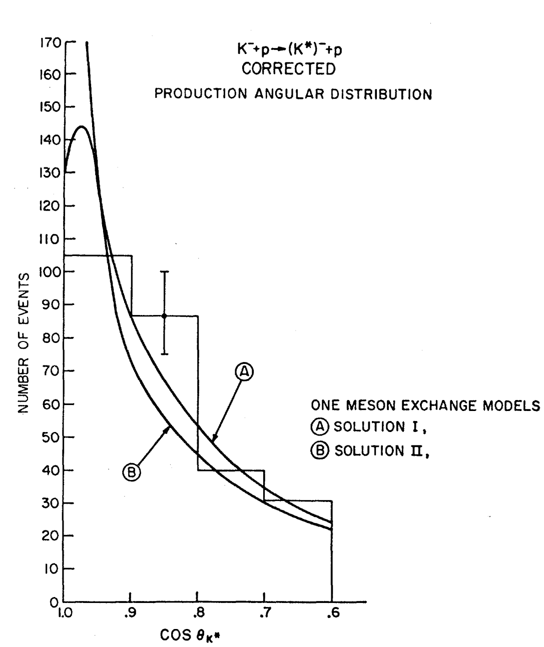

FIG. 61. Corrected K^*-production angular distribution for $K^-p \rightarrow K^{*-}p$ events compared to two Jackson solutions (see text).

coupling (solution A), and the other corresponding to destructive interference and a zero tensor coupling (solution B). Both of these solutions, which contain absorption effects, are in rough agreement with the observed K^* production angular distribution as shown in Fig. 61. Further information is obtained from a study of K^* decay.

In its own rest frame the decay angular distribution of the K^* is given by[182]

$$W(\theta_J,\phi_J) \approx \{\rho_{00}\cos^2\theta_J + \rho_{11}\sin^2\theta_J - \rho_{1-1}^2\sin^2\theta_J\cos 2\phi_J - \sqrt{2}\,\mathrm{Re}\rho_{10}\sin 2\theta_J\cos\phi_J\}\,d(\cos\theta_J)d\phi_J, \quad (52)$$

[181] S. Goldhaber *et al.*, paper presented at The International Conference on High Energy Physics, 1964, Dubna, USSR.

[182] K. Gottfried and J. D. Jackson, Nuovo Cimento 33, 309 (1964); Phys. Letters 8, 144 (1964).

TABLE XIV. Comparison of best fits to decay angular distribution of K^* (in K^*p final state) with the calculated density matrix elements.

	$\rho_{0,0}$	$\rho_{1,-1}$	$\mathrm{Re}\rho_{1,0}$
Expt.	0.47±0.06	0.33±0.04	−0.067±0.028
Theory Sol. A	0.37	0.19	−0.12
Theory Sol. B	0.27	0.21	−0.10

where the density matrix elements ρ_{ij} and decay angles are defined in the coordinate system of Fig. 62(a). The observed angular distributions are compared with the predictions corresponding to solutions A, B, in Fig. 62(b). Table XIV compares the calculated and experimental density matrix elements. Although there is qualitative agreement, neither solution appears to be entirely satisfactory. However, with the experience gained in our study of other meson exchange reactions,[183] we anticipate that the fit may easily be improved if the vector exchange amplitude is increased. The integrated K^* production cross section for the peripheral region $\cos\theta_{K^*} \geqslant 0.6$ is about 1.55 mb, in reasonable agreement with the ≈ 1.3 mb predicted by the exchange model with absorption.

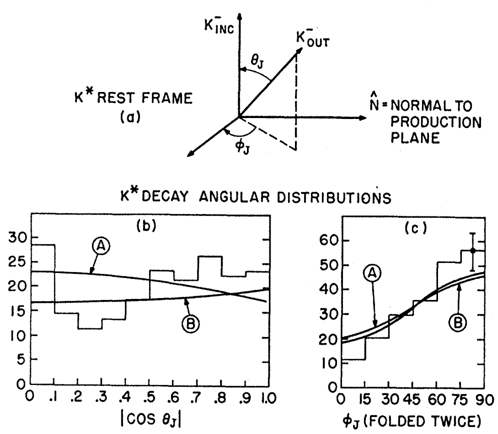

FIG. 62. (a) Definition of coordinate system for K^* decay. (b) K^* polar and (c) azimuthal decay angular distributions, compared to two Jackson solutions (see text).

3. Other Two-Body Reactions

The center-of-mass angular distributions of the reactions described in Table XII are shown in Figs. 59, 61, 63(a)–63(j) and 64. For the two-body reactions discussed previously, see Figs. 19, 26, 35, 44, 56. The dominant characteristics of all these angular distributions are summarized in Table XV. A summary of permissible exchange processes is also given. One sees that the vast majority of all two-body reactions are in qualitative agreement with the hypothesis that one-particle-exchange processes dominate the production process. If one excludes the Ξ^*K reaction because of its nearness to threshold, it appears that most reactions are dominated by meson exchange when they are allowed, and otherwise by baryon exchange. Only the

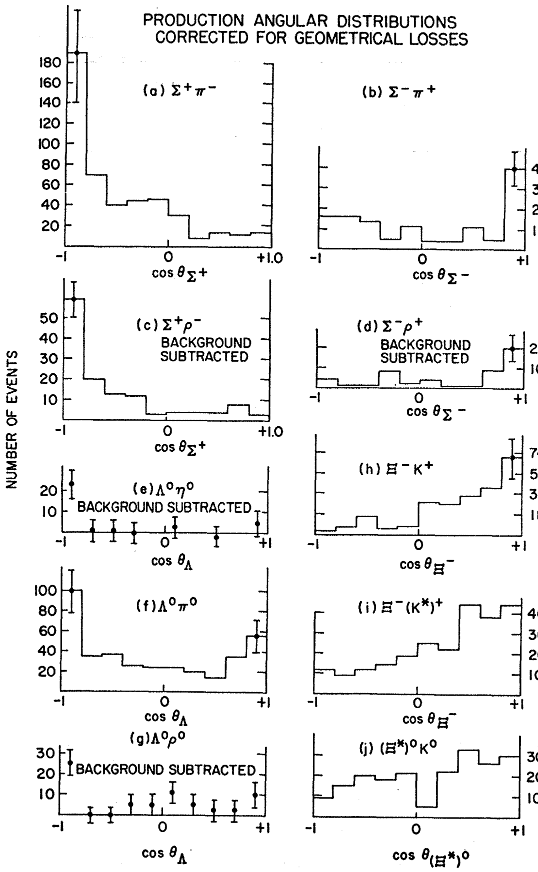

FIG. 63. (a) Σ^+ production angular distribution for $\Sigma^+\pi^-$ final state. (b) Σ^- production angular distribution for $\Sigma^-\pi^+$ final state. (c) Σ^+ production angular distribution for $\Sigma^+\rho^-$ final state. (d) Σ^- production angular distribution for $\Sigma^-\rho^+$ final state. (e) Λ^0 production angular distribution for $\Lambda^0\eta^0$ final state. (f) Λ^0 production angular distribution for $\Lambda^0\pi^0$ final state. (g) Λ^0 production angular distribution for $\Lambda^0\rho^0$ final state. (h) Ξ^- production angular distribution for Ξ^-K^+ final state. (i) Ξ^- production angular distribution for $\Xi^-(K^*)^+$ final state. (j) $(\Xi^*)^0$ production angular distribution for $(\Xi^*)^0K^0$ final state.

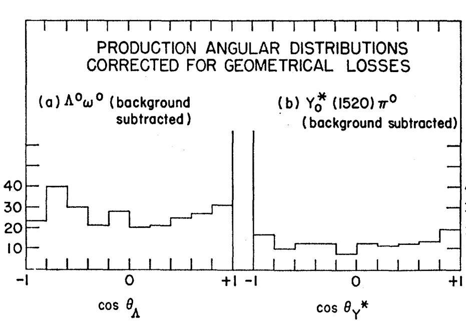

FIG. 64. (a) Λ^0-production angular distribution for $\Lambda^0\omega^0$ final state. (b) $Y_0^*(1520)$ production angular distribution for $Y_0^*(1520)\pi^0$ final state.

[183] J. D. Jackson (private communication).

TABLE XV. Dominant characteristics of production angular distributions for various two-body final states. See text.

	Hyperon ang. dist.	Allowed meson exchange	Allowed baryon exchange
$\bar{K}^0+N$	Backward-peaked	ρ	Forbidden
$\bar{K}^0+(N^*)^0$	Backward-peaked	ρ	Forbidden
$\Lambda+\eta^*$	Backward-peaked	K^*	p
$\Lambda+\eta^0$	Backward-peaked	K^*	p
$\Lambda+\rho^0$	Backward-peaked	K^*, K	p
$\Sigma^++\pi^-$	Backward-peaked	K^*	$(N^*)^{++}$
$\Sigma^++\rho^-$	Backward-peaked	K^*, K	$(N^*)^{++}$
$Y_1^*(1385)^++\pi^-$	Backward-peaked	K^*	$(N^*)^{++}$
$Y_0^*(1405)+\pi^0$	Backward-peaked	K^*	p
$Y_1^*(1660)^++\pi^-$	Backward-peaked	K^*	$(N^*)^{++}$
$\Lambda\phi$	Backward-peaked	K^*, K	p
$\Lambda\pi^0$	Backward and forward	K^*	p
$\Sigma^-+\pi^+$	Forward-peaked	Forbidden	N
$\Sigma^-+\rho^+$	Forward-peaked	Forbidden	N
Ξ^-+K^+	Forward-peaked	Forbidden	Λ^0
$\Xi^-+(K^*)^+$	Forward-peaked	Forbidden	Λ^0
$Y_1^*(1385)^-+\pi^+$	Forward-peaked	Forbidden	N
$\Xi^*(1530)^0+K^0$	Isotropic	Forbidden	Σ^+
$\Lambda\omega$	Isotropic	K^*, K	p
$Y_0^*(1520)+\pi^0$	Isotropic	K^*	p

$\Lambda\pi^0$ reaction appears to require both. The exceptions to this "exchange dominance" model are the $\Lambda\omega^0$ and $Y_0^*(1520)\pi^0$ reactions.

A few speculative remarks concerning these "anomalous" reactions are in order. When contrasted with the relatively normal behavior of the $\Lambda\phi$ reaction, the $\Lambda\omega$ reaction must be considered anomalous. Within the framework of the peripheral model, the observed disagreement must be attributed to differences in the final-state interactions of the physical ϕ and physical ω. It is difficult to reconcile such a difference with the proposed 60:40 SU(3) mixture properties of the ϕ and ω.

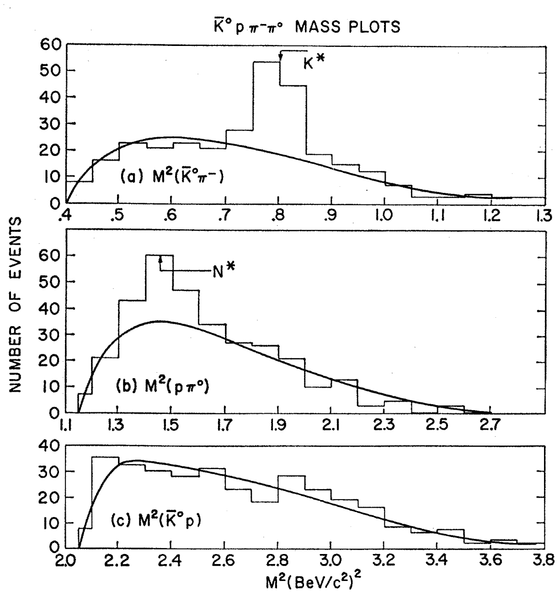

FIG. 65. (a) $M^2(\bar{K}^0\pi^-)$ histogram for 321 $K^-p\rightarrow\bar{K}^0p\pi^-\pi^0$ events. (b) $M^2(p\pi^0)$ histogram for same sample. (c) $M^2(\bar{K}^0p)$ histogram for same sample.

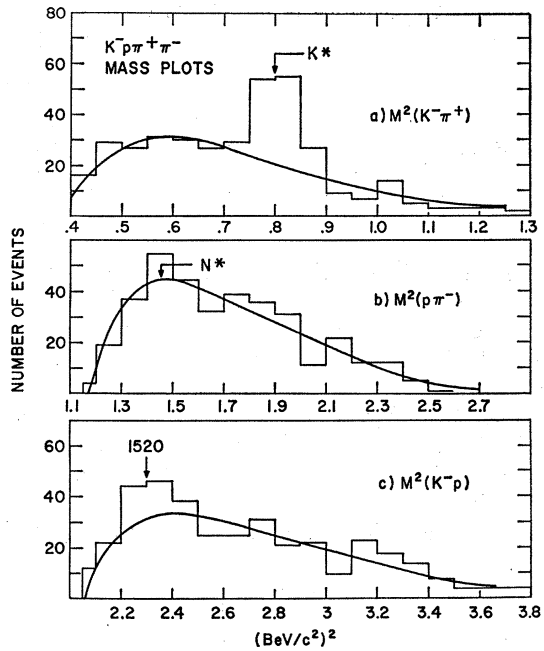

FIG. 66. (a) $M^2(K^-\pi^+)$ histogram for 371 $K^-p\rightarrow K^-p\pi^+\pi^-$ events. (b) $M^2(p\pi^-)$ histogram for same sample. (c) $M^2(K^-p)$ histogram for same sample.

Finally, we note that the isotropy of $Y_0^*(1520)$ production is in direct contrast to the extreme peripherality of $Y_1^*(1385)$, $Y_0^*(1405)$, and $Y_1^*(1660)$ production. The contrast is heightened by the fact that all three of the latter resonances have different quantum numbers and (presumably) belong to different $SU(3)$ multiplets, and yet are consistent with K^* exchange, while $Y_0^*(1520)$ is not.[184] To attribute the $Y_0^*(1520)$ isotropy to coherent contributions from *both* meson and baryon exchange seems unwarranted in view of the relatively small role played by baryon exchange in similar reactions. Thus $Y_0^*(1520)+\pi^0$ production cannot easily be understood on the basis of peripheral mechanisms and may, in fact, require a qualitatively different model.[185]

B. Some Three-Body Reactions

We shall now briefly describe those multiparticle final states which contain identifiable three-body reac-

[184] For the sake of obtaining a quantitative estimate of the disagreement with K^* exchange, we have calculated the expected angular distribution assuming E_1 dominance (since $J^P=\frac{3}{2}^-$ for the 1520) and standard absorption parameters. The results are in violent disagreement with isotropy, predicting a factor of 3 decrease from $\cos\theta_{Y^*(1520)}=-1$ to $\cos\theta_{Y^*(1520)}=-0.6$.

[185] A simple, (but far-reaching) possibility is the existence of a new resonance of mass in the neighborhood of 2330 MeV/c^2, i.e., the available c.m. energy in this experiment. The creation of a virtual $Y_1^*(\approx 2300)$ with subsequent preferential decay into $Y_0^*(1520)+\pi^0$ could produce the observed isotropy.

tions. These final states are:

$$\bar{K}^0 p\pi^-\pi^0, \quad \text{(a)}$$
$$K^- p\pi^+\pi^-, \quad \text{(b)}$$
$$\bar{K}^0 N\pi^+\pi^-, \quad \text{(c)}$$
$$\Sigma^+\pi^-\pi^+\pi^-\pi^0, \quad \text{(d)}$$
$$\Sigma^-\pi^+\pi^+\pi^-\pi^0, \quad \text{(e)}$$
$$\Sigma^{\mp}\pi^{\pm}+\text{missing neutrals}(\geq 2m_{\pi^0}). \quad \text{(f)}$$

There is negligible ambiguity in the identification[186] of these final states. The four-body kaon channels (a), (b), and (c), containing 321, 371 and 301 events, respectively, are analyzed for intermediate resonance production in Figs. 65, 66, and 67. The effective-mass plots clearly indicate that the $K^*(888)$, $N^*(1238)$, and $Y_0^*(1520)$ are involved. There is no significant evidence for the production of $Y_1^*(1660)$, $Y_1^*(1765)$, $Y_0^*(1815)$, or ρ. From these data we estimate the contributions to the final states (a), (b), and (c) as follows:

(a) Final state $\bar{K}^0 p\pi^-\pi^0$

Intermediate state	Relative contribution
$(K^*)^- p\pi^0$	0.2
$(K^*)^0 p\pi^-$	0.05
$(N^*)^0\bar{K}^0\pi^0$	0.12
$\bar{K}^0 p\pi^-\pi^0$	0.63

(b) Final state $K^- p\pi^+\pi^-$

Intermediate state	Relative contribution
$(K^*)^0 p\pi^-$	0.2
$(N^*)^{++}K^-\pi^-$	0.2
$Y_0^*(1520)\pi^+\pi^-$	0.08
$K^- p\pi^+\pi^-$	0.52

(c) Final state $\bar{K}^0 n\pi^+\pi^-$

Intermediate state	Relative contribution
$(K^*)^- n\pi^+$	0.2
$(N^*)^-\bar{K}^0\pi^+$	0.05
$Y_0^*(1520)\pi^+\pi^-$	0.05
$\bar{K}^0 n\pi^+\pi^-$	0.7

It is interesting to note that the $Y_0^*(1520)$ plays a relatively minor role in the formation of (b) and (c). This is in direct contrast to the situation at lower energies.[187] Also, there is no significant production ($<3\%$) of the two-body reaction

$$K^- + p \rightarrow N^*(1238) + K^*(888).$$

[186] The fitted final states are estimated to be $\gtrsim 95\%$ pure, since ambiguous fits are not used in this study. The $\Sigma^{\mp}\pi^{\pm}$+missing mass sample is undoubtedly omission-biased at low effective masses since each event can easily satisfy the loose 1C fit criteria for $\Sigma^{\pm}\pi^{\mp}\pi^0$. This is only a $\lesssim 15\%$ effect, however.

[187] S. P. Almeida and G. R. Lynch, Phys. Letters 9, 204 (1964).

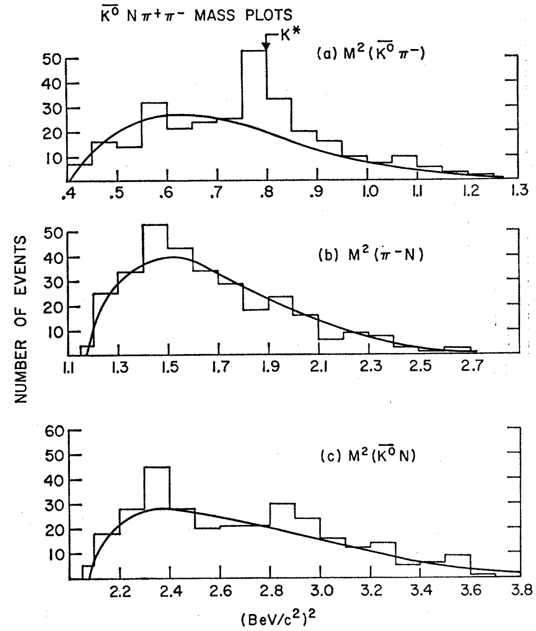

FIG. 67. (a) $M^2(\bar{K}^0\pi^-)$ histogram for 301 $K^-p\rightarrow\bar{K}^0N\pi^+\pi^-$ events. (b) $M^2(\pi^-N)$ histogram for same sample. (c) $M^2(\bar{K}^0N)$ histogram for same sample.

Finally, we turn to the five-body Σ final states. A study of the relevant two-body effective masses (not shown) indicates no appreciable Y^* or ρ production. On the other hand, the 3-pion mass spectra from (d) and (e) shown in Fig. 68 reveal that the latter are dominated by ω^0 and η^0 production. A study of the neutral-missing-mass spectrum from (f) (see Fig. 69) provides additional evidence for $\Sigma^{\pm}\pi^{\mp}\eta^0$ production. Following a suggestion by Gyuk and Tuan,[188] we have searched for indications of $\Sigma\eta$ and $\Sigma\omega$ resonances (see Fig. 70) and find a null result, corresponding to an upper limit for the production of such resonances of $\lesssim 5\ \mu$b.

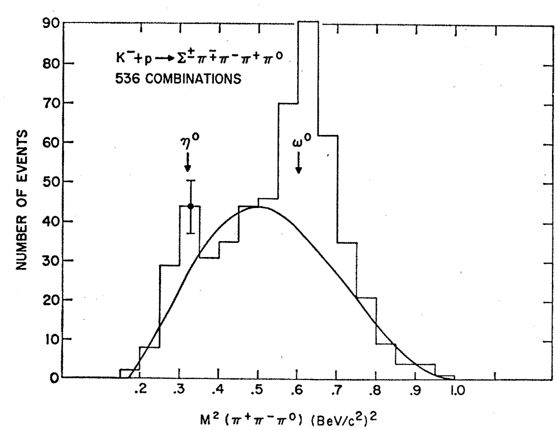

FIG. 68. $M^2(\pi^+\pi^-\pi^0)$ histogram for 268 $K^-p\rightarrow\Sigma^{\pm}\pi^{\mp}\pi^+\pi^-\pi^0$ events, each event plotted twice.

[188] I. P. Gyuk and S. F. Tuan, Phys. Rev. Letters 14, 121 (1965).

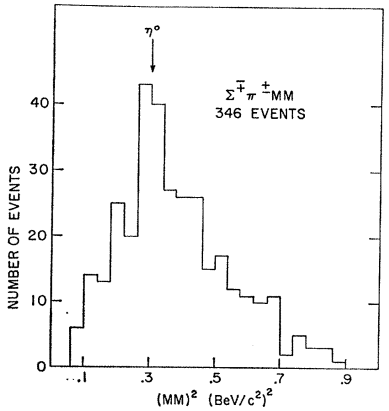

FIG. 69. (MM)^2 histogram for 346 $K^-p \rightarrow \Sigma^{\pm}\pi^{\mp}MM$ events.

V. THE CASCADE HYPERON

The identification of Ξ^- and Ξ^0 hyperons has been discussed in detail in Secs. III and IV. In this section we consider the determination of several properties of the Ξ^- and Ξ^0. The data permit a relatively complete study of the Ξ^-, providing significant information[189] on its mass, lifetime, decay modes, and all three of its weak-interaction parameters α_{Ξ^-}, β_{Ξ^-}, and γ_{Ξ^-}. In contrast, the data on the Ξ^0 are sufficient only to determine its mass and asymmetry parameter α_{Ξ^0}.

A. Properties

1. Masses

Mass determinations are made by computing the invariant mass of Ξ^- decay products,

$$M^2(\Lambda\pi) = (E_\Lambda + E_\pi)^2 - (\mathbf{P}_\Lambda + \mathbf{P}_\pi)^2, \qquad (53)$$

using only well measured events. In all cases the *fitted* value of the Λ momentum is used. For Ξ^0 decay in which the decay π^0 is not observed, its 4-momentum is determined by refitting the entire event without assumption as to the Ξ^0 mass. That is, the reaction $K^- + p \rightarrow \Xi^0 + K^+ + \pi^-$ is refitted to the hypothesis $K^- + p \rightarrow \Lambda^0 + \pi^0 + K^+ + \pi^-$. For Ξ^- decay, the most direct approach, i.e., using the measured values of $\mathbf{P}_\pi$ and E_π in (53), clearly involves a different systematic treatment of the data. Therefore, in addition to the direct approach, the decay π^- momentum was also obtained in a manner identical to that used in Ξ^0 decay, i.e. by refitting the event $K^- + p \rightarrow \Xi^- + K^+$ to the hypothesis $K^- + p \rightarrow \Lambda^0 + \pi^- + K^+$ ignoring the measured π^- data. This approach is appropriate to a measurement of the $\Xi^- - \Xi^0$ mass difference inasmuch as Ξ^0 and Ξ^- events are analyzed by the same method. The direct approach serves as a check for hidden systematic errors in the best mean mass.

The $\Lambda\pi$ effective-mass histograms for 108 Ξ^- and 29 Ξ^0 decays in which *refitted* decay pion momenta are used, are shown in Figs. 71(a) and 71(b), respectively. These yield best-fit values of

$$M_{\Xi^0} = 1313.5 \pm 2.2 \text{ MeV}/c^2$$

and

$$M_{\Xi^-} = 1321.4 \pm 1.1 \text{ MeV}/c^2,$$

giving a mass difference of

$$M_{\Xi^-} - M_{\Xi^0} = 6.9 \pm 2.2 \text{ MeV}/c^2.$$

The Ξ^- mass histogram for 299 events in which the measured decay-pion momentum was used is shown in Fig. 72. Assuming a purely statistical error assignment of ± 0.3 MeV/c^2, the mean mass of 1320.4 MeV/c^2 is consistent with the previous determination. As a further check on over-all systematics, the mass of the decay Λ^0 was determined from the measured value of its decay products. The results, shown in Fig. 73, yield a mass $M_\Lambda = 1115.6 \pm 0.4$ MeV/c^2, which compares well with the latest compiled[162] value, 1115.44 ± 0.12 MeV/c^2. Additional tests, such as the variation of the size of the fiducial acceptance region and magnetic field, showed that the mean mass of the Ξ^- was stable to within ± 0.5 MeV/c^2.

The cascade masses given above are all in good agreement with those found by other groups[190]; comparison is made in the summary table, Table XVI.

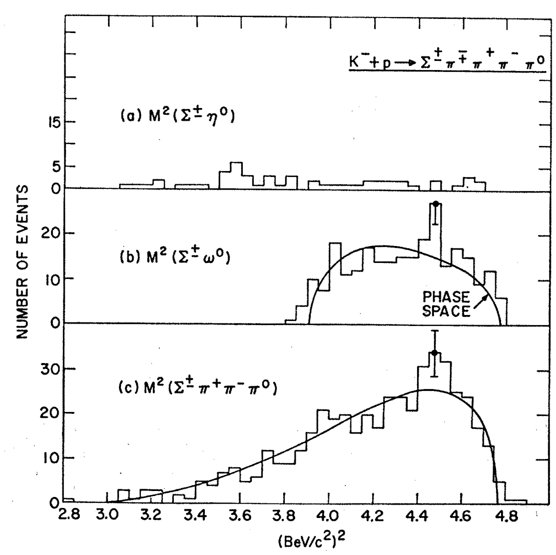

FIG. 70. (a) $M^2(\Sigma^{\pm}\eta^0)$, (b) $M^2(\Sigma^{\pm}\omega^0)$, and (c) $M^2(\Sigma^{\pm}\pi^+\pi^-\pi^0)$ histograms for $K^-p \rightarrow \Sigma^{\pm}\pi^{\mp}\pi^+\pi^-\pi^0$ final state.

[189] Preliminary results concerning the properties of the Ξ have been reported in L. Bertanza *et al.*, Phys. Rev. Letters , 229 (1962). P. L. Connolly *et al.*, *Proceedings of the Sienna Conference on Elementary Particles, 1963,* edited by G. Bernardini and G. P. Puppi (Società Italina di Fisica, Bolagna 1964), Vol. I, p. 34.

[190] A list of references may be found in the summary talk of H. Ticho, *Proceedings of the International Conference on Fundamental Aspects of Weak Interactions, 1963,* edited by G. C. Wick and W. J. Willis (Brookhaven National Laboratory, Upton, New York, 1963), p. 410.

TABLE XVI. Summary of world information on Ξ^-, Ξ^0 properties.

Group	M_{Ξ^-} (MeV/c^2)	M_{Ξ^0} (MeV/c^2)	$M_{\Xi^-}-M_{\Xi^0}$ (MeV/c^2)	τ_{Ξ^-} (10^{-10} sec)	τ_{Ξ^0} (10^{-10} sec)	α_{Ξ^-}	α_{Ξ^0}	β_{Ξ^-}	γ_{Ξ^-}
BNL-SYR	1320.9±0.5	1313.5±2.2	6.9±2.2	1.80±0.16	...	+0.47±0.12	+0.2 ±0.4	0.0 ±0.3	+0.88±0.14
LRL[a]	...	...	...	1.69±0.07	$2.5_{-0.3}^{+0.4}$	+0.41±0.08	+0.36±0.3	−0.08±0.26	+0.91±0.03
UCLA[a]	...	...	6.1±1.6	1.77±0.12	$3.5_{-0.8}^{+1.0}$	+0.62±0.12	−0.1 ±0.4	+0.63±0.16	+0.46±0.22
EP and others[a] (heavy liquid)	1321.4±0.6	1314.6±1.5	6.8±1.6	1.91±0.16	$3.8_{-0.7}^{+1.0}$	+0.53±0.16	+0.49±0.65	−0.25±0.5	+0.85±0.05

2. *Lifetime*

In order to obtain an unbiased sample of Ξ^-, we use only those events in which the Ξ^- and the Λ^0 decay visibly within a restricted fiducial region *and* such that the decay length of the Ξ^- is ≥ 0.5 cm. These criteria lead to a 311-event sample whose differential-decay-time distribution is shown in Fig. 74. The approximate straight-line behavior shows that the detection biases are not severe. The best value of the Ξ^- lifetime τ (or decay rate λ) is found from a maximum-likelihood analysis based upon the standard[191] Bartlett method. Taking into account the detection probability that both the Ξ^- and Λ decay within the fiducial region, the likelihood function[192] takes the form of a product of three factors:

$$L(\tau)=\prod_{i=1}^{N}\left[\exp(-\lambda l_i/q_i)\frac{\lambda}{q_i}\right]\left[P_\Lambda(l_i,q_i)\right]\left[\frac{1}{\bar{p}(q_i,\tau)}\right] \quad (54)$$

representing, respectively, (1) the probability that a Ξ^-

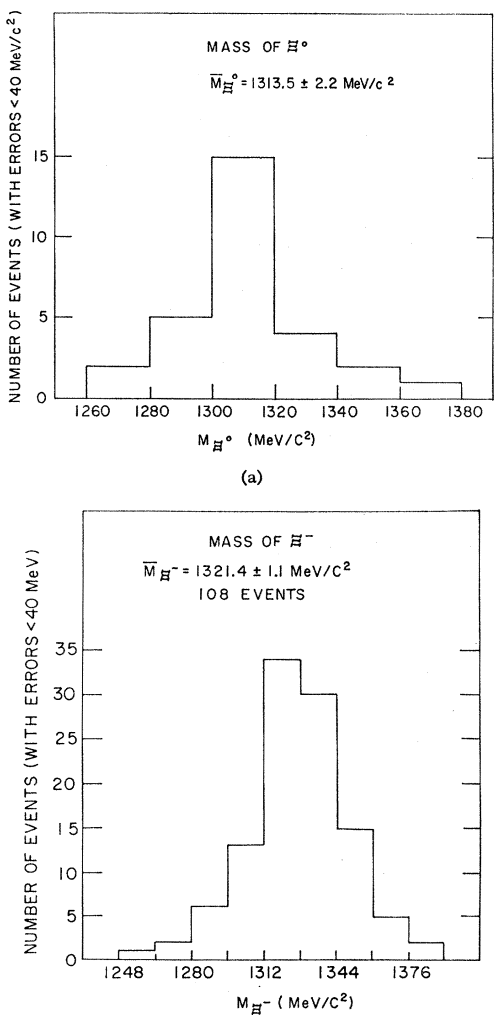

FIG. 71. (a) Ξ^0 mass distribution from 29 $K^-p\rightarrow\Xi^0K^+\pi^-$ events. (b) Ξ^- mass distribution from 108 $K^-p\rightarrow\Xi^-K^+$ events, using fitted π^- (see text).

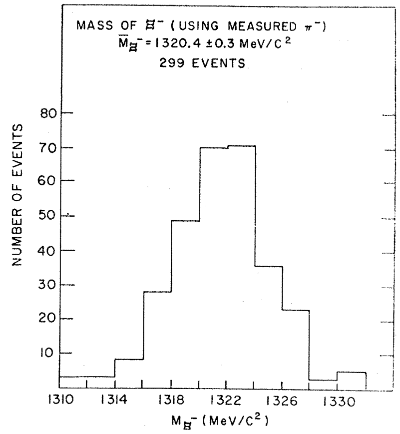

FIG. 72. Ξ^- mass distribution from 299 $K^-p\rightarrow\Xi^-K^+\pi^0$ and $\Xi^-K^0\pi^+$ events, using measured π^- (see text).

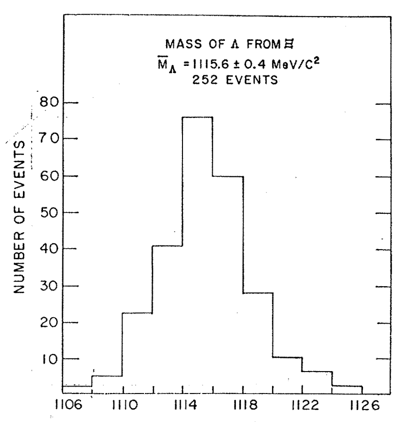

FIG. 73. Λ mass distribution from 252 $\Xi^-\rightarrow\Lambda\pi^-$ decays.

---

191 M. S. Bartlett, Phil. Mag. 44, 249 (1953).

192 G. C. Moneti, Brookhaven Bubble Chamber Group Internal Report L24(1962) (unpublished).

with momentum q_i decays with length l_i, (2) the probability that a Λ decay within the acceptance region and finally, (3) the total probability of detecting such a decay chain (a normalization factor). Specifically,

$$P_\Lambda(l_i,q_i)=1-\int_\Omega\left[\exp-\frac{\lambda_\Lambda L_\Lambda(\theta)}{q_\Lambda(\theta)}\right]f(\theta)d\Omega \qquad (55)$$

and

$$\bar{P}(q_i,\tau)=\int_0^L P_\Lambda(x,q_i)\left[\exp\left(-\frac{\lambda x}{q}\right)\right]\frac{\lambda}{q}dx, \qquad (56)$$

where λ, q, L = decay rate, laboratory momentum and potential path of the Ξ^-, and λ_Λ, $q_\Lambda(\theta)$, $L_\Lambda(\theta)$ = decay rate, laboratory momentum and potential path of the Λ^0 and $f(\theta)$ = the normalized decay angular distribution of the Λ from Ξ^- decay. In actual application of this analysis, two simplifying assumptions are made: (1) θ is small and the curvature of the Ξ^- is neglected so that $L_\Lambda(\theta)X\cong L$ for all θ; and (2) the ratio $q/q_\Lambda(\theta)$ in (56) is constant and is taken from tables of decay kinematics. The average value for $q/q_\Lambda(\theta)$ for our sample is consistent with the tables. The best mean life is obtained directly from the Bartlett S function

$$S(1/\tau)=\left(\frac{\partial\ \ln\mathcal{L}}{\partial\tau}\right)\left[-\left(\frac{\partial^2\mathcal{L}}{\partial\tau^2}\right)_{\partial(\ln\mathcal{L})/\partial\tau=0}\right]^{-1/2}. \qquad (57)$$

If the events have a Gaussian distribution, it can be shown that $S(1/\tau)$ is linear in $1/\tau$ with a mean value of 0 and a variance of 1. The linear behavior is exhibited

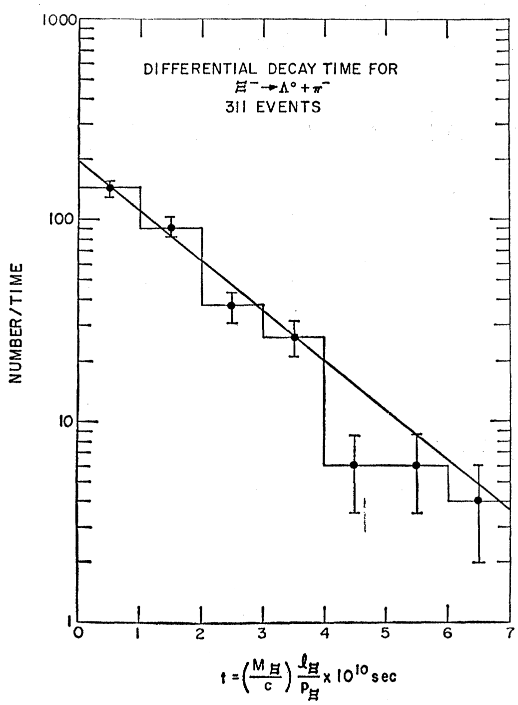

FIG. 74. Differential-decay-time distribution for 311 $\Xi^-\rightarrow\Lambda\pi^-$ decays.

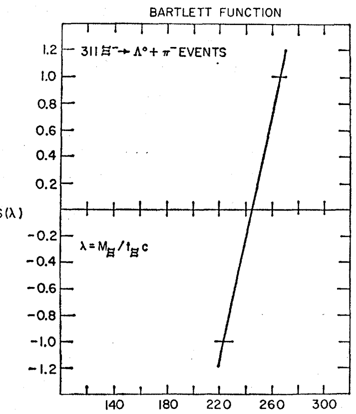

FIG. 75. Bartlett S function versus the decay rate, λ, for 311 $\Xi^-\rightarrow\Lambda\pi^-$ decays.

directly in Fig. 75. From the values of $1/\tau$ at $S=0$ and $S=\pm1$, we find

$$\tau_{\Xi^-}=(1.80_{-0.15}^{+0.16})\times10^{-10}\ \mathrm{sec},$$

in excellent agreement with other determinations[190]—see Table XVI. This value is not appreciably altered if the minimum Ξ^- decay length or the fiducial acceptance region is varied, and the corrections for Ξ^- interactions in flight are negligible compared with the statistical error. For the sake of completeness, we note that an attempt was made to estimate the Ξ^0 lifetime from the 46 $\Xi^0K^+\pi^-$ events. Because the calculated lifetime is extremely sensitive to the minimum Ξ^0-length cutoff, we are not able to quantitatively test the $\Delta I=\frac{1}{2}$ rule. Qualitatively, however, the Ξ^0 lifetime is between 2×10^{-10} and 4×10^{-10} sec.

This completes our discussion of Ξ^- properties.[193]

B. The β Decay of the Ξ^- ($\Delta S=1$)

Because of the rarity of background reactions which look like Ξ^- events, the latter can be identified on the basis of their over-all topology and production vertex information, *independent* of decay vertex information. In fact, the criteria

(i) negative decay plus visible V^0, or
(ii) negative decay plus identified K^+ at production suffice to select a sample which are:

Ξ^- production events (2- or 3-body) (a)

$$\left.\begin{array}{l}K^-+p\rightarrow\Sigma^-+\bar{K}^0+K^+\\ \text{or}\quad \pi^-+p\rightarrow\Sigma^-+\bar{K}^0+\pi^+(+\pi^0)\end{array}\right\} \qquad (b)$$

$$\left.\begin{array}{l}K^-+p\rightarrow\Sigma^-+\pi^++MM\\ \qquad\qquad\quad\searrow\\ \qquad\qquad\qquad\Lambda^0+e^-+\bar{\nu}\end{array}\right\}. \qquad (c)$$

[193] We have attempted, unsuccessfully, to measure the Ξ^- spin using three methods: (i) The Lee-Yang spin tests—T. D. Lee and C. N. Yang, Phys. Rev. **109**, 1755 (1958); (ii) A modified Byers-Fenster approach—N. Byers and S. Fenster, Phys. Rev. Letters **11**, 52 (1963); (iii) and a modified Adair analysis—R. K. Adair, Phys. Rev. **100**, 1540 (1955); F. Eisler *et al.*, Nuovo Cimento **7**, 222 (1958).

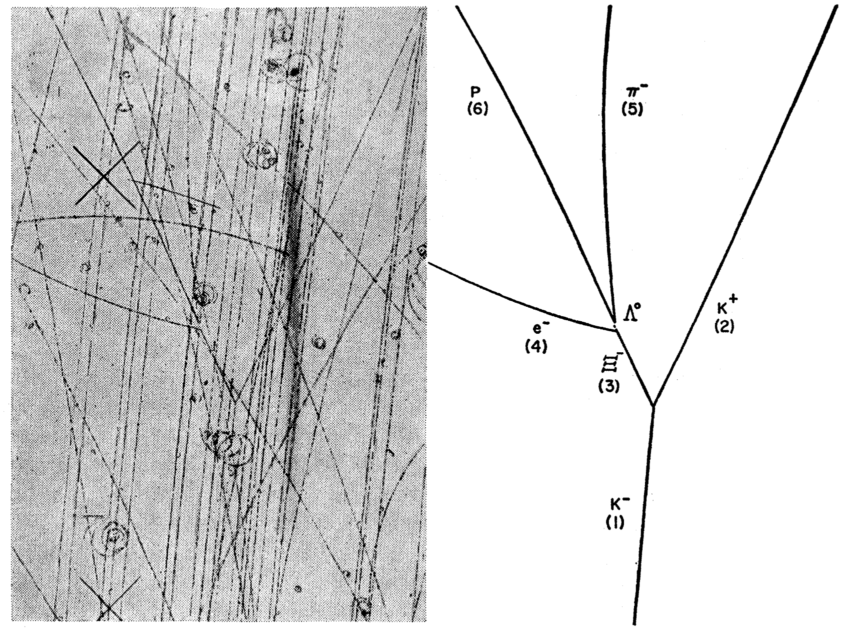

FIG. 76. Photograph and line drawing of possible Ξ^- beta decay event.

Of 330 candidates, the 20 Σ^- background reactions of type (b) were easily separated, leaving 310 Ξ^- production events (or $\Sigma^-\beta$ decays). We have searched for examples of the $\Xi^-\beta$ decay:

$$\Xi^- \rightarrow \Lambda^0 + e^- + \bar{\nu} \tag{58}$$

within the sample defined above.

Such examples can be found using either of two *nonexclusive* techniques. On the one hand, one can require positive identification of the electron together with kinematical consistency with the hypothesis (58) (the "ionization technique"). On the other hand, one can require incompatibility with the normal pionic-decay[194] kinematics together with consistency with (58) (the "fitting technique"). In either case, of course, to achieve unambiguous identification, one must be able to rule out the $\Sigma^-\beta$-decay possibility. In the 310 event sample, we have found two examples of $\Xi^-\beta$ decay, one unambiguous, and one probable but ambiguous with the hypothesis (c). The first event was found by the fitting technique, while the second (ambiguous) event was found by the ionization technique. The latter has been described previously,[195] but for the sake of completeness, we describe both events below.

Pictures and sketches of the events are shown in Fig. 76 and 77, respectively. Complete kinematical specifications of the events are given in Tables XVII and XVIII. Beginning with the first event, Table XVII shows that the decay secondary (track 4) cannot be identified by ionization although the decaying hyperon is either a Ξ^- or Σ^-. Kinematic fitting shows that the V^0 must be a Λ^0 from the decay vertex and the normal Ξ^- pionic decay hypothesis fails to fit with a χ^2 probability $\lesssim 10^{-3}$. Additional fitting at the decay vertex shows that the event is compatible with $\Xi^-\beta$ decay, but incompatible with $\Sigma^-\beta$ decay. The crucial point here is that the transverse momentum is so large that it alone rules out all possible decay fits except (58). Finally, the production fit to the hypothesis $\Xi^- + K^+$ is excellent (χ^2 probability of 88%). One therefore concludes that the event is an unambiguous example of $\Xi^- \rightarrow \Lambda^0 + e^- + \bar{\nu}$.

Turning now to the second event, one sees from Table XVIII that the charged decay product (track 4) is a positively identified election. The pion hypothesis leads one to expect an ionization density of 4.5 compared with the observed density of 1.5. Kinematic fitting shows that the V^0 is a Λ from the decay vertex. The problem then is to distinguish between the Σ^- and $\Xi^-\beta$ decay hypothesis. Neither kinematic fitting at the decay vertex, nor ionization information is of any help in this respect, as indicated in Table XVIII. Moreover, the fit at the production vertex is consistent with either

$$\Xi^- + \pi^+ + (\mathrm{MM})_A; \quad (\mathrm{MM})_A = 563 \pm 77 \ \mathrm{MeV}/c^2 \tag{d}$$

$$\Sigma^- + \pi^+ + (\mathrm{MM})_B; \quad (\mathrm{MM})_B = 764 \pm 25 \ \mathrm{MeV}/c^2. \tag{e}$$

Thus the event cannot be uniquely identified. As indicated in Ref. 195, one can obtain an estimate of the relative probabilities of (d) versus (e) on the basis of production information alone, i.e. from the total cross sections and missing mass spectra for events of type (d) and (e). This yields an estimate for the a priori probability of (d) versus (e) of the order of $\lesssim 5/1$ with an uncertainty of the same order, so that no resolution of the ambiguity is afforded on this basis.

Even assuming that the latter event is real, we can-

[194] Of the 310 candidates, all but two were consistent with the pionic hypothesis, but $\approx 85\%$ were also kinematically consistent with the leptonic hypothesis.

[195] L. Bertanza *et al.*, Phys. Rev. Letters **9**, 19 (1962).

TABLE XVII. Measured and fitted quantities of cascade beta-decay event.

			Measured		Fitted		Bubble density	
Track	Particle	ϕ(Azim)	θ(Dip)	p(MeV/c)	p(prod)	p(decay)	Meas.	Exp.
1	K^-	353.9±1.1	0.6±0.4[a]	2226.9±45.0[b]	2244±38		1.0±0.1	1.0
2	K^+	333.1±0.1	−4.0±0.1	1569 ±94	1502±30		1.4±0.1	1.1
3	Ξ^-	25.8±0.7	6.0±0.9	unmeasurable	1001±15	1094±58	3.6±0.6	2.8
4	e^-	75.2±0.3	35.9±0.3	180 ± 5		180± 5	2.0±0.4	1.2
5	π^-	7.3±0.1	6.9±0.2	247 ± 2		250± 3	1.3±0.1	1.3
6	p	23.4±0.1	−3.4±0.2	697 ±28		667±16	2.6±0.4	3.0
7	Λ	22.0±0.4	2.7±1.9			907±19		

[a] Mean dip angle of K^- beam.
[b] Mean momentum of K^- beam.

not use both events simultaneously in our estimate of the $\Xi^-\beta$-decay branching ratio because they were identified using different criteria. For the first event (obtained by the "fitting technique"), the efficiency of the search may be obtained as follows. First, all events are refitted at production without making use of any information concerning the Ξ^- decay products. The resulting Ξ^- momentum spectrum, shown in Fig. 78(a), may then be used to transform the momentum of the charged secondary into the Ξ^- rest frame. This transformation is carried out assuming that the secondary is an *electron* so that the resultant distribution may be compared with the expected[196] phase-space distribution for the electron momentum ($p_{e^-}{}^*$) from (58). The results are shown in Fig. 78(b).

The peak corresponds to the dominant pionic-decay contribution, although it is shifted from the value $p_{\pi^-}=137$ MeV/c^2 because the "wrong" (electron) mass was used in the transformation. The identified β decay (event #1) appears well outside the peak. Except for this case, all other events with $p^*\leq 100$ MeV/c were found to be consistent with pionic ionization and all had extremely large momentum errors, accounting for their position outside the peak. The fraction of phase

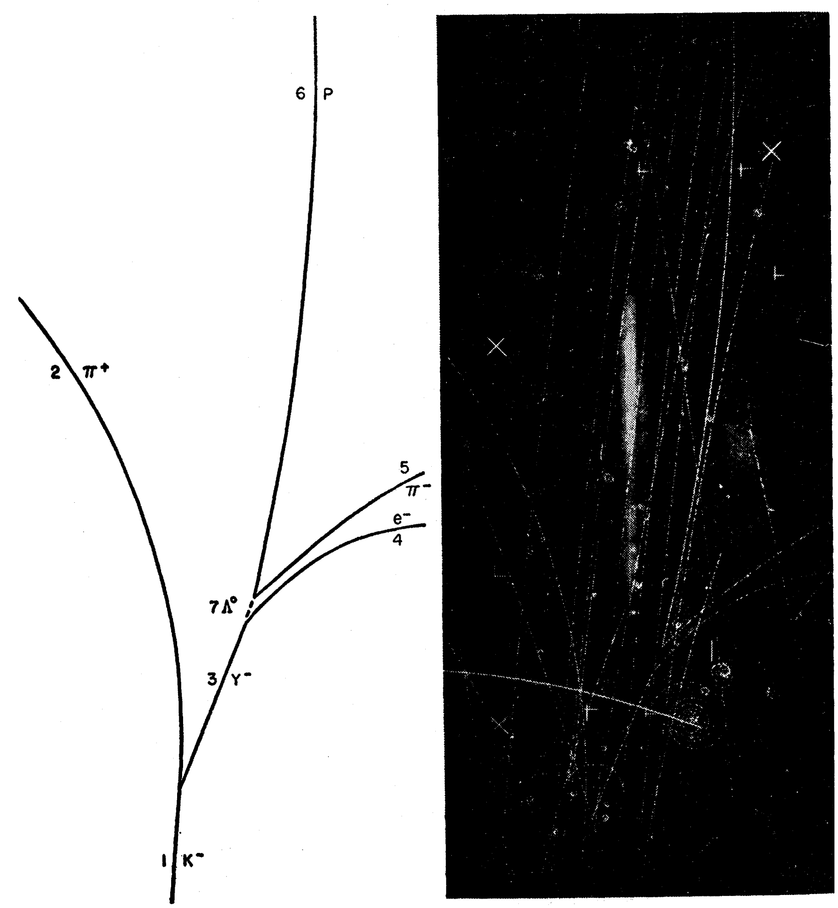

FIG. 77. Photograph and line drawing of Ξ^- beta decay event.

[196] Here we neglect the small effect of baryon recoil.

TABLE XVIII. Measured and fitted quantities of possible cascade-beta-decay event.

Track No.	Assigned particle	Measured angles, momenta and bubble density ϕ(Azimuth)	θ(Dip)	p(MeV/c)	Observed bubble density	Ξ^- Fit p	Expected bubble density	Σ^- Fit p	Expected bubble density
1	K^-	354.9±0.5	−0.5±0.5	2240± 45[a]					
2	π^+	354.5±0.2	+0.1±1.2	168± 4	1.9±0.2		1.7		1.7
3	Ξ^-, Σ^-	340.5±0.2	19.3±1.0	940±141	2.7±0.3	935±17	3.1	1023±21	2.4
4	e^-	325.8±0.4	45.0±2.0	83± 3	1.5±0.2	84± 4	1.4	84± 4	1.4
5	π^-	313.8±0.2	6.9±1.1	200± 8	1.5±0.2	204± 2	1.5	204± 2	1.5
6	p	347.7±0.1	19.0±0.5	765± 15	2.8±0.2	759±15	2.7	759±15	2.7
7	Λ^0	340.5±0.8	16.1±4.0			933±16		932±15	

[a] Mean momentum of K^- beam.

space below 100 MeV/c($\approx 50\%$) represents the efficiency of the search. This yields the crude estimate,

$$r_\beta = \frac{\Xi^- \to \Lambda + e^- + \nu}{\Xi^- \to \Lambda + \pi} \cong \frac{(1 \times 1/0.5)}{310} = (6 \pm 6) \times 10^{-3}$$

for the Ξ^- beta decay rate.

For the second event, identified by means of the ionization technique, the efficiency of the search may be obtained from a study of the *laboratory* momentum of the charged decay secondary. The data are shown in Fig. 77(c), together with the expected distribution due to the normal $\Xi^- \to \Lambda + \pi^-$ decay. [The latter is obtained by using the Ξ^- momentum spectrum of Fig. 77(a)]. The (ambiguous) β-decay event No. 2 is marked at 80 MeV/c. Since electrons with momenta below ≈ 125 MeV/c can be identified with very high probability, the efficiency of the search is $\approx 50\%$, i.e., the ratio of the shaded to the total area of Fig. 78(c). Thus, once again one obtains $r_\beta \approx (6 \pm 6) \times 10^{-3}$.

It is interesting to note that only one other certain example of (58) has been observed.[197] The results of the search for Ξ^- beta decay at various laboratories[190] is summarized in Table XIX. The best estimate for r^β from the world data is

$$r_\beta \approx 2/950 = (2 \pm 1) \times 10^{-3}.$$

This number is in reasonable agreement with the value

TABLE XIX. β Decay of the Ξ^-.

Laboratory	Number found	Effective denominator
BNL-SYR Search 1	1	310×0.5=150
BNL-SYR Search 2	1	310×0.5=150
LRL[a]	0	400
UCLA[a]	1	194×0.8=155
EP+CERN[a]	0	300×0.8=250
Total[b]	2	950

[a] Ref. 190.
[b] Using search 2 only.

[197] D. D. Carmony and G. M. Pjerrou, Phys. Rev. Letters **10**, 381 (1963).

($\lesssim 10^{-3}$) predicted by the Cabibbo[198] version of the universal Fermi interaction, as given by Willis *et al.*[199]

C. Weak-Interaction Parameters

The decay of a spin-J cascade via the usual modes,

$$\begin{aligned} \Xi^- &\to \Lambda^0 + \pi^-, \\ \Xi^0 &\to \Lambda^0 + \pi^0, \end{aligned} \tag{59}$$

may be described by means of 2 complex partial wave amplitudes, $A_{J-1/2}$ and $A_{J+1/2}$. Since an over-all phase is not measurable, there are only three independent real numbers which characterize the decay. It turns out to be convenient to use the four parameters

$$|A_J|^2 = |A_{J-1/2}|^2 + |A_{J+1/2}|^2, \tag{60}$$

$$\alpha_\Xi = \frac{2\,\mathrm{Re}[A_{J-1/2}{}^* A_{J+1/2}]}{|A_J|^2}, \tag{61}$$

$$\beta_\Xi = \frac{2\,\mathrm{Im}[A_{J-1/2}{}^* A_{J+1/2}]}{|A_J|^2}, \tag{62}$$

$$\gamma_\Xi = \frac{|A_{J-1/2}|^2 - |A_{J+1/2}|^2}{|A_J|^2}, \tag{63}$$

in conjunction with the subsidiary condition

$$\alpha_\Xi{}^2 + \beta_\Xi{}^2 + \gamma_\Xi{}^2 = 1. \tag{64}$$

This choice is convenient because these parameters enter naturally in the density-matrix analysis of the decays (59) and the subsequent decay, $\Lambda \to \pi +$nucleon. In addition, these parameters are directly related to the invariance of weak interactions with respect to P, C, and T.

Experimentally, the parameter $|A_J|^2$ is just a normalization factor proportional to total decay rate. The parameters α_Ξ, β_Ξ, and γ_Ξ may be determined from the decay-Λ polarization, using $\Lambda \to \pi^- p$ decay as an analyzer. In the ensuing discussion we forego the advantage of simplicity which results from the assumption

[198] N. Cabibbo, Phys. Rev. Letters **10**, 531 (1963).
[199] W. J. Willis *et al.*, Phys. Rev. Letters **13**, 291 (1964).

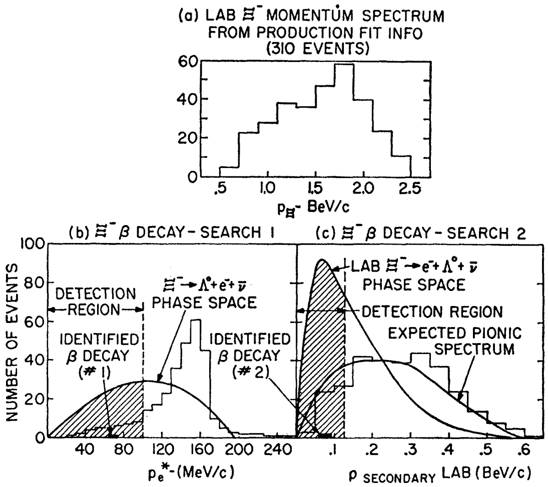

FIG. 78. (a) Ξ^- laboratory momentum spectrum from production fit only. (b) Charged secondary momentum spectrum from Ξ^- decay in Ξ^- rest frame, assuming the secondary is an electron. (c) Charged secondary momentum spectrum from Ξ^- decay in laboratory system, compared to normal $\Xi^- \to \Lambda\pi^-$ decay spectrum.

that $J=\frac{1}{2}$, (although this is most likely the case), in order to emphasize the generality of our determination. We adopt the following notation:

$\hat{q}_\Xi = \Xi$ direction in the over-all K^-p center-of-mass system,

$\hat{q}_B =$ incoming K^- direction in the over-all K^-p center-of-mass system,

$\hat{q}_\Lambda = \Lambda$ direction in the Ξ rest frame,

$\hat{q}_n =$ nucleon direction in the Λ rest frame,

$\hat{N} =$ normal to the production plane $= \hat{q}_B \times \hat{q}_\Xi / |\hat{q}_B \times \hat{q}_\Xi|$,

$\hat{X} = \hat{N} \times \hat{q}_\Lambda / |\hat{N} \times \hat{q}_\Lambda|$, $\hat{Y} = \hat{q}_\Lambda \times \hat{X}$,

$a_m =$ parameters determining the alignment of the Ξ^- for a given J, $-J \leqslant m \leqslant J$,

$I_i(a_m,J) =$ known function[200] of a_m.

Then it can be shown[201] that the parameters α_Ξ, β_Ξ and γ_Ξ can be determined from five possible dot-product correlations among the vectors described above. These have the form

$$1+\alpha_\Lambda\alpha_\Xi(\hat{q}_\Lambda\cdot\hat{q}_n), \tag{65}$$

$$1+\frac{\pi}{4}\alpha_\Lambda\beta_\Xi I_1(a_m,J)(\hat{X}\cdot\hat{q}_n), \tag{66}$$

$$1-\frac{\pi}{4}\alpha_\Lambda\gamma_\Xi I_1(a_m,J)(\hat{Y}\cdot\hat{q}_n), \tag{67}$$

$$1-\alpha_\Xi I_2(a_m,J)(\hat{N}\cdot\hat{q}_\Lambda), \tag{68}$$

$$1-\alpha_\Lambda\frac{[1+(2J+1)\gamma_\Xi]}{J(J+1)}I_3(a_m,J)(\hat{N}\cdot\hat{q}_n). \tag{69}$$

Noting that (65) is independent of J *and* independent of alignment parameters, it follows that $\alpha_\Xi\alpha_\Lambda$ may be determined from a complete sample of Ξ's no matter what their production mode. As discussed in III, there are 46 (well identified) Ξ^0 events, coming from the final-state $\Xi^0K^+\pi^-$, while there are 364 Ξ^- events with visible Λ decay coming from both two and three-body reactions of the type $\Xi^-K^+(\pi^0)$ and $\Xi^-\pi^+K^0$. The $\hat{q}_\Lambda\cdot\hat{q}_n$ correlations of these samples are shown in Figs. 79 and 80, respectively. From least-squares straight-line fits, one finds

$$\alpha_\Lambda\alpha_{\Xi^0} = -0.12\pm0.23,$$

$$\alpha_\Lambda\alpha_{\Xi^-} = -0.34\pm0.09.$$

Using $\alpha_\Lambda = -0.62\pm0.07$ due to Cronin and Overseth,[202] one has

$$\alpha_{\Xi^0} = +0.20\pm0.37 \quad \text{and} \quad \alpha_{\Xi^-} = +0.56\pm0.15.$$

The situation for β_Ξ and γ_Ξ is not so simple because the correlation functions (66)–(69) depend upon J and the precise state of Ξ alignment. Now, as emphasized in V, the three-body production events arise mainly from the decay of intermediate resonant states, and as one might expect, show no indication of alignment, so the remainder of the study is carried out using the 131 two-body event sample. The correlations [(66)–(69)] for this sample are shown in Fig. 81. We notice that the ratio of the correlation coefficients in (66) and (67) is *spin-independent.* We then have

$$\xi = \frac{\beta_{\Xi^-}}{\gamma_{\Xi^-}} = -\left[\frac{0.0\pm0.14}{-0.49\pm0.15}\right] = 0.0\pm0.3.$$

This, together with the previous determination of α_{Ξ^-} and the constraint equation (64), is sufficient to de-

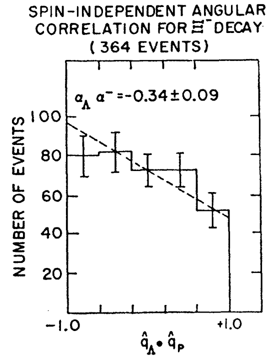

FIG. 79. Angular correlation in $\hat{q}_\Lambda\cdot\hat{q}_p$ for 364 $\Xi^-\to\Lambda\pi^-$ decays.

[200] Y. Ueda and S. Okubo, Nucl. Phys. **49**, 345 (1963). This reference contains a mistake. Right mutually orthogonal vectors should read $\hat{z}=\hat{p}_\Lambda$, $y=(1/\sin\theta)(\hat{p}_\Lambda\times\hat{s}_\Xi)$ and $\hat{x}=\hat{y}\times\hat{p}_\Lambda$ in their notation. See Y. Ueda, thesis, University of Rochester, 1965 (unpublished).

[201] T. D. Lee and C. N. Yang, Phys. Rev. **108**, 1645 (1957); W. B. Teutsch, S. Okubo, and E. C. G. Sudarshan, Phys. Rev. **114**, 1148 (1959).

[202] J. W. Cronin and O. E. Overseth, Phys. Rev. **129**, 1795 (1963).

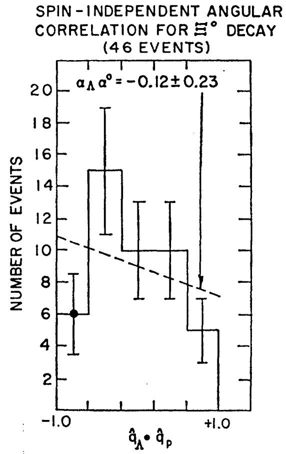

FIG. 80. Angular correlation in $\hat{q}_\Lambda \cdot \hat{q}_p$ for 46 $\Xi^0 \to \Lambda\pi^0$ decays.

termine β_{Ξ^-}, γ_{Ξ^-} from

$$\beta_{\Xi^-} = \pm\xi\left(\frac{1-\alpha_{\Xi^-}^2}{1+\xi^2}\right)^{1/2} = \pm 0.0 \pm 0.30$$

$$\gamma_{\Xi^-} = \pm\left(\frac{1-\alpha_{\Xi^-}^2}{1+\xi^2}\right)^{1/2} = \pm 0.83 \pm 0.10$$

to within an ambiguity of sign which reflects the fact that the determination is independent of the sign of I_1. For the general case this ambiguity is hard to remove because there are too many alignment parameters to fit. However, for either $J=\frac{1}{2}$ or $J=\frac{3}{2}$, the sign ambiguity can be removed by measuring the ratio of the correlation coefficients in (68) and (69). One finds

$$\frac{3\alpha_{\Xi^-}}{\alpha_\Lambda(1+2\gamma_{\Xi^-})} \quad \text{for} \quad J=\tfrac{1}{2},$$

and

$$\frac{3\alpha_{\Xi^-}}{\alpha_\Lambda(1+4\gamma_{\Xi^-})} \quad \text{for} \quad J=\tfrac{3}{2}.$$

The experimental ratio of the slopes of (68) and (69) is -0.64 ± 0.39. Using the α_{Ξ^-} previously determined, we solve for γ_{Ξ^-} and compare to the previous rexults. A positive solution for γ_{Ξ^-} is favored over a negative solution by about two standard deviations for both spin assignments. To this extent, we have resolved our sign ambiguity. The *spin-independent results* are, therefore

$$\alpha_{\Xi^-} = 0.56\pm0.15,$$
$$\beta_{\Xi^-} = 0.00\pm0.30,$$
$$\gamma_{\Xi^-} = 0.83\pm0.10.$$

Although it is not conclusive, there exists some direct evidence[203] for $J=\frac{1}{2}$. Moreover, the apparent success of $SU(3)$ suggests that all ground-state baryons have spin $\frac{1}{2}$. For these reasons, it is profitable to reanalyze the data using the simplified $J=\frac{1}{2}$ versions of (65)–(69), in which the correlation coefficients take the form

$$+\alpha_{\Xi^-}\alpha_\Lambda, \tag{65'}$$
$$+\tfrac{1}{4}\pi\bar{P}_{\Xi^-}\alpha_\Lambda\beta_{\Xi^-}, \tag{66'}$$
$$-\tfrac{1}{4}\pi\bar{P}_{\Xi^-}\alpha_\Lambda\gamma_{\Xi^-}, \tag{67'}$$
$$-\alpha_{\Xi^-}\bar{P}_{\Xi^-}, \tag{68'}$$
$$-\alpha_\Lambda(1+2\gamma_{\Xi^-})\bar{P}_{\Xi^-}/3, \tag{69'}$$

where $\bar{P}_{\Xi^-}$ is the average polarization of the Ξ^-. Eliminating γ_{Ξ^-} from the constraint equation (64), we are left with 5 equations in three independent unknowns of the form

$$f_i(\alpha_{\Xi^-},\beta_{\Xi^-},\bar{P}_{\Xi^-}) = Z_i \pm \Delta Z_i, \tag{70}$$

where Z_i, ΔZ_i are the experimental values of the correlation coefficients and their errors. A χ^2 minimization of the entire set of relations gives:

$$\alpha_{\Xi^-} = 0.47\pm0.12,$$
$$\beta_{\Xi^-} = 0.00\pm0.30,$$
$$\gamma_{\Xi^-} = 0.88\pm0.09,$$
$$\bar{P}_{\Xi^-} = 0.85\pm0.14.$$

These results are consistent with our previous determination and are compared in Table XVI with those from similar experiments carried out by Berkeley, UCLA, and CERN groups.[190] All results for α_{Ξ^-} are in good accord. γ_{Ξ^-} and β_{Ξ^-} are highly correlated because

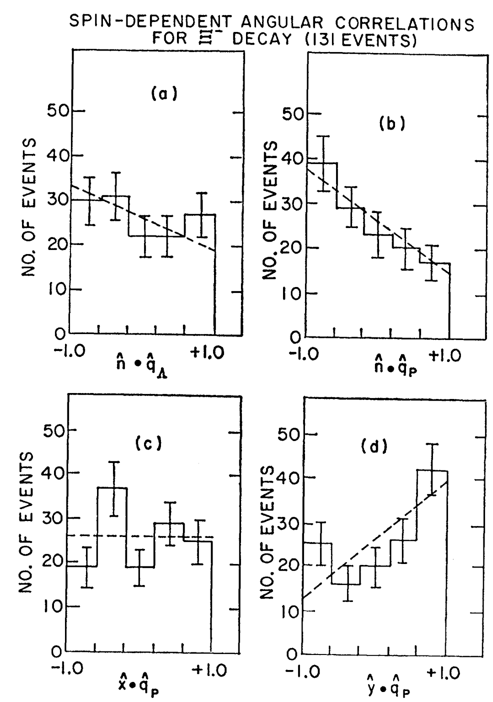

FIG. 81. Angular correlation in (a) $\hat{n}\cdot\hat{q}_\Lambda$; (b) $\hat{n}\cdot\hat{q}_p$; (c) $\hat{x}\cdot\hat{q}_p$; and (d) $\hat{y}\cdot\hat{q}_p$ for 131 Ξ^- decays from $K^-p \to \Xi^- K^+$.

[203] D. D. Carmony *et al.*, Phys. Rev. Letters **12**, 482 (1964).

of the constraint equation (64). Errors in β_{Ξ^-} are large, and the spread in β_{Ξ^-}, γ_{Ξ^-} values are correspondingly large. Even so, our β_{Ξ^-} value is only two standard deviations from the largest value of β_{Ξ^-}, that given by the UCLA group.

Before we interpret our results, it is necessary to consider how final-state interactions (FSI) affect the analysis. Lee *et al.* have shown[204] that the observed partial wave amplitudes $A_{J\pm1/2}$ are related to the true weak-decay amplitudes $A_J'\pm\frac{1}{2}$ by

$$A_{J-1/2}\rightarrow A_{J-1/2}'e^{i\delta_{J-1/2}}, \tag{71}$$

$$A_{J+1/2}\rightarrow A_{J+1/2}'e^{i\delta_{J+1/2}}, \tag{72}$$

where $\delta_{J\pm1/2}$ are the phase shifts in the $\Lambda\pi^-$ system at an energy equal to the Q value of Ξ^- decay (65 MeV/c^2). The phases of the true weak amplitudes are determined (up to an over-all sign) if one assumes invariance under either time reversal (T) or charge conjugation (C). With T invariance both $A_{J-1/2}'$ and $A_{J+1/2}'$ may be chosen real, while with C invariance if we choose $A_{J-1/2}'$ real, then $A_{J+1/2}'$ is pure imaginary. With the notation

$$|A_J'|^2=|A_{J-1/2}'|^2+|A_{J+1/2}'|^2 \tag{73}$$

$$\Delta_J=\delta_{J+1/2}-\delta_{J-1/2}, \tag{74}$$

one has

T invariance

$$\alpha_{\Xi^-}=\pm\frac{2(A_{J-1/2}')(A_{J+1/2}')\cos\Delta_J}{|A_J'|^2},$$

$$\beta_{\Xi^-}=\pm\frac{2(A_{J-1/2}')(A_{J+1/2}')\sin\Delta_J}{|A_J'|^2},$$

$$\gamma_{\Xi^-}=\frac{|A_{J-1/2}'|^2-|A_{J+1/2}'|^2}{|A_J'|^2},$$

C invariance

$$\alpha_{\Xi^-}=\pm\frac{2(A_{J-1/2}')(A_{J+1/2}')\sin\Delta_J}{|A_J'|^2},$$

$$\beta_{\Xi^-}=\pm\frac{2(A_{J-1/2}')(A_{J+1/2}')\cos\Delta_J}{|A_J'|^2},$$

$$\gamma_{\Xi^-}=\frac{|A_{J-1/2}'|^2-|A_{J+1/2}'|^2}{|A_J'|^2}.$$

From these expressions and previous results we note the following:

(1) Independent of assumptions concerning FSI and J, the nonzero value of α_Ξ means that parity is violated in Ξ decay.

(2) The assumption of T invariance requires

$$\beta_{\Xi^-}/\alpha_{\Xi^-}=\tan\Delta_J=0.0\pm0.14 \quad\text{or}\quad \Delta_J=0\pm17°$$

while the assumption of C invariance requires

$$\beta_{\Xi^-}/\alpha_{\Xi^-}=\cot\Delta_J=0.0\pm0.14 \quad\text{or}\quad \Delta_J=90\pm17°.$$

Thus the data are consistent with either T or C invariance *but not* both. In the latter case one must infer a very large phase shift difference. From the point of view of $SU(3)$ where $J=\frac{1}{2}$, the $\Lambda\pi$ phase shifts are expected to be the order of the nucleon-π phase shifts (which are close to zero at this energy). Consequently, the assumption of T invariance is preferred.

(3) Independent of FSI and J, the large value of γ_{Ξ^-} indicates a strong preference for non-spin-flip decay. As a measure of this preference, we find

$$\left|\frac{A_{J+1/2}}{A_{J-1/2}}\right|^2=0.09\pm0.05.$$

(4) Within the poor statistics, we see that $\alpha_{\Xi^0}\approx\alpha_{\Xi^-}$ as predicted by the $\Delta\mathbf{I}=\frac{1}{2}$ rule.

In principle, the above results may be used to test various assumptions concerning the nature of the nonleptonic weak interactions. Assuming unbroken $SU(3)$, octet dominance, and CP invariance,[205] Gell-Mann[206] has derived a relation among the parity-violating (s-wave) amplitudes, A_y for the decays $\Lambda\rightarrow p+\pi^-$, $\Xi^-\rightarrow\Lambda+\pi^-$ and $\Sigma^+\rightarrow p+\pi^0$, namely:

$$2A_{\Xi^-}=A_\Lambda+\sqrt{3}A_{\Sigma_0^+}. \tag{75}$$

Using the additional assumption of RP invariance,[207] Lee,[208] and Sugawara[209] have shown that the relation (75) holds not only for A_y but also for the parity-conserving (p-wave) amplitudes B_y. The latter is equivalent to a triangular relationship among the Ξ^-, Λ, and Σ_0^+ amplitude:

$$2\mathbf{A}_{\Xi^-}=\mathbf{A}_\Lambda+\sqrt{3}\mathbf{A}_{\Sigma_0^+}. \tag{76}$$

In the ensuing analysis we assume the usual interaction Hamiltonian

$$\bar{u}(A_y-\gamma_5B_y)u,$$

which leads to nonleptonic hyperon decay rates of the form

$$\Gamma=(q/8\pi M^2)\{|A_y|^2[(M+m)^2-\mu^2] + |B_y|^2[(M-m)^2-\mu^2]\}. \tag{77}$$

Here $\bar{u}$ and u are Dirac spinors; M, m, μ are the masses of the initial-state baryon, final-state baryon and decay pion, respectively; q is the c.m. momentum. It is important to note that the decay amplitudes A_y, B_y (which do not contain phase-space factors) are related in a

[204] T. D. Lee *et al.*, Phys. Rev. **106**, 1367 (1957).

[205] There is no evidence of significant CP violation in nonleptonic baryon decays, although the recent observation of $K_1^0\rightarrow2\pi$ decay leaves this an open question.

[206] M. Gell-Mann, Phys. Rev. Letters **12**, 155 (1964).

[207] M. Gell-Mann (unpublished); J. J. Sakurai, Phys. Rev. Letters **7**, 426 (1961).

[208] B. W. Lee, Phys. Rev. Letters **12**, 83 (1964).

[209] J. Sugawara (to be published).

TABLE XX. World averages.

Particle	Mean life, τ (in 10^{-10} sec)	Neutral decay branching ratio	Asymmetry parameter, α_y	s amplitude [in 10^5 (Mev sec)$^{-1/2}$]	p amplitude [in 10^5 (Mev sec)$^{-1/2}$]
Λ	2.58 ± 0.25	0.675 ± 0.027	-0.62 ± 0.07	$+0.131 \pm 0.007$	-0.843 ± 0.119
Ξ^-	1.74 ± 0.07	1.00	$+0.48 \pm 0.08$	$+0.169 \pm 0.004$	$+0.681 \pm 0.130$
Σ^+	0.813 ± 0.025	0.52 ± 0.02	...	...	...

simple way to the phenomenological decay parameters A_s and A_p defined in Eqs. (60)–(64), i.e.

$$\frac{A_p}{A_s}=\frac{B_y}{A_y}\left[\frac{(M-m)^2-\mu^2}{(M+m)^2-\mu^2}\right]^{1/2}. \tag{78}$$

Using the values of the lifetimes, branching ratios, and asymmetry parameters listed[210] in Table XX, we have obtained values of A_y, B_y by taking a proper weighted average.[211] This procedure yields well determined values for the Λ and Ξ^-. For the Σ^+, however, the errors are large and uncertain.[212] Thus, although it is clear that $\alpha_{\Sigma_0^+}$ is close to unity, no significant average can be given. From Table XX, one sees that the relationship (75) is satisfied for values[213] of $|\alpha_{\Sigma_+^0}| \gtrsim 0.9$ and fails for $|\alpha_{\Sigma_0^+}| \leq 0.8$. It appears likely therefore that the requirements of $SU(3)$ with octet dominance are satisfied.

The situation regarding the more stringent requirement (76) is illustrated in Fig. 82. Here, the solid vectors correspond to the (well-determined) decay amplitudes for the Λ and Ξ^- decays. The dashed line represents the Σ^+ amplitude assuming $\alpha_{\Sigma_0^+}=+1$. The shaded band corresponds to the locus of $\mathbf{A}_{\Sigma^+}$, as $|\alpha_{\Sigma_0^+}|$ is varied from 0.8 to 1.0. The triangle closes for $\alpha_{\Sigma'^+} \approx +0.97$. However, the sensitivity of the test precludes any strong conclusions until $\alpha_{\Sigma_0^+}$ is determined with a precision of $\approx 5\%$.

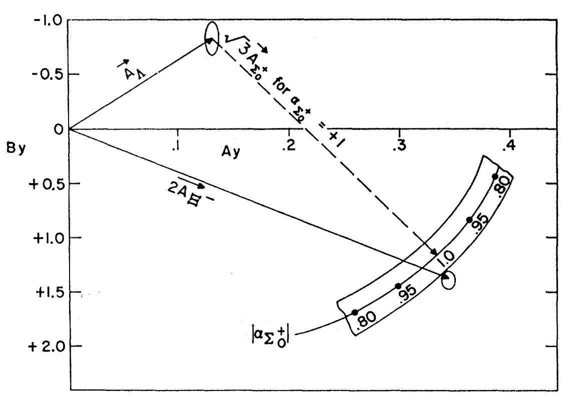

FIG. 82. Test of triangular relationship among Ξ^-, Λ^0, and Σ_0^+ decay amplitudes.

VI. CROSS SECTIONS

In this section, we present cross sections for all identifiable final states[214] and reaction channels. The general criteria used to identify final states are described in detail in Sec. II C. The techniques of separating a given reaction channel from the various final states to which it contributes are elaborately discussed in Secs. III and IV. In general, except for Σ^0-Λ^0 confusion, final states are identified with very little ambiguity. On the other hand, reaction channels involving resonances are identified with a degree of reliability ranging from poor to excellent, depending upon the signal-to-background ratio, production angular distribution, etc.

The number of events used to determine the cross sections of all identifiable final states is given in the second column of Table XXI. These numbers represent *complete* samples[215] from data runs I and II, after proper apportionment of ambiguous event types,[216] and subtraction of pion contamination.[217] The errors reflect both statistical and systematic uncertainties. Although the samples listed in Table XXI are directly comparable, it must be noted that no fiducial acceptance criteria were imposed on the $\Xi^- K(\pi)$, $(\Lambda^0,\Sigma^0)K^0\bar{K}^0$ or $\Sigma^\pm K^\mp K^0$ events, while other event types were accepted only if they occurred within a restricted volume. In order to

[210] See Summary in the *Proceedings of the International High Energy Physics Conference 1962*, edited by J. Prentki (CERN, Geneva, 1962).

[211] Because the spread in the observed mean values exceeds that expected from the internal errors, we use the prescription:

$$\bar{\sigma}_{\text{mean}}=\left[\Sigma\left(\frac{\text{deviation from mean}}{\text{measurement error}}\right)^2\right]^{1/2} \Big/ \left[\Sigma\left(\frac{1}{\text{measurement error}}\right)^2\right]^{1/2}.$$

[212] The error in the determination of $\alpha_{\Sigma_0^+}$ by E. F. Beall *et al.* [Phys. Rev. Letters **8**, 75 (1962)] is incorrect. The authors are presently re-evaluating it (private communication).

[213] It is no accident that the value of $\alpha_{\Sigma_0^+}$ needed to satisfy (75) is the same as that needed to satisfy the requirements of the $|\Delta I|=\frac{1}{2}$ rule for Σ^+ decay. The assumption of octet dominance guarantees both. See R. H. Dalitz, *Proceedings of the International School of Physics, "Enrico Fermi" June 1964* (Academic Press, New York, 1964).

[214] The terms "final state" and "reaction channel" are not mutually exclusive, of course. By "final state," we mean an identified group of *metastable* particles which may or may not come from intermediate resonance production and decay.

[215] It should be noted that the numbers in Column 2 of Table XXI do not necessarily represent the samples studied in Secs. II and IV. In general, the latter contain data from Run III as well as I and II.

[216] This includes correction for omission of nonmeasurable and/or nonanalyzable events. See Secs. IIC and IIID for discussion.

[217] Some of the pion contamination corrections were obtained from a study of our own data (see Sec. IIIA). The remaining corrections are based upon cross sections given by G. Smith, Lawrence Radiation Laboratory Physics Note #443, 1963 (unpublished). In all cases the corrections are roughly proportional to the beam pion contamination, i.e., $\approx 5\%$.

TABLE XXI. Cross sections for identifiable final states.

Final state	No. of events Run I+Run II after apportionment of ambiguities and removal of pion contamination	Completely corrected total	σ (μb)
$\Lambda^0\pi^0$ [a]	291± 35	568± 85	315± 47
$(\Lambda^0,\Sigma^0)MM$	900± 50	1680±130	932± 72
$(\Lambda^0,\Sigma^0)\pi^+\pi^-$	940± 55	1700±100	943± 55
$(\Lambda^0,\Sigma^0)\pi^+\pi^-\pi^0$	1810±100	3280±230	1819±128
$(\Lambda^0,\Sigma^0)\pi^+\pi^-MM$	477± 30	810± 73	449± 40
$(\Lambda^0,\Sigma^0)\pi^+\pi^-\pi^+\pi^-$	100± 12	204± 28	113± 16
$(\Lambda^0,\Sigma^0)\pi^+\pi^-\pi^+\pi^-\pi^0$	41± 8	84± 16	47± 9
$\bar{K}^0N$	347± 20	1410±130	782± 72
$\bar{K}^0MM$	823± 35	3160±253	1753±140
$\bar{K}^0\pi^-p$	681± 30	2500±180	1387±100
$\bar{K}^0\pi^-p\pi^0$	355± 23	1240±112	688± 62
$\bar{K}^0N\pi^+\pi^-$	324± 23	1140±103	632± 57
$K^-p\pi^+\pi^-$	788± 48[b]	857±105	476± 58
$\Sigma^+\pi^-$	409± 35	532± 52	295± 29
$\Sigma^+\pi^-\pi^0$	945± 60	1260±150	699± 83
$\Sigma^+\pi^-MM$	130± 20	164± 42	91± 25
$\Sigma^+\pi^-\pi^+\pi^-$	290± 23	358± 35	199± 19
$\Sigma^+\pi^-\pi^+\pi^-\pi^0$	93± 15	115± 19	64± 8
$\Sigma^-\pi^+$	93± 12	118± 17	65± 9
$\Sigma^-\pi^+\pi^0$	738± 35	885±100	491± 55
$\Sigma^-\pi^+MM$	194± 25	233± 60	129± 35
$\Sigma^-\pi^+\pi^+\pi^-$	212± 20	254± 31	141± 17
$\Sigma^-\pi^+\pi^+\pi^-\pi^0$	102± 15	122± 20	68± 11
Ξ^-K^+	68± 8	190± 33	91± 16
$\Xi^-K^+\pi^0$	39± 7	112± 28	54± 13
$\Xi^-\pi^+K^0$	65± 8	249± 62	119± 30
$\Xi^0K^+\pi^-$	35± 8	90± 27	50± 15
$\Lambda^0K^0\bar{K}^0$	34± 6	149± 35	71± 17
$\Lambda^0K^+K^-$	55± 8	93± 13	52± 7
$\Sigma^0K^0\bar{K}^0$	6± 3	30± 16	14± 8
$\Sigma^0K^+K^-$	9± 3	15± 6	8± 3
$\Sigma^-K^+\bar{K}^0$	5± 2	16± 7	8± 3
$\Sigma^+K^-K^0$	2± 1	7± 4	3± 2

[a] This contains some contamination of $\Sigma^0\pi^0$ events, estimated to be $\lesssim 15\%$.
[b] Scaled up from a $20\approx\%$ sample.

obtain cross sections, each final state must be corrected for the following effects[218]:

(1) over-all scanning efficiency,

(2) loss due to escape of unstable particles before decay,

(3) loss due to very short decays of strange particles,

(4) loss due to neutral decay modes of strange particles,

(5) omission due to final-state pion decays which were ignored in analysis.

With the exception of (4), these corrections are in general quite small. For example, the over-all scanning efficiency averaged over all event types is 0.95±0.03. The average escape probability is negligible[219] for Σ's and less than 10% for Λ's. The loss due to short decays varies from (3±3)% for Λ^0's to (20±5)% for Σ^+'s. Finally, we note that the correction (5) amounts to about (4±2)% for a two-charged-pion final state. Fully corrected numbers, corresponding to complete samples for data runs I and II, are given in the third column of Table XXI.

Similar considerations apply to reaction channels involving resonances, the data for which are shown in Table XXII. Here, the numbers of events in the third column represent the contributions from all final states in which identification of the resonance is reasonably certain, after subtraction of background. The specific final states involved are listed in the second column of Table XXII. For the most part, effective-mass information[220] is used to identify the resonance contribution within each final state, along the lines indicated in Table XII of Sec. IV. However, in certain cases where the background is large or hard to interpret, a production-angle cutoff[221] must be used in order to obtain a sample of reasonable purity. In such cases the numbers represent the partial sample in the detectable angular interval. In all cases the errors reflect both statistical and systematic (background subtraction) uncertainties. The former dominates in all cases. The numbers in the third column of Table XXII are obtained after compensation for resonance decay into unidentifiable final states as well as correction for the effects (1) through (5).

In order to obtain cross sections, knowledge of the kaon flux is required. The total number of incoming kaons was determined from the observed number of beam decays of the one-prong and three-prong varieties. Single-prong decays were recorded, provided the decay secondary made an angle of $\geq 5°$ with the beam direction.[222] All three-prong vertices were recorded. After correcting for (a) scanning efficiency, (b) the 5° cutoff for two-body and leptonic modes, (c) spurious "τ" events due to the decay "π^-+Dalitz pair," and (d) loss of effective path length due to K^- interactions, one finds that the total number of kaons[223,224] is 1.43×10^6.

[218] These corrections are in general different for the resonant and nonresonant contributions to each final state. The information of Table XXII (together with known branching ratios) is used to make the necessary adjustments.

[219] The $\Xi^-\rightarrow\Lambda+\pi^-$ decay chain is an exception. Here, because *both* the Ξ^- and Λ^0 decays are required to be visible, and because Ξ^-'s are produced in the forward direction, the escape probability averages to about 40%.

[220] Where appropriate, we take into account the finite width of the resonance.

[221] For reactions dominated by meson exchange, a peripheral cutoff is used. For reactions dominated by baryon exchange, an "anti-peripheral" cutoff is used (see Sec. IVC).

[222] This angle is larger than the maximum pion decay angle at 2.24 BeV/c.

[223] An internal check on the measured kaon flux is afforded by the observed ratio of τ's to all K^- decays. We find 5.9±0.2% in excellent agreement with the accepted value.

[224] Part of this paper forms the subject of a thesis submitted in partial fulfillment of the requirements for the degree of Doctor of Philosophy, Syracuse University (1964).

TABLE XXII. Cross sections for reaction channels.

Reaction channel	Final states used	Raw number	Fully corrected number	σ (μb)	$\cos\theta_y$ acceptance interval[a]
$\Lambda\eta$	ΛMM	31 ± 9	55 ± 18	31 ± 10	
$\Lambda\eta^*$	ΛMM, $\Lambda\pi^+\pi^-\pi^0$, $\Lambda\pi^+\pi^- MM$, $\Lambda 5\pi$	94 ± 18	164 ± 31	91 ± 15	≤ -0.6
$\Lambda\phi$	$\Lambda\bar{K}^0\bar{K}^0$, ΛK^+K^-	57 ± 8	141 ± 15	73 ± 8	
$\Sigma^0\phi$	$\Sigma^0K^+K^-$	8 ± 3	25 ± 8	14 ± 4	
$\Lambda\omega$	$\Lambda\pi^+\pi^-\pi^0$	246 ± 30	502 ± 65	278 ± 36	
$\Lambda\rho^0$	$\Lambda\pi^+\pi^-$	85 ± 15	150 ± 26	83 ± 14	
$Y_1^*(1385)^+\pi^-$	$\Lambda\pi^+\pi^-$	205 ± 20	374 ± 45	207 ± 25	
$Y_1^*(1385)^-\pi^+$	$\Lambda\pi^+\pi^-$	32 ± 11	83 ± 33	46 ± 18	
$Y_0^*(1405)\pi^0$	$\Sigma^\pm\pi^\mp\pi^0$	53 ± 20	97 ± 40	54 ± 22	
$Y_0^*(1520)\pi^0$	$\Sigma^\pm\pi^\mp\pi^0$	106 ± 16	350 ± 70	194 ± 39	
$Y_1^*(1660)^+\pi^-$ [b]	$\Sigma^\pm\pi^\mp\pi^+\pi^-$	41 ± 8	82 ± 15	46 ± 8	≤ -0.6
$\Sigma^+\rho^-$	$\Sigma^+\pi^-\pi^0$	110 ± 22	143 ± 36	79 ± 20	
$\Sigma^-\rho^+$	$\Sigma^-\pi^+\pi^0$	22 ± 11	29 ± 15	16 ± 8	≤ -0.6
$\Xi^-(K^*)^+$	$\Xi^-K^+\pi^0$, $\Xi^-K^0\pi^+$	24 ± 6	72 ± 16	34 ± 8	
$(\Xi^*)^-K^+$	$\Xi^-\pi^0K^+$	6 ± 2	46 ± 15	22 ± 7	
$(\Xi^*)^0K^0$	$\Xi^-\pi^+K^0$	25 ± 5	117 ± 24	56 ± 11	
$(\Xi)^0(K^*)^0$	$\Xi^0\pi^+K^-$	8 ± 3	30 ± 12	16 ± 7	
$\Xi^-\kappa^+$	$\Xi^-K\pi$	$\lesssim 6$	$\lesssim 18$	$\lesssim 10$	
$(K^*)^-p$	$\bar{K}^0\pi^-p$	292 ± 25	1860 ± 190	1030 ± 140	≤ -0.6
$\bar{K}^0N^*(1238)^0$	$\bar{K}^0MM$	38 ± 15	224 ± 100	124 ± 55	
$Y_0^*(1405)\pi^+\pi^-$	$\Sigma^\pm\pi^\mp\pi^+\pi^-$	45 ± 25	75 ± 45	42 ± 25	
$Y_0^*(1520)\pi^+\pi^-$	$\bar{K}^0N\pi^+\pi^-$, $K^-p\pi^+\pi^-$, $\Sigma^\pm\pi^\mp\pi^+\pi^-$	136 ± 35	262 ± 70	145 ± 39	
$Y_1^*(1385)^+\pi^-\pi^0$		230 ± 35	368 ± 60	204 ± 33	
$Y_1^*(1385)^-\pi^+\pi^0$	$\{\Lambda\pi^+\pi^-\pi^0\}$	183 ± 30	294 ± 30	163 ± 33	
$Y_1^*(1385)^0\pi^+\pi^-$		212 ± 30	340 ± 60	189 ± 33	
$\Sigma^+\pi^-\omega$	$\Sigma^+\pi^-\pi^+\pi^-\pi^0$	41 ± 9	50 ± 15	28 ± 8	
$\Sigma^+\pi^-\eta$	$\Sigma^+\pi^-\pi^+\pi^-\pi^0$, $\Sigma^+\pi^-MM$	23 ± 13	27 ± 15	15 ± 8	
$\Sigma^-\pi^+\omega$	$\Sigma^-\pi^+\pi^+\pi^-\pi^0$	39 ± 9	47 ± 14	26 ± 8	
$\Sigma^-\pi^+\eta$	$\Sigma^-\pi^+\pi^+\pi^-\pi^0$, $\Sigma^-\pi^+MM$	45 ± 18	49 ± 20	27 ± 11	
$(K^*)^-p\pi^0$	$\{\bar{K}^0\pi^-p\pi^0\}$	73 ± 15	540 ± 108	300 ± 60	
$(N^*)^+\bar{K}^0\pi^-$		49 ± 10	245 ± 50	136 ± 28	
$(K^*)^0p\pi^-$	$\{K^-p\pi^+\pi^-\}$	150 ± 40	320 ± 80	177 ± 44	
$(N^*)^{++}K^-\pi^-$		150 ± 40	160 ± 40	89 ± 22	
$(K^*)^-N\pi^+$	$\{\bar{K}^0N\pi^+\pi^-\}$	48 ± 10	364 ± 70	202 ± 39	
$(N^*)^-K^0\pi^+$		20 ± 10	70 ± 35	39 ± 19	

Using this number, together with the total path length of 35.0 cm, appropriate for $\Xi^-K(\pi)(\Lambda,\Sigma^0)K^0\bar{K}^0$ and $\Sigma^\pm K^\mp K^0$, or the restricted path length, 32.4 cm, appropriate for all other final states, we obtain the partial reaction cross sections of Tables XXI and XXII.

ACKNOWLEDGMENTS

This work was carried out over a period of four years. It is obvious that an effort of this magnitude is possible only with the aid of large numbers of people of vitality and imagination. We would like to take this opportunity to acknowledge the following individual efforts: Dr. R. P. Shutt for his continued support, advice, encouragement and hospitality. Dr. G. C. Moneti and Dr. I. O. Skillicorn whose efforts and ideas in beam design, programming, and analysis contributed significantly in the formative stages of the experiment and specifically to the work concerning the Ξ^-, $Y_1^*(1385)$, φ, and $\Xi^*(1530)$. Dr. J. K. Kopp for his general systems programming, which provided the essential kinematic analysis. Dr. L. Bertanza, Dr. V. Brisson, Dr. P. L. Connolly, Dr. M. Gundzik, Dr. E. L. Hart, Dr. T. Kikuchi, Dr. K. W. Lai, Dr. I. S. Mittra, Dr. J. Westgard,[224] and Dr. R. Wolfe for their participation in one or more aspects of this experiment. Dr. M. H. Blewett, Dr. H. Brown, Dr. G. K. Green and Dr. J. Sanford, the AGS staff and technicians; C. Hedberg, H. Genia, J. Ferrante and the 20-in.-hydrogen-chamber staff of technicians for their invaluable aid in obtaining the pictures, as well as J. Garfield and his staff for the excellent developing and processing of the film. Professors N. Horwitz, J. D. Jackson, T. Kalogeropoulos, R. Peierls, L. O'Raifeartaigh, F. Rohrlich, J. J. Sakurai, E. C. G. Sudarshan and W. J. Willis for many stimulating and informative discussions. Mrs. Mary Burns and Mrs. Betty Osborne for their efficient supervision of the day-by-day activities connected with the processing of the data. And finally the many scanners, measurers, and secretaries whose constant efforts are in no small measure responsible for the fruition of all our efforts.

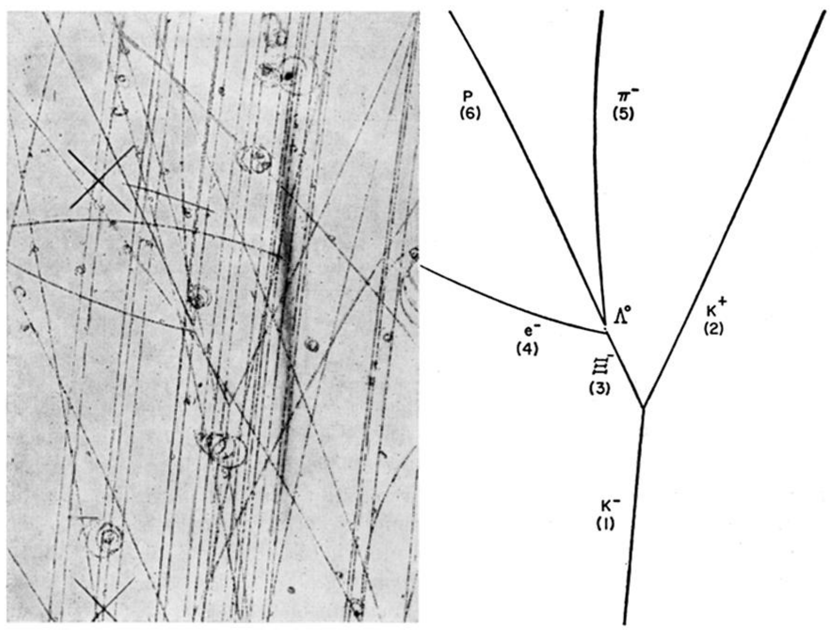

FIG. 76. Photograph and line drawing of possible Ξ^- beta decay event.

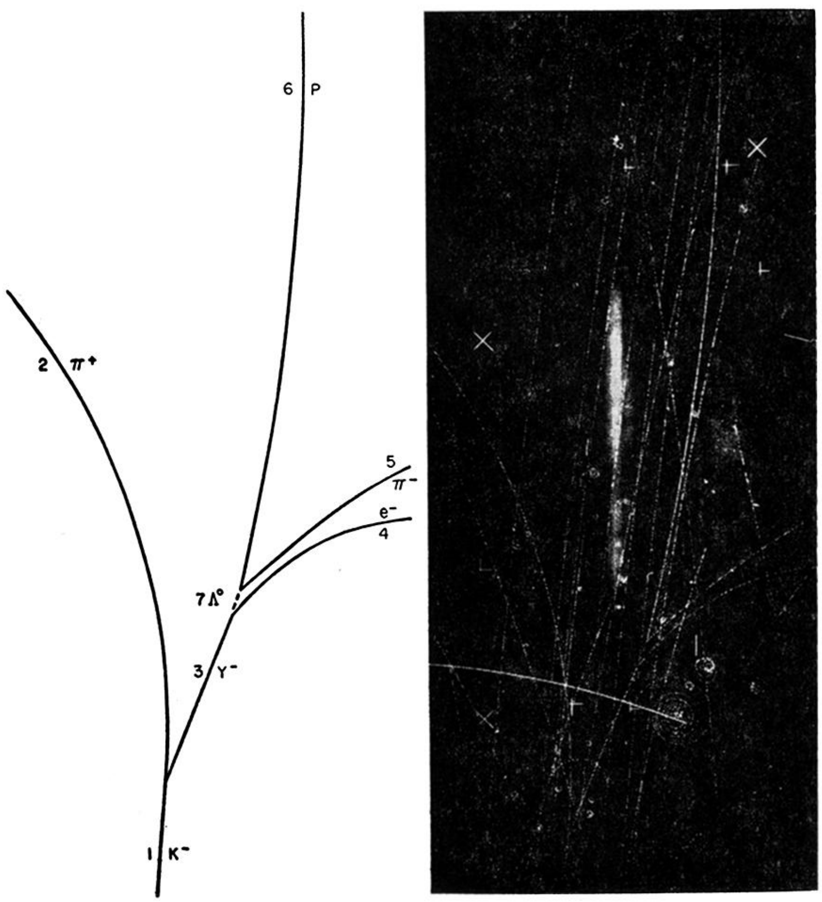

FIG. 77. Photograph and line drawing of Ξ^- beta decay event.